

Regulation of histone proteins
with cell volume and genome content
in *Saccharomyces cerevisiae*

Dissertation

DER FAKULTÄT FÜR BIOLOGIE
DER LUDWIG-MAXIMILIANS UNIVERSITÄT MÜNCHEN



Kora-Lee Claude

München 2022

This dissertation was completed at the Helmholtz Centre Munich

German Research Centre for Environment and Health (GmbH)

Institute of Functional Epigenetics

under the supervision of Dr. Kurt Schmoller

First examiner: Prof. Robert Schneider

Second examiner: Prof. Christof Osman

Date of submission: March 31, 2022

Date of oral examination: November 10, 2022

Eidesstattliche Erklärung

Ich versichere hiermit an Eides statt, dass die vorliegende Dissertation von mir selbstständig und ohne unerlaubte Hilfe angefertigt ist.

Kora-Lee Claude

Munich, December 11, 2022

Erklärung

Hiermit erkläre ich, dass die Dissertation nicht ganz oder in wesentlichen Teilen einer anderen Prüfungskommission vorgelegt worden ist.

Ich erkläre weiter, dass ich mich nicht anderweitig einer Doktorprüfung ohne Erfolg unterzogen habe.

Kora-Lee Claude

Munich, December 11, 2022

Acknowledgements

This thesis is the result of a lot of effort and energy on my part. However, I did not work on it alone. I truly believe in teamwork and am convinced that science gets better when people work together. Here, I would like to thank everyone who actively helped me on the scientific side and also the people who helped me on an emotional level.

First and foremost, I wish to thank my supervisor, **Dr. Kurt Schmoller**, for believing in me and entrusting me with this topic. With my background as a physicist, I knew very little about cell biology when I first started this thesis. Nevertheless, Kurt gave me the opportunity to work on this project and I have learned so much over the past years. I would like to thank you for always being patient and always being there to explain things or teach me new experimental methods.

I also express my gratitude to the two other members of my thesis committee, **Prof. Barbara Conradt** and my official doctorate supervisor **Prof. Robert Schneider**, for regularly taking the time to assess my scientific progress and for being open to discussions. I am grateful that you shared your professional experiences with me.

I would like to particularly thank two members of the Schmoller group for their extensive help with experiments and discussions: **Daniela Bureik** and **Dimitra Chatzitheodoridou**. This project would not have been as successful as it was without your help, and for that you deserve my deepest thanks and respect. You have also always been a moral support and I am very grateful to you.

In addition, I express my deep appreciation for the other members of the Schmoller Group with whom I have had the pleasure of working: **Anika Seel**, **Yagya Chadha**, **Francesco Padovani**, **Alissa Finster** and **Benedikt Mairhörnmann**, as well as my former students

Petia Adarska and **Adil Temirgaliyev**. My gratitude extends to all current and former members of the Institute of Epigenetics, and particularly to **Scarlett Dornauer**, **Dr. Igor Kukhtevich**, **Dr. Lara Zorro Shahidian**, **Dr. Poonam Bheda** and **Nada Al-Refaie**. You all made the lab a peaceful and joyful environment to work in, and for this, I want to thank you.

Furthermore, I want to say thank you to **Sükriye Kocçayir** and **Hanife Hisenaj**. With your work in the background you make our work so much easier, and I don't think you get enough recognition. Thank you!

I would also like to thank **Dr. Thomas Hofer** from the HMGU Immunoanalytics Core Facility for the collaboration, teaching me and helping me with flow cytometry measurements.

Moreover, I thank **Prof. Abhyudai Singh** from the University of Delaware for his collaboration and for helping with the mathematical modelling in this project.

Last but not least, I would like to express my deepest appreciation to my parents, my brother, and mostly to my friends: **Viktoria Kunzelmann**, **Simona Našiščionytė**, **Sahand Yousefpour**, **Johannes Hochholzer**, **Nathalie Claus** and **Annalena Ruff**. You were the ones who supported me emotionally and I will be forever grateful.

Abstract

This thesis addresses the fundamental biological question of how cells achieve different regulations of protein subgroups with cell volume and ploidy (ch. 1). For most proteins, the production is coupled to cell volume, leading to constant concentrations with increasing cell volume. However, strongly DNA-bound proteins, such as histones, are likely needed at constant amounts, which would lead to decreasing concentrations as a function of cell volume. It still remains unclear how cells could achieve to couple the production of some protein subgroups to cell volume, but decouple it from cell volume for other protein subgroups.

To answer this question, I focused on the regulation of histone proteins, using the model organism *Saccharomyces cerevisiae* and made use of genetics in order to achieve a wider range of observable cell volumes (ch. 2.1). Additionally, I performed live-cell fluorescence microscopy (ch. 2.3), reverse-transcription quantitative PCR (ch. 2.4), flow cytometry (ch. 2.5) and single-molecule fluorescence *in situ* hybridization (ch. 2.6).

First, I demonstrate that histone protein and mRNA concentrations decrease with cell volume and are coupled to their respective gene copy number (ch. 3.2 & 3.3). Then, I show that this regulation is achieved by the histone promoter (ch. 3.4), is not an effect of the cell cycle dependent production of histones (ch. 3.7), and most likely does not require direct transcriptional feedback or degradation mechanisms (ch. 3.8). I also detail a minimal mathematical model that describes the dependence of promoter transcription rates with cell volume (ch. 3.5). This model predicts that the behaviour of a histone promoter can be changed to that of most promoters, solely by decreasing its transcription initiation rate. Using a series of promoter truncations, I confirm this theoretical prediction experimentally (ch. 3.6).

In summary, this work shows that the regulation of histone proteins with cell volume and genome content is likely an intrinsic property of histone promoters, where direct transcriptional feedback or degradation mechanisms might play a role but are not necessary. The model introduced during this work lays a foundation for a deeper understanding of protein regulation with cell volume and ploidy in general. Interestingly, this regulation is likely conserved across most eukaryotic cells.

Publication:

Claude, K.-L., Bureik, D., Chatzitheodoridou, D., Adarska, P., Singh, A., and Schmoller, K. M. (2021) Transcription coordinates histone amounts and genome content. *Nature Communications*, 12:4202.

Contents

Acknowledgements	v
Abstract	vii
List of Terms	xv
List of Figures	xvii
List of Tables	xix
1 Introduction	1
1.1 Protein homeostasis with cell size	1
1.1.1 Cell size affects cellular physiology and protein homeostasis	1
1.1.2 Most proteins are kept at constant concentrations as a function of cell size	2
1.1.3 Some protein subsets show a different regulation with cell size	4
1.1.4 Aim of this thesis: investigating the regulation of histones as an example	5
1.2 The model organism <i>Saccharomyces cerevisiae</i>	6
1.2.1 Why use <i>Saccharomyces cerevisiae</i> as a model organism?	6
1.2.2 Cell cycle of budding yeast	7
1.2.3 Tuning budding yeast cell volume	8
1.2.4 Regulation of histones in budding yeast	10
1.3 Outline of this thesis	12
1.4 A generalisable mechanism for the regulation of all protein subsets	13

2	Materials and Methods	15
2.1	Inducible- <i>Whi5</i> budding yeast strains	15
2.2	Measurements on yeast populations	16
2.2.1	Growth curves and doubling times	16
2.2.2	Budding indexes	18
2.2.3	Cell volume distributions	19
2.3	Live-cell fluorescence microscopy	20
2.3.1	Experimental procedure	21
2.3.2	Quantification of histone amounts and concentrations	22
2.3.3	Estimation of cell cycle phases	23
2.3.4	Normalisation of single cell fluorescent intensity traces	24
2.3.5	Estimation of <i>mCitrine</i> synthesis rate	25
2.4	Reverse-transcription quantitative PCR	25
2.4.1	Experimental procedure	26
2.4.2	Test for qPCR primer specificity	27
2.5	Flow cytometry	28
2.5.1	Experimental procedure	29
2.5.2	Calculation of fluorescent concentrations	31
2.5.3	Analysis of cell cycle phases	31
2.6	Single-molecule fluorescence <i>in situ</i> hybridization	32
2.6.1	Experimental procedure	32
2.6.2	Quantification of mRNA spots	34
2.6.3	Classification of cell cycle phases	35
3	Results	37
3.1	Characterisation of inducible- <i>Whi5</i> strains	38
3.1.1	Inducible- <i>Whi5</i> strains allow tuning of cell volume	38
3.1.2	Inducible- <i>Whi5</i> system does not impair on cell growth	40
3.2	Histone protein concentrations depend on cell volume & gene copy number	43

3.2.1	Histone protein amounts stay constant over cell volume and increase with ploidy	43
3.2.2	Histone protein concentrations decrease with increasing cell volume and increase with ploidy	46
3.2.3	Htb2 protein concentrations depend on <i>HTB2</i> gene copy number . .	47
3.3	Histone mRNA concentrations depend on cell volume & gene copy number	50
3.3.1	Histone mRNA concentrations decrease with increasing cell volume	50
3.3.2	<i>HTB2</i> mRNA concentrations depend on <i>HTB2</i> gene copy number .	54
3.4	Histone promoters regulate histone concentrations with cell volume and gene copy number	57
3.4.1	Histone promoters determine the dependence of transcripts on cell volume	57
3.4.2	Histone promoters determine the dependence of transcripts on gene copy number	59
3.5	Model for the dependence of transcription rate on cell volume and ploidy .	62
3.5.1	Introducing the model	62
3.5.2	Model predictions for the behaviour of transcript concentrations . .	65
3.6	Change behaviour of histone promoters experimentally	68
3.6.1	Create histone promoter truncations	68
3.6.2	Histone promoter truncations change the dependence of transcript concentrations on cell volume	69
3.6.3	Histone promoter truncations lead to switch from histone-like to actin-like behaviour	71
3.7	Cell cycle dependent production of histone transcripts	75
3.7.1	S-phase duration does not decrease for larger cells	75
3.7.2	Decrease of histone-promoter-mediated transcript concentrations is achieved during S-phase	77
3.7.3	Cell cycle dependent regulation is not disrupted in histone promoter truncations	81

3.8	Taking a closer look at degradation and transcriptional feedback	85
3.8.1	Degradation of mRNA through the nuclear exosome might play a role for the accurate cell volume dependence of histone transcript concentrations	85
3.8.2	Transcriptional feedback involving HIR complex is not necessary for cell volume dependence of histone transcript concentrations	87
3.8.3	Transcriptional feedback might contribute to the cell volume dependent regulation by the <i>HTB1</i> promoter	89
3.8.4	<i>HTB1</i> promoter does not show dosage compensation upon deletion of <i>HTB2</i>	92
4	Discussion and Outlook	95
4.1	Overall discussion	95
4.1.1	Histone protein and mRNA concentrations decrease with increasing cell volume, and increase with gene copy number	95
4.1.2	Histone promoters are sufficient for regulation of histone concentrations	96
4.1.3	Mathematical model for the dependence of transcription rates on cell volume and ploidy	96
4.2	Outlook	98
4.2.1	Limitations of the current minimal model	98
4.2.2	Possible further experiments	100
4.2.3	Cells need a general mechanism for the regulation of all protein subsets	101
A	Parameter sets for the minimal model	103
B	Statistical analyses and error estimations	105
B.1	Testing significance of the Volume-Dependence-Parameter	105
B.2	Comparison of population means	106
B.3	Error estimation of concentrations at a set cell volume	106

C qPCR primer	109
D Yeast strains	111
References	121
Scientific curriculum vitae	135

List of Terms

ACT1 Gene encoding for Act1 in budding yeast, a structural protein in the cytoskeleton.

ADH1 Gene encoding for Adh1 in budding yeast, an alcohol dehydrogenase. The *ADH1* terminator is used in all the promoter constructs in this thesis.

CLN3 Gene encoding for Cln3 in budding yeast, a G1 cyclin promoting G1- to S-phase transition.

CSE4 Gene encoding for centromeric histone H3-like protein in budding yeast.

ENO2 Gene encoding for Eno2 in budding yeast, a phosphopyruvate hydratase. Catalyst during glycolysis and gluconeogenesis.

HHF1 One of two gene copies encoding for histone H4 in budding yeast.

HHF2 One of two gene copies encoding for histone H4 in budding yeast.

HHO1 Gene encoding for histone H1 in budding yeast.

HHT1 One of two gene copies encoding for histone H3 in budding yeast.

HHT2 One of two gene copies encoding for histone H3 in budding yeast.

HIR1 Gene encoding for Hir1 in budding yeast, a subunit of the HIR nucleosome assembly complex. HIR complex is involved in the regulation of histone gene transcription.

HTA1 One of two gene copies encoding for histone H2A in budding yeast.

HTA2 One of two gene copies encoding for histone H2A in budding yeast.

HTB1 One of two gene copies encoding for histone H2B in budding yeast.

HTB2 One of two gene copies encoding for histone H2B in budding yeast.

HTZ1 Gene encoding for histone variant H2AZ in budding yeast.

mCitrine Yellow fluorescent protein used in this thesis. Derived from *Aequorea victoria*.

NEG element Common motif found in the *HTA1-HTB1*, *HHT1-HHF1* and *HHT2-HHF2* promoters. Involved in repression of histone genes outside S-phase.

RRP6 Gene encoding for Rrp6 in budding yeast, a component of the nuclear exosome exonuclease.

RTT106 Gene encoding for Rtt106 in budding yeast, a histone chaperone. Part of the HIR complex.

SPT10 Gene encoding for Spt10 in budding yeast, a histone H3 acetylase. Spt10 binds to pairs of UAS elements in core histone promoters. Involved in activation of histone genes during S-phase.

UAS Histone upstream activating sequence elements found in all core histone promoters. Act as binding sites for Spt10.

VDP Volume Dependence Parameter. Quantitative measure introduced to describe behaviour of concentration as function of cell volume. $VDP = 0$ means constant concentration. $VDP = -1$ means decrease of concentration with $c \approx 1/V$.

WHI5 Gene encoding for Whi5 in budding yeast, an inhibitor of the G1- to S-phase transition. A β -estradiol-inducible *WHI5* is used in this thesis to tune the cell volume of budding yeast cells.

List of Figures

1.1	Illustration: regulation of most protein concentrations vs. DNA-bound proteins	5
1.2	Illustration: tuning volume of budding yeast cells	9
1.3	Illustration: histone genes and their regulation in budding yeast	11
2.1	Illustration: example growth curve of budding yeast	17
2.2	Illustration: calculation of the H-period in live-cell fluorescence microscopy	23
3.1	Inducible-Whi5 strains - tune budding yeast cell volume	39
3.2	Inducible-Whi5 strains - controls	41
3.3	Inducible-Whi5 strains - cell cycle phases	42
3.4	Htb1- and Htb2-mCitrine amounts	45
3.5	Htb2-mCitrine concentration with cell volume	46
3.6	Htb2-mCitrine concentration with ploidy	49
3.7	Constant mRNA concentrations with cell volume	51
3.8	Histone mRNA concentrations decrease with cell volume	53
3.9	Control experiments on decrease of histone mRNA concentrations	54
3.10	<i>HTB2</i> mRNA concentrations with gene copy number	56
3.11	Illustration: histone promoters experiments	57
3.12	Histone promoters regulate histone concentrations - RT-qPCR	58
3.13	Histone promoters regulate histone concentrations - flow cytometry	60
3.14	Histone promoters regulate histone concentrations - Summary	61
3.15	Illustration: minimal mathematical model	63
3.16	Minimal mathematical model - predictions	66
3.17	Minimal mathematical model - change behaviour of promoter	68

3.18	Illustration: promoter truncation experiments	69
3.19	Change <i>VDP</i> of histone promoters - flow cytometry	70
3.20	Illustration: UAS elements on the <i>HHF1</i> and <i>HTB1</i> promoter	71
3.21	Manipulation of histone promoter behaviour - flow cytometry	72
3.22	Manipulation of histone promoter behaviour - RT-qPCR	74
3.23	Histone promoters are cell cycle dependent - live-cell fluorescence microscopy	76
3.24	Histone promoters - S-phase duration	77
3.25	Illustration: single-molecule FISH experiments	78
3.26	Histone promoters are cell cycle dependent - smFISH	79
3.28	Truncated histone promoters are cell cycle dependent - live cell fluorescence microscopy	82
3.29	Truncated histone promoters are cell cycle dependent - smFISH	84
3.30	Summary of <i>VDPs</i> for <i>rrp6Δ</i>	86
3.31	Summary of <i>VDPs</i> for <i>hir1Δ</i> and <i>rtt106Δ</i>	88
3.32	<i>HIR1</i> -dependent regulation on the transcript level	91
3.33	<i>HTB1</i> promoter does not exhibit dosage compensation	93
4.1	Graphical summary	98

List of Tables

C.1 qPCR primer specificity	109
C.2 qPCR primer	110
D.1 Yeast strains	119

Chapter 1

Introduction

1.1 Protein homeostasis with cell size

1.1.1 Cell size affects cellular physiology and protein homeostasis

Looking at different biological organisms, it becomes clear that cell sizes can vary drastically depending on the type or function of cells [Ginzberg et al., 2015]. Prokaryotic cells, for example, typically range from 0.1 - 5.0 μm in diameter, whereas eukaryotic cells are much bigger, normally with diameters of 1 - 100 μm . In fact, cell size plays an important role for cell survival, as it severely impacts on cell physiology [Goehring and Hyman, 2012, Chan and Marshall, 2010]. In particular, many sub-cellular structures, such as the nucleus or mitochondria, increase in proportion to cell size [Jorgensen et al., 2007, Neumann and Nurse, 2007, Rafelski et al., 2012, Seel et al., 2022]. Therefore, cells use various mechanisms to control and regulate their size in order to stay healthy [Lloyd, 2013, Turner et al., 2012, Robert, 2015, Ginzberg et al., 2015, Schmoller and Skotheim, 2015].

But, even with these control mechanisms, cells can still be subject to drastic changes in their cell size. Changes in nutrient conditions can for example have severe impact on cell growth and therefore cell size [Conrad et al., 2014]. Other biological processes, such as embryogenesis or cell differentiation also lead to such changes in cell size [Aiken et al., 2004, Tsihlaki and FitzHarris, 2016]. In addition, most proliferating cells grow bigger whilst they are cycling through their cell cycle.

In general, most biological processes in a cell are dependent on the appropriate concentrations of proteins involved in the reactions [Alberts et al., 2002]. Misregulation in the expression of genes can severely impact on cell fitness, and can lead to many diseases of the whole organism [Lee and Young, 2013]. Thus, concentrations of most proteins need to be kept constant with cell growth. Normally, this is achieved by coupling the protein production to cell size: bigger cells typically have higher transcription and protein synthesis rates [Zhurinsky et al., 2010, Marguerat and Bähler, 2012, Padovan-Merhar et al., 2015, Schmoller and Skotheim, 2015, Sun et al., 2020]. This leads to increasing amounts of proteins [Williamson and Scopes, 1961, Crissman and Steinkamp, 1973, Wu and Pollard, 2005] resulting in roughly constant concentrations as a function of cell size.

1.1.2 Most proteins are kept at constant concentrations as a function of cell size

The literature has been discussing how cells could achieve to couple general biosynthesis to cell size for some time. Some studies indicate that the coupling of protein production to cell size is mostly established by mRNA synthesis, rather than by mRNA turnover rates [Marguerat and Bähler, 2012]. Bigger cells typically have more mRNAs as a result of higher transcriptional output [Schmidt and Schibler, 1995, Elliott and McLaughlin, 1979]. In contrast, mRNA degradation rates are mostly independent of cell size [Zhurinsky et al., 2010, Padovan-Merhar et al., 2015]. However, it is now also believed that mRNA synthesis and degradation are linked to each other by some feedback mechanism [Sun et al., 2012]. The general understanding follows the idea that some part of the transcriptional machinery, some general transcription factors, or chromatin structures could be responsible for coupling general transcription rates to cell size [Marguerat and Bähler, 2012]. For example, it has been shown that tuning the expression level of the RNA Polymerase II, or several general transcription factors, had an impact on the levels of most mRNAs [Lee et al., 2005, Sharma et al., 2006]. In addition, some subunits of the RNA Polymerase II have also been shown to be haplo-insufficient, both in *Saccharomyces cerevisiae* and in *Schizosaccharomyces pombe* [Kim et al., 2010, Pir et al., 2012]. This means that for some

of those Polymerase II subunits, a diploid cell needs to have both gene copies encoding for them in order to exhibit proper growth.

This leads to the common idea that some subunit of the transcriptional machinery is limiting for the availability of the transcriptional machinery, and thus limiting for general transcription rates. Increasing the availability of the transcriptional machinery by increasing the amounts of this limiting component then leads to increased general transcription rates. If the amount of this limiting component increased with increasing cell size, this would allow cells to couple general transcription rates to cell size. Additionally, the idea of a limiting component whose amount is linked to cell size also explains the fact that total RNA and mRNA levels are not affected by ploidy, when comparing diploids and haploids of similar size [Ogur et al., 1952, Galitski, 1999, Wu et al., 2010]. The genome content of diploids is twice as much as the one of haploids. Thus, if a limiting component is responsible for tuning general transcription rates, the mRNA production per gene should drop in diploids, compared to haploids of similar size. This is because the limiting component is now spread out across twice as many genes. As diploids have two copies of each gene, though, the overall mRNA concentration should be similar to the one in haploids [Wu et al., 2010, Lin and Amir, 2018, Sun et al., 2020].

In addition to transcription rates, translation rates also need to increase with cell size in order to couple total protein production to cell size. This could be established by an increase of ribosomes with cell size [Marguerat and Bähler, 2012]. In accordance with this assumption, rRNA and total ribosomal protein synthesis indeed increase with cell size [Padovan-Merhar et al., 2015, Elliott et al., 1979]. Additionally, the amount of many ribosomal proteins increases in direct proportion to cell size [Schmoller and Skotheim, 2015].

In summary, if both global transcription rates and global translation rates increase in direct proportion to cell size, the production of total proteins can also increase in direct proportion to cell size (Fig. 1.1). This then leads to constant concentrations of most proteins with growth, as is needed for most biochemical reactions [Alberts et al., 2002]. Transcription rates are thought to be mediated by the availability of a limiting component

of the transcriptional machinery. Translation rates are thought to be mediated by the availability of ribosomes.

1.1.3 Some protein subsets show a different regulation with cell size

Coupling protein production to cell size is, however, not appropriate for all proteins in a cell. In *Saccharomyces cerevisiae* for example, it has been shown that the production of the G1/S inhibitor Whi5 is independent of cell size [Schmoller et al., 2015]. This leads to a decrease of Whi5 concentration with increasing cell size and allows cells to sense and control their size. A similar finding was also recently reported for the G1/S inhibitor Rb in mammalian cells [Zatulovskiy et al., 2020]. In fact, recent studies suggest that many cell cycle regulators [Chen et al., 2020], as well as other proteins [Swaffer et al., 2021a, Lanz et al., 2021] are subject to a different regulation with cell size than most proteins. Some proteins might show a super-scaling behaviour, where the concentration increases with increasing cell size. Other proteins, such as histones and Whi5, display a sub-scaling behaviour, where the concentration decreases with increasing cell size [Lanz et al., 2021]. For instance, focusing on histones highlights the cell's need for another method of regulation than just increasing production with cell size. As building blocks of nucleosomes [Cox et al., 2005], they are strongly DNA-bound proteins and are likely needed at a constant DNA-to-protein ratio. It is known that accurate histone homeostasis is necessary for biochemical processes in the cell [Amodeo et al., 2015, Joseph et al., 2017, Hauer et al., 2017, Chari et al., 2019], and in order to avoid toxicity [Kim et al., 1988, Han et al., 1987, Meeks-Wagner and Hartwell, 1986], histones are subject to several layers of regulation through transcription, translation and degradation [Eriksson et al., 2012, Kurat et al., 2014a, Gunjan and Verreault, 2003]. Thus, it is indeed more likely that the production of histone proteins is not coupled to cell size, but rather to the genomic DNA content of the cell (Fig. 1.1).

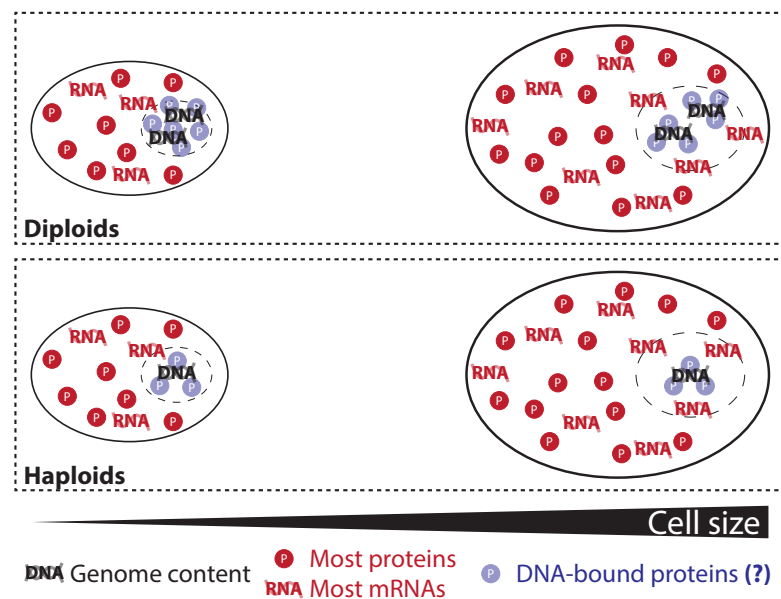


Figure 1.1: **Illustration of the regulation of most protein concentrations in contrast to the possible regulation of DNA-bound proteins.** General biosynthesis is linked to cell size leading to increased amounts of most proteins and mRNAs in bigger cells (adapted from [Marguerat et al., 2012]). This way, cells keep constant concentrations with increasing cell size. DNA-bound proteins, such as histones, however, might be subject to a different regulation. Their production could be decoupled from cell size, and coupled to genome content instead.

1.1.4 Aim of this thesis: investigating the regulation of histones as an example

At the beginning of this thesis however, it remained unclear how exactly cells could achieve to uncouple the production of some proteins from cell size. How could they instead couple it to genome content, even though global biosynthesis increases with cell size? In particular, the precise regulation of histone proteins with cell size and genome content had not been investigated yet. Thus, as a first aim, I focused on histones to get a better understanding on how exactly they are regulated both with cell size and genome content. Going further, the second aim of this project was to investigate the molecular mechanisms involved in the cell size dependent production of histones.

In addition to being essential proteins conserved across eukaryotes, histones are also a good

example of tightly DNA-bound proteins, which are likely subject to a different regulation with cell size than most proteins. Thus, focusing on histones might help identify a general mechanism that could allow cells to couple the production of some protein subsets to cell size, and the production of other protein subsets to genome content.

1.2 The model organism *Saccharomyces cerevisiae*

1.2.1 Why use *Saccharomyces cerevisiae* as a model organism?

To gain insights into histone synthesis and regulation, I used the model organism *Saccharomyces cerevisiae*, also known as budding yeast. Budding yeast is a single-celled, eukaryotic model organism, whose cells are roughly spherical, typically with a diameter of around 5 μm and a cell volume of about 30 fL [Duina et al., 2014]. This places them in between the size of typical bacterial cells and mammalian cells. Under optimum laboratory conditions, budding yeast can reproduce rather rapidly, as fast as once every 90 minutes. It is also easily possible to grow yeast cells both as haploids (one set of chromosomes) and as diploids (two sets of chromosomes). Generally, it requires only simple growth conditions and is therefore inexpensive and easy to grow. In addition, glycerol stocks of yeast strains can be stored at $-80\text{ }^{\circ}\text{C}$ and kept for years. New cultures can then be started from those stocks, simply by taking out small amounts of frozen cells, plating them on solid medium agar plates and letting them grow at $30\text{ }^{\circ}\text{C}$ in an incubator for several days.

One striking aspect of budding yeast that has made it an established model organism for cellular biology, is the ease to genetically modify it. Since homologous recombination works with high efficiency in budding yeast, transformation protocols are easy and fast to perform, usually resulting in high amounts of clones with the desired genetic modification [Duina et al., 2014]. Thus, integrating, deleting or modifying genes in the genome can be done easily and fast. One of the most used budding yeast strains, S288C [Mortimer and Johnston, 1986], was also the first eukaryotic organism to be fully sequenced [Goffeau et al., 1996]. This strain is used as a reference genome for most other strains used in

laboratories, which further simplifies the possibilities of genetic modifications. For this work, the yeast strains used are based on the W303 strain, that has itself also been fully sequenced [Ralsler et al., 2012] and whose genome is derived from S288C to 85 %. In addition, a powerful online tool, the Saccharomyces Genome Database [Cherry et al., 2012], facilitates experimental design and interpretation of data by providing wide and open access information on the budding yeast genome.

Moreover, the cell size control of budding yeast is relatively well understood [Schmoller et al., 2015, Chandler-Brown et al., 2017] and, thus, it is possible to experimentally manipulate the size of budding yeast cells in order to investigate a wider range of sizes [Schmoller et al., 2015, Kukhtevich et al., 2020]. Here, I want to note that cell size can be measured as a variety of different parameters, such as the diameter, the length or the volume of cells. Since budding yeast cells are roughly spherical, I used the total cell volume as a measure for cell size.

In summary, budding yeast is a powerful model organism to address fundamental biological questions, such as the regulation of histone proteins with cell volume and genome content. In addition, budding yeast has a total of eleven histone genes [Eriksson et al., 2012], an amount small enough to perform analyses on all of them. Many landmark discoveries shaping our today's understanding of basic cellular processes were made in budding yeast [Duina et al., 2014]. Furthermore, the structure and function of histone proteins are in general mostly conserved throughout eukaryotic cells [Cox et al., 2005]. Thus, it is very likely that the underlying mechanism of histone regulation with cell volume and genome content in budding yeast is largely conserved across most eukaryotes.

1.2.2 Cell cycle of budding yeast

Budding yeast cells can reproduce asexually by an asymmetric process called budding both as haploids and diploids [Duina et al., 2014]. During this process a daughter cell emerges from the mother cell and grows until it detaches. When a cell is born, it first starts growing during a phase called G1. Then, it enters the phase of DNA replication, called S-phase. Just before and during S-phase a small bud starts emerging and growing

from the mother cell. During the rest of S-phase the bud keeps growing bigger and stays attached to the mother cell. When DNA replication is completed, the divided new nucleus is transported from the mother cell into the bud. At the end of this process, the bud detaches from the mother and enters its own cell cycle. Those last steps within the cell cycle are commonly referred to as G2/M-phase, since the usual G2-phase of rapid cell growth just before mitosis is not well defined for budding yeast [Morgan, 2007].

In addition, haploid cells can reproduce sexually by a process called mating [Merlini et al., 2013]. Haploid cells can either be of mating type a (Mat a) or mating type α (Mat α), both releasing typical pheromones. In the presence of the other mating type's pheromone, Mat a and Mat α cells can then initiate "shmooing" and start the process of mating, resulting in a stable diploid cell Mat a/Mat α . Under nitrogen-poor growth conditions, diploid cells can then undergo meiosis and form four haploid spores [Neiman, 2011]. Those spores can then germinate into four cells, two of each mating type. In nature, budding yeast haploid cells can switch between Mat a and Mat α , allowing them to form diploid cells easily [Haber, 2012]. For most laboratory strains, however, this switching possibility is disabled in order to work with stable haploid cells of either Mat a or Mat α .

1.2.3 Tuning budding yeast cell volume

The first aim of this thesis is to quantitatively and accurately investigate the concentration of histones as a function of cell volume. For this, it is of importance to increase the range of observable cell volumes. Commonly used experimental methods include the arrest of cells in G1 for varying amounts of time and subsequent release into S-phase [Futcher, 1999]. This allows for the creation of synchronous yeast populations with different mean cell volumes. On the down side, using such methods means heavily interfering into the cell cycle and growth dynamics of yeast cells, potentially resulting in artefacts. Another possibility is to use strains bearing mutations that lead to smaller or bigger cells than wild-type cells [Jorgensen et al., 2002, Zhang et al., 2002]. However, most of the mutants resulting in high changes in cell volume usually display very slow growth rates compared to wild-type strains.

As an alternative, it is possible to make use of the relatively well understood cell-size control in budding yeast [Schmoller et al., 2015, Chandler-Brown et al., 2017] in order to tune the volume of cells. The regulation of budding yeast cell volume depends on the interplay between the G1/S inhibitor *WHI5* [Jorgensen et al., 2002] and the G1 cyclin *CLN3* [Nash et al., 1988, Mortimer et al., 1992]. It was shown that the protein synthesis rate of *WHI5* stays constant and is independent of cell volume, while the synthesis rate of *CLN3* increases with cell volume [Schmoller et al., 2015]. This leads to a constant Cln3 concentration and a decrease of Whi5 concentration with increasing cell volume during G1-phase. With decreasing Whi5 concentration, the probability of initiating the start of S-phase is increased. Since the *WHI5* production is independent of cell volume, smaller cells are typically born with a higher concentration of Whi5. Thus, they need to grow for a longer time in G1 (i.e. become bigger) in order to achieve lower Whi5 concentrations and increase the probability of starting S-phase. Thus, dilution of Whi5 through growth during G1-phase allows budding yeast cells to regulate their cell volume.

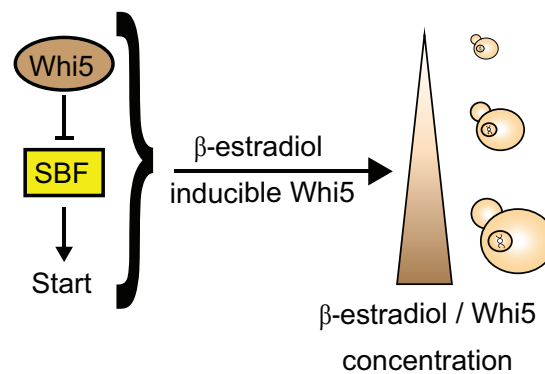


Figure 1.2: **Inducible-Whi5 concentration tunes volume of budding yeast cells.**

To manipulate cell volume, *WHI5* is expressed from a β -estradiol-inducible promoter. Higher β -estradiol concentration results in increased mean cell volumes.

Using this understanding, a system of hormone (β -estradiol) inducible *WHI5* has been described and used in previous studies to successfully tune the volume of budding yeast cells [Ottoz et al., 2014, Schmoller et al., 2015, Kukhtevich et al., 2020]. Briefly, the Whi5 concentration in cells can be tuned by addition of β -estradiol, ultimately resulting in a wide range of cell volumes (Fig. 1.2). The first effect of longer G1-phase, due to

higher Whi5 concentrations, evens out after a few generations, since bigger mother cells typically produce bigger daughter cells. This β -estradiol inducible *WHI5* system was also used during this thesis in order to tune the volume of investigated budding yeast cells.

1.2.4 Regulation of histones in budding yeast

Each of the four core histones in budding yeast is encoded by two gene variants, which show high sequence similarity between each other (*HTA1* & *HTA2* for H2A, *HTB1* & *HTB2* for H2B, *HHT1* & *HHT2* for H3, and *HHF1* & *HHF2* for H4). In the genome, they are expressed from bidirectional promoters, which each control pairs of H2A-H2B [Hereford et al., 1979] or H3-H4 [Smith and Murray, 1983] (Fig. 1.3a). Thus, in total there are four of these histone loci, and as a result of the redundancy in each core histone gene, the deletion of any one of those loci - except the *HTA1-HTB1* locus - is not lethal to the cells [Cross and Smith, 1988, Libuda and Winston, 2006]. Additionally, the gene *HHO1* encodes for the linker histone H1, and *CSE4* & *HTZ1* encode for two histone variants. For this thesis, I decided to restrain my analyses to the eight core histone genes and the linker histone gene.

The core histone genes are subject to both positive (i.e. activating) and negative (i.e. repressive) regulation on the transcript level [Osley, 1991, Eriksson et al., 2012]. Additionally, the degradation of excess histones through the proteasome is known to be regulated by the protein kinase Rad53, as was discovered through the lethal accumulation of histones in *rad53* Δ cells [Gunjan and Verreault, 2003]. Despite the high degree of sequence similarity between the individual gene variants coding for the same histone protein, the different core histones are still subject to strikingly different regulations. For example, only the *HTA1-HTB1* pair is known to exhibit dosage compensation upon deletion of *HTA2-HTB2* [Norris and Osley, 1987, Cross and Smith, 1988, Moran et al., 1990]. This means that both *HTA1* and *HTB1* react with higher expression when the *HTA2-HTB2* locus is deleted.

Each of the core histone gene promoters contains multiple upstream activating sequence (UAS) elements [Osley, 1991] (Fig. 1.3a), that are absent in the sequence of the H1

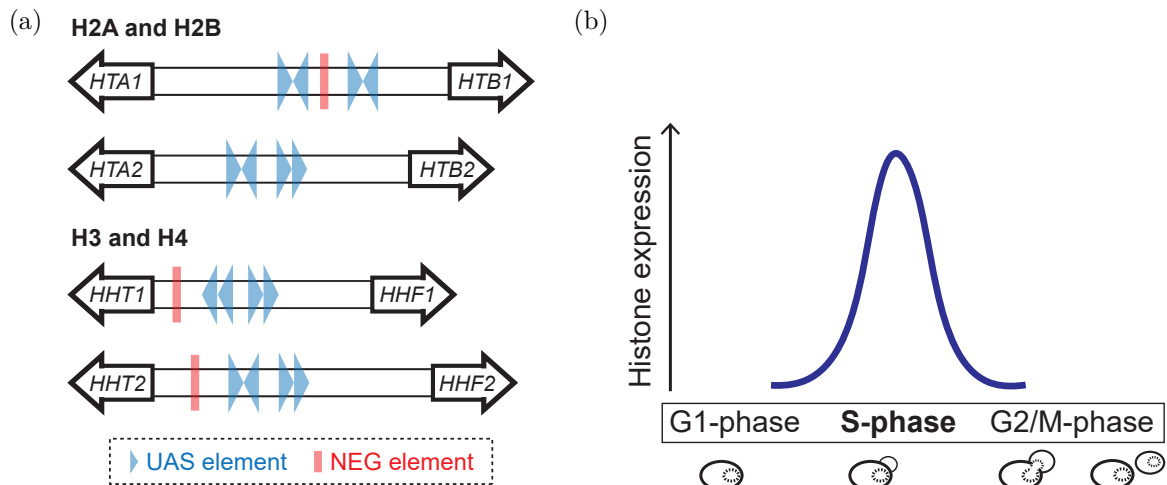


Figure 1.3: **Illustration of the core histone genes in budding yeast, and the restriction of their expression to S-phase.** (a) The eight core histone gene copies, grouped by the histone genes they encode for, are shown as a schematic illustration. The locations of the upstream activating sequence (UAS) elements [Osley et al., 1986] are indicated as blue arrowheads, with the direction indicating their orientation. The UAS elements act as binding sites for Spt10, known to activate histone gene expression in S-phase. The NEG elements [Osley, 1991, Mariño-Ramírez et al., 2006], possibly important for the repression of histone expression outside of S-phase, are indicated as red boxes. (adapted from [Eriksson et al., 2012]). (b) The expression of the core histone genes is restricted to late G1-phase and S-phase, corresponding to the time of DNA replication (adapted from [Kurat et al., 2014a]).

gene *HHO1*. Those UAS elements act as binding sites for the transcription factor Spt10, which interestingly requires two UAS elements for high-affinity binding [Eriksson et al., 2005]. Spt10 binding on the histone promoters is thought to activate and restrict the transcription of the core histone genes to S-phase (Fig. 1.3b). Additionally, binding of the major transcription factor complexes that activate transcription during the G1/S transition of cells, SBF and MBF, might also be involved in this cell cycle dependent activation of core histone genes [Eriksson et al., 2005, Eriksson et al., 2011]. However, the exact mechanism of when and why those transcription factors bind to the histone promoters remains unclear [Eriksson et al., 2012].

In addition, histone gene transcription is actively repressed outside of S-phase. Except for the *HTA2-HTB2* gene pair [Osley and Lycan, 1987, Xu et al., 1992], this repression is thought to be mediated by the HIR complex, which includes the histone chaperones Rtt106 and Hir1 [Fillingham et al., 2009, Feser et al., 2010, Zunder and Rine, 2012]. The HIR complex is in general thought to play an important part in the coupling of histone expression to DNA replication, since it is also involved in the repression of histone genes upon replication stress, again not including the *HTA2-HTB2* pair [Eriksson et al., 2012, Libuda and Winston, 2010]. The HIR complex dependent regulation seems to be controlled by the NEG element, a short sequence that can be found in all core histone gene pair promoters, except the *HTA2-HTB2* pair [Osley and Lycan, 1987, Osley, 1991, Mariño-Ramírez et al., 2006] (Fig. 1.3a).

In summary, many studies have investigated the cell cycle dependent expression of histones and their coordination in response to replication stress [Osley, 1991, Eriksson et al., 2012]. However, how exactly histones are regulated with respect to cell volume remained unclear at the beginning of this thesis.

1.3 Outline of this thesis

Chapter 2 will give an overview over all the experimental techniques used during this work, highlighting the general working principle, which questions were addressed with these experiments and describe the experimental protocols. It will also give more information on the inducible *WHI5* strains used for this thesis.

Chapter 3 will describe and interpret the experimental results in light of the assumptions made and in accordance with the literature. First, I make sure that the biological system used to increase the range of observable cell volumes during this work [Ottoz et al., 2014, Schmoller et al., 2015, Kukhtevich et al., 2020] does not have a drastic impact on cell growth (ch. 3.1). Then, in order to investigate the regulation of histone proteins with cell volume, I use live-cell fluorescence microscopy together with microfluidics to quantify the fluorescence amount of tagged histone genes in single cells. I show that histone protein concentrations decrease with increasing cell volume (ch. 3.2), and con-

firm that this is already achieved at the mRNA level for all histone genes by performing reverse-transcription quantitative PCR (RT-qPCR) on bulk cell populations (ch. 3.3). Going further, again using RT-qPCR and adding flow cytometry, I show that the histone promoters alone are sufficient to achieve the decrease of transcript concentrations with increasing cell volume (ch. 3.4). At this point, I introduce a minimal mathematical model to describe a general mechanism that cells could be employing to couple histone production to genome content, and the production of most other proteins to cell volume (ch. 3.5). This model predicts that the regulation of transcripts with cell volume and genome content is an intrinsic property of the promoter, and that it can be changed by tuning the initiation rate (binding affinity to the transcriptional machinery) of the promoter. Using flow cytometry, RT-qPCR and a series of promoter truncations, I confirm this theoretical prediction experimentally (ch. 3.6). Then, again using live-cell fluorescence microscopy and adding single molecule fluorescence *in situ* hybridization, I take a closer look at the cell cycle dependent production of histones (ch. 3.7). Lastly, using RT-qPCR, I investigate possible mRNA degradation and transcriptional feedback mechanisms that could be involved in the regulation of histones with cell volume and genome content (ch. 3.8). I show that, while such mechanisms could play a role in the exact regulation of some histone transcripts, they are at least not necessary for it.

Chapter 4 will summarise the findings and critically discuss them in relation to the literature. Additionally, chapter 4.2 will address the limitations of the current stage and give an outlook on what other experiments could be performed in order to gain even more mechanistic insights into the regulation of proteins with cell volume and genome content.

1.4 A generalisable mechanism for the regulation of all protein subsets

Throughout this thesis, I focus on the regulation of histone proteins with cell volume and ploidy as an example. They are a good model to study a regulation that is likely different than the regulation of most other proteins, which are kept at constant concentrations.

In fact, numerous different subsets of proteins might display a different regulation than being held at constant concentrations as a function of cell volume. As stated above, the production of many cell cycle regulators is likely independent on cell volume, leading to a decrease of concentration [Schmoller et al., 2015, Zatulovskiy et al., 2020, Chen et al., 2020]. Another recent study also suggests that protein subunits of the proteasome are produced in a super-scaling manner, meaning that their concentrations is increasing with cell volume [Lanz et al., 2021]. The aim of this thesis is to describe a general mechanism that can explain the cell volume- and ploidy-dependent regulation of all protein subsets within a cell. Thus, this thesis addresses a fundamental biological question, which is likely conserved throughout most eukaryotes.

Chapter 2

Materials and Methods

This chapter will describe the genetic background of the inducible *WHI5* strains (ch. 2.1) and give an overview of the experimental methods used for the scope of this thesis. In order to estimate growth dynamics, I performed several measurements on bulk populations (ch. 2.2). Additionally, to calculate histone protein concentrations and histone mRNA concentrations, I performed live-cell fluorescence microscopy (ch. 2.3) and reverse-transcription quantitative PCR (ch. 2.4). As a fast read-out method to quantify fluorescence amounts, I also performed flow cytometry measurements (ch. 2.5). Lastly, to get more insights on the production of histone mRNA molecules, I used single-molecule fluorescence *in situ* hybridization (ch. 2.4). Each of those methods will be introduced by explaining the basic working principle and stating what was measured. Moreover, the experimental procedures and protocols will be described. Where applicable, this chapter will also detail the analyses performed on the measured data.

2.1 Inducible-*Whi5* budding yeast strains

The basis of this thesis is the ability to measure a wide range of cell volumes. For single cell measurements it allows for the increase of the observable cell volume range. For bulk measurements it is even more essential, since increasing the range of budding yeast cells allows the creation of yeast populations with different mean cell volumes. This makes it possible to measure properties of bulk populations as a function of the mean cell volumes of the populations.

For this purpose, during this thesis, I made use of β -estradiol-inducible *WHI5* strains, previously described in other studies [Schmoller et al., 2015, Kukhtevich et al., 2020]. In those strains, the endogenous alleles of *WHI5* is deleted and a copy of *WHI5* expressed from an artificial, β -estradiol inducible promoter system [Ottoz et al., 2014] is integrated into the genome. In-detail, this inducible promoter system consists of an artificial β -estradiol-dependent transcription factor and an artificial promoter, both integrated into the genome of the yeast strains. In the presence of β -estradiol, the artificial transcription factor can bind the artificial promoter, and thus activate its transcription. This artificial promoter is used to regulate the expression of *WHI5*. Therefore, addition of β -estradiol leads to the activation of *WHI5* transcription. Variable addition of β -estradiol concentrations then results in variable concentrations of Whi5 within the cells and allows the tuning of yeast cell volumes (Fig. 1.2). Higher β -estradiol concentrations lead to cells with larger volumes.

2.2 Measurements on yeast populations

A population of growing yeast cells can be described by its growth dynamics, i.e. its growth curve and doubling time during exponential growth, and the distribution of cell cycle phases. Additionally, the distribution of cell volumes within the population and thus the mean cell volume of the population is of special interest for this study.

This chapter will give a brief description on how I measured and calculated those parameters for this work.

2.2.1 Growth curves and doubling times

Typically, a growing population of yeast cells will undergo four stages of growth, which can be visualised by a growth curve (Fig. 2.1). When starting a new culture of yeast cells, the cells first undergo a phase during which they need to adapt to the new growth conditions (new media, new temperature, etc.) and little to no cell division happens, resulting in a nearly constant total number of cells N . This phase is called the lag phase and typically

lasts a couple of hours. When cells start dividing, they enter the log phase, during which the cell population exhibits exponential growth with a constant growth rate r_g . When the cell culture becomes too dense and nutrients are depleted, usually after several hours of growth, the cells enter the stationary phase where growth rate r_g and death rate r_d are equal and the total number of cells N within the population stays constant. If the culture is not supplied with new nutrients or diluted, the cells will eventually enter the death phase with a death rate r_d higher than the growth rate r_g , leading to a decline of the total number of cells N within the population.

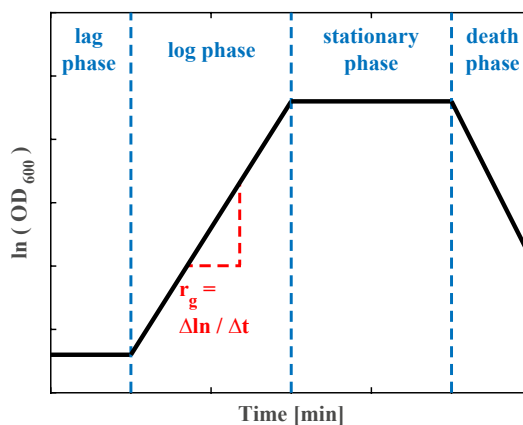


Figure 2.1: **Schematic illustration of a growth curve for budding yeast.** The growth rate r_g of the cell population can be calculated in the log phase of the growth curve.

The duration of those phases can be influenced by the media in which the cells are being grown. Rich media will lead to faster growth whereas poor media will lead to slower or no growth at all. It is worth to note that budding yeast cells can grow through fermentation when supplied with sugar but also through respiration by ethanol import if no source of sugar is available. Thus, depending on the media, budding yeast cells can also undergo a diauxic shift [Olivares-Marin et al., 2018]: when the source of sugar is depleted, the metabolism of the cells switches from fermentation to respiration, if ethanol is available. This results in a first log phase with specific growth rate $r_{g,1}$ until the population reaches an intermediate plateau in total number of cells N_1 . Then, after the diauxic shift, the population undergoes a second log phase with a different growth rate $r_{g,2}$.

During the log phase (exponential growth of the population) the number of cells N within the population can be described by the following equation:

$$N(t) = N_0 \cdot e^{r_g \cdot t} \quad (2.1)$$

with N_0 describing the number of cells at time point zero. Since the optical density OD of low-density liquid yeast cultures and the number N of cells within the culture are roughly proportional to each other, a similar exponential relationship is also true for the optical density OD of liquid cultures [Myers et al., 2013].

In order to determine growth curves, I measured optical densities OD at 600 nm using a spectrophotometer (Perkin Elmer, Lambda Bio+). I grew liquid cultures of yeast cells and measured the optical density OD_{600} at pre-defined time points over several hours. Visualising the OD_{600} data points on a logarithmic scale leads to a linear relationship between $\ln(OD_{600})$ and time t for the exponential growth phase of the population (Fig. 2.1). The growth rate r_g can then be calculated as the slope of the linear relationship:

$$r_g = \frac{\ln(OD_{600}(t_2)) - \ln(OD_{600}(t_1))}{t_2 - t_1} \quad (2.2)$$

Another parameter describing growth dynamics of the population during the log phase, is the doubling time t_D , i.e. the average time needed for a cell to undergo a full cell cycle and produce a new daughter cell. Knowing the growth rate r_g from the measured growth curves, I calculated t_D as:

$$t_D = \frac{\ln(2)}{r_g} \quad (2.3)$$

2.2.2 Budding indexes

During growth, a budding yeast cell will pass through the different cell cycle phases, namely G1-phase, S-phase and G2/M-phase (ch. 1). The average time a cell spends in each of those phases, determines the fraction of cells within a population that will be in each cell cycle phase. A method to get an estimate about the distribution of cell cycle phases in a growing yeast population, is to count the amount of budded (S-phase

or G2/M-phase) and non-budded cells (G1-phase) within the population [Zettel et al., 2003]. The ratio between budded and total cells is called the budding index. To measure budded and non-budded cells, I grew populations of yeast cells to an exponential stage, before mounting 15 – 30 μL between glass microscopes slides (EpreDia, X5000 Slides 90°, 26x76x1 mm) and cover slides (EpreDia, 24x50 mm No. 1). I then visualised the cells using a bright-field microscope (VWR International, VisiScope BL114) and counted the amount of budded cells within a total of 100 – 150 cells. Each sample was measured twice, once by myself and once by a member of the lab. To ensure the absence of bias while counting the cells, I made sure to conceal which specific yeast strain was being measured by numbering the samples. The final budding index of a population was then determined as the mean between the budding index determined by my counting and the budding index determined by the counting of a lab member.

2.2.3 Cell volume distributions

Even though budding yeast cell volume is regulated through coupling growth and division by dilution of the G1/S-phase inhibitor Whi5 [Schmoller et al., 2015], newborn cells and cells entering S-phase are still subject to a natural variation in their cell volume. Additionally, in a population of growing cells, each individual cell is in a different stage of its cell cycle. Thus, for population of growing cells, this results in a distribution of cell volumes around a mean. Since accurately assessing the mean cell volume of populations is of key interest for this study, I measured the distribution of cell volumes in growing yeast populations using a Coulter counter (Beckman Coulter, Z2 Particle Counter). A Coulter counter uses the system of resistive pulse sensing (RPS): when particles are suspended in a conducting fluid and pass through a narrow constriction, in parallel with an electric current, they produce a change in electric resistance that is proportional to their volume [Coulter, 1953, de Blois and Bean, 1970]. Using this principle, it is possible to count the number of cells in a sample volume and assess the distribution of cell volumes within a cell population.

In order to determine the cell volume distributions and mean cell volumes of budding

yeast cultures, I diluted small volumes of growing liquid cultures (10 μL to 1000 μL , depending on the optical density OD_{600} of the culture) in 10 mL of a conductive medium (Beckman Coulter, ISOTON®II diluent). Before measuring the samples in the Coulter counter, I sonicated them for 5 s (Bandelin electronics, HD2070 & UW2070) to break apart possible cell aggregates that would distort the measured cell volume distributions. To get an accurate estimation of the cell volume distributions and make measurements comparable, I made sure to measure a total of 20000 – 40000 cells per sample culture. For further analyses and calculations, I used the calculated mean cell volume of the measured cell volume distributions.

2.3 Live-cell fluorescence microscopy

Live-cell fluorescence microscopy allows imaging of living cells and following their evolution through the cell cycle on a single cell level. For this work, I used both phase-contrast microscopy [Zernike, 1942a, Zernike, 1942b] and fluorescence microscopy [Stockert and Blazquez-Castro, 2017], simultaneously. Phase-contrast microscopy makes imaging of living unstained cells possible, while parallel fluorescence microscopy allows to observe specific fluorescently tagged proteins or stained components of the cells. For this work, I mainly used the fluorescent protein *mCitrine* ($\lambda_{excitation} = 516 \text{ nm}$, $\lambda_{emission} = 529 \text{ nm}$) [Zacharias et al., 2002] to tag histone proteins and thus measure their amounts in living budding yeast cells. However, those fluorescent tags can impair on the fitness of the cells, and bleach over the time of the experiment. In addition, using light of too strong intensity to image the cells can lead to phototoxicity, ultimately resulting in cell death [Laissue et al., 2017]. In order to avoid such effects, the imaging settings, such as the intensity of the LEDs used for imaging and the time during which the cells are being imaged, need to be carefully thought through and selected.

This chapter will give an overview of the experimental procedure I used for live-cell fluorescence microscopy measurements, as well as explain the analyses I performed to quantify the amount and concentrations of histone proteins, calculate the length of cell cycle phases and determine the synthesis rate of *mCitrine*, when expressed from histone promoters.

2.3.1 Experimental procedure

First, I grew liquid cell cultures (3 mL) at 30 °C in synthetic complete media containing 2% glycerol and 1% ethanol (SCGE) for at least 6 h in a shaking incubator at 250 rpm (Infors, Ecotron). Then, I added appropriate β -estradiol concentrations to inducible cells (0 nM and 30 nM for haploids or 50 nM for diploids) and let the cultures grow for at least 24 h to ensure steady-state conditions. During growth, I maintained optical densities $OD_{600} < 1.0$ through appropriate dilutions. For imaging, I used 1 mL of cells ($OD_{600} < 1.0$), that I spun down at 10k g-force for 1 min (Thermo Fisher Scientific, Pico 17), resuspended in 200 μ L SCGE and finally sonicated for 5 s. I then introduced 100 μ L of this cell suspension in a Cellasic microfluidics Y04C (haploids and non-induced diploids) or Y04D (induced diploids) plate. Here, I note that I did not add any β -estradiol in the microfluidic device during the microscopy experiments. This results in a gradual decrease of cell volume of induced cells after the start of the experiment.

I performed the live-cell fluorescence microscopy experiments on a Zeiss LSM 800 microscope (software installed: Zen 2.3, blue edition) with additional epifluorescence setup. The microscopy setting was additionally equipped with a Cellasic microfluidics device (Cellasix, ONIX 2). With this device, the microfluidics plates could be vacuum sealed, and a constant pressure of 13.8 kPa was applied on the chambers containing the media (SCGE). This ensured a constant media flow throughout the experiment. The experiments ran at 30 °C (Zeiss, Heating unit XLS) for 12 h, over-night, with images being taken every 3 min using an automated stage (WSB Piezo Drive Can), a plan-apochromat 40x/1.3 oil immersion objective and an axiocam 506 camera. For phase-contrast images I set the illumination voltage to 4.5 V and the exposure time to 30 ms. For the *mCitrine* images, I used the Colibri 511 LED module at 25% power and set the exposure time to 10 ms. For each condition, I measured at least two independent biological replicates on different days.

For this work, I measured cells with fluorescently tagged *HTB2* and *HTB1*, as well as cells carrying an additional promoter driving *mCitrine* expression. For the experiments performed on cells with tagged *HTB1* and cells carrying an additional promoter, a micro-

scope maintenance service had to be performed between imaging of biological replicates, which resulted in increased illumination intensities. To avoid photo toxicity and bleaching, I had to adjust the imaging parameters for the *mCitrine* channel: images were then taken using the Colibri 511 LED module at 5 % power and an exposure time of 100 ms. Subsection 2.3.4 will explain how the measured intensities between two biological replicates were normalized in order to pool the datasets.

2.3.2 Quantification of histone amounts and concentrations

To correct for inaccuracies of the x-y-stage between time points of the experiment, I first aligned the microscopy movies using a custom Fiji47 script [Schindelin et al., 2012], written by Dr. Kurt Schmoller. Then, I used MATLAB 2017b and previously elaborated and described methods [Doncic et al., 2013, Schmoller et al., 2015, Chandler-Brown et al., 2017] to perform the cell segmentation and quantification of the fluorescent signal as well as the subtraction of background fluorescence and cell-volume-dependent autofluorescence (determined from control strains not expressing a fluorescent protein), and also the determination of time points of cell birth, bud emergence, and cytokinesis. For further analyses, I only included cells born during the experiment.

For the quantification of total histone protein amounts, I used total *mCitrine* fluorescent amount after background- and autofluorescence correction as a proxy for total protein amounts. In order to determine total protein concentrations as the total protein amounts divided by cell volume, I calculated cell volumes based on the phase-contrast images, using MATLAB 2017b. Briefly, after the segmentation, the cell areas are aligned along their major axis. Then, the cells are divided into slices perpendicular to their major axis, each 1 pixel in width. Rotational symmetry of each slice around its middle axis parallel to the cell's major axis is assumed. Finally, to calculate the total cell volume, the volumes of each slice are summed up. This allowed me to analyse protein amounts and protein concentrations as a function of cell volume on a single cell level.

Here, I note that the calculated fluorescence amounts, and therefore histone protein amounts and concentrations, are displayed in arbitrary units (arb. units), as is common

for fluorescence measurements. Since the experimental settings were the same throughout the experiments (exception between and after a microscope maintenance service, details are described in chapter 2.3.4), the results can therefore be compared with each other. However, the calculated absolute protein concentrations can not be compared quantitatively with results from other studies.

2.3.3 Estimation of cell cycle phases

Since histones are only produced during the late G1 and S-phase of cells [Eriksson et al., 2012], the *mCitrine* fluorescence traces measured in this work display the following profile: First, the fluorescent amount stays constant over time, leading to a plateau. Then, when the mother cell starts histone production, the fluorescent amount increases with time until it reaches a second plateau when the cell finishes histone production. I aimed to estimate the duration of the histone production period (H-period; referred to as mCitrine production period for strains in which a histone promoter is driving *mCitrine* expression), and the duration of G1 and G2/M-phase from the *mCitrine* fluorescent intensity traces (Fig. 2.2).

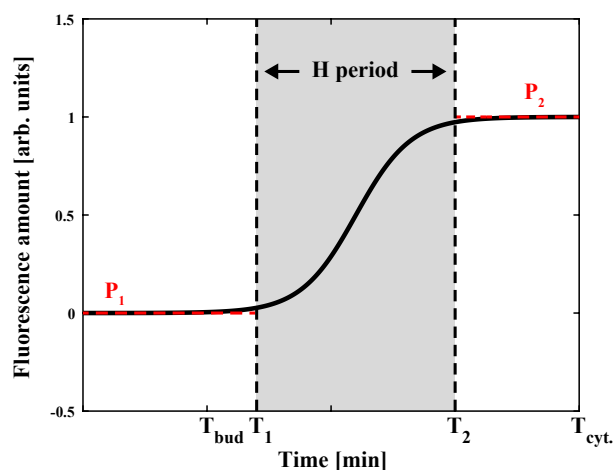


Figure 2.2: **Schematic illustration of the calculation of the histone production phase (H-period) in live-cell fluorescence microscopy.** After fitting P_1 and P_2 , setting a threshold defines T_1 and T_2 . The H-period is then calculated as the difference between those time points.

For each single cell, I first performed a constant linear fit in each of the two plateaus, linked to G1 or G2/M-phase, respectively, and denoted them as P_1 and P_2 . I obtained P_1 by performing the linear fit through the data points of the fluorescence trace from cell birth to first bud emergence, and P_2 by performing the linear fit through the last 30 minutes of the fluorescence trace. Then, I set a threshold of 5%, determined the last time point, T_1 , for which $I_{mCitrine} < P_1 + 0.05 \cdot P_1$, and defined this time point as the beginning of the H-period. Similarly, I defined the first time point, T_2 , for which $I_{mCitrine} > P_2 - 0.05 \cdot P_2$ as the end of the H-period.

Finally, I calculated the duration of the H-period as the difference, $T_2 - T_1$, between those two time points. G1-phase duration was defined as the time from cell birth to first bud emergence, and G2/M duration as the time between the end of the H-period and cytokinesis. I excluded cells for which this approach failed from the analysis of cell cycle phases.

2.3.4 Normalisation of single cell fluorescent intensity traces

As mentioned above (ch. 2.3.1), a microscope maintenance service had to be performed whilst I was still performing microscopy experiments. This maintenance service led to a drastic increase of illumination intensities. For a subset of experiments, on cells with tagged *HTB1* and on cells with an additional promoter driving *mCitrine* expression, this resulted in the following situation: one biological replicate had been imaged with certain imaging parameters whilst the other biological replicate had to be imaged with a different set of imaging parameters in order to avoid phototoxicity.

In order to be able to pool experimental data from those two biological replicates, I normalized the intensities of the single cell traces. Specifically, the single cell traces of the experiments taken before maintenance service were normalized to the intensities of experiments performed after maintenance service. For this purpose, I calculated the mean of P_1 of all single cell traces before and after the maintenance service and defined a normalisation factor, a , as:

$$a = \frac{P_{1,mean}^{After}}{P_{1,mean}^{Before}} \quad (2.4)$$

For each set of experiment, I then multiplied all single cell traces taken before maintenance service with a and pooled those normalized single cell traces with the single cell traces obtained after maintenance service.

2.3.5 Estimation of *mCitrine* synthesis rate

For some experiments, I measured the fluorescent amount of mCitrine, expressed from either a full histone promoter or a truncated histone promoter. To characterise whether the cell-cycle-dependent transcription of *mCitrine* changed when comparing the truncated promoters with the full promoter, I estimated the *mCitrine* synthesis rates from the mCitrine fluorescence traces. For this purpose, I calculated the difference in mCitrine intensity between frame x_{n+1} and frame x_n , for each frame of the single cell traces. This difference corresponds to the mCitrine synthesis as a function of time. To remove measurement noise, I then calculated moving averages over 3 frames for the *mCitrine* synthesis curves. Finally, I calculated the mean of those smoothed single cell curves, all aligned at bud emergence, to show a single mean *mCitrine* synthesis rate curve. In the figures (ch. 3.7, Figs. 3.23 & 3.28), I show this mean curve for the time span during which at least 10 single cell traces were included in the average.

2.4 Reverse-transcription quantitative PCR

Reverse-transcription quantitative PCR (RT-qPCR) allows measuring the relative concentration of mRNA expressed by a specific gene within a cell population. For this, the total RNA of the cells within the investigated cell population must first be extracted. Then, the extracted RNA is reverse transcribed into complementary DNA (cDNA) by reverse-transcription (RT). Lastly, performing a quantitative PCR (qPCR) using a fluorescent dye and mRNA specific primers, allows measuring the relative concentration of mRNA expressed by the genes of interest. This chapter will describe the experimental procedures I used to perform the RT-qPCR experiments during this thesis. Additionally, it will describe how the specificity of the qPCR primers was tested, in order to ensure a

proper quantification of mRNA concentrations.

The basis of the qPCR lies in using a fluorescent dye that only binds to double stranded DNA fragments. With each cycle of the qPCR, the amount of generated DNA fragments doubles, and thus, higher amounts of the dye are bound to DNA. After each cycle, the sample is briefly illuminated with light of a specific wavelength to excite the bound fluorescent dye. The emitted fluorescence is then measured by the PCR cycler. For each gene measured, the PCR cycle at which the fluorescence emitted by the bound dye exceeds a certain pre-defined threshold is referred to as C_P^{Gene} . Measuring a control reference gene, whose amount is known to be stable within the cells, during the same experiment, allows the estimation of the relative concentration of mRNA expressed from the gene of interest by using following equation:

$$\log_2(\text{relative concentration}) = -(C_P^{Gene} - C_P^{Reference}) \quad (2.5)$$

2.4.1 Experimental procedure

RNA extraction

To start, I grew liquid cultures (25 mL) at 30 °C in yeast peptone media containing 2% glucose (YPD) for at least 6 h in a shaking incubator at 250 rpm, before washing and transferring them to SCGE. The cultures then grew for at least 16 h before I added appropriate β -estradiol concentrations to inducible cells (0 nM, 10 nM and 30 nM). To ensure steady-state conditions, the cultures (final volume of 50 mL) then grew for at least 24 h. During culture growth, I maintained $OD_{600} < 1.0$ through appropriate dilutions. Before continuing with the extraction of total RNA, I measured cell volume distributions of the cultures with a Coulter counter after sonication for 5 s.

Then, I spun down the remaining cell cultures at 4000 rpm for 5 min and resuspended the cell pellet in 50 μ L nuclease-free water (Qiagen). For extraction of total RNA, I used a hot acidic phenol (Sigma-Aldrich) and chloroform (Thermo Fisher Scientific) extraction method adapted from an established protocol [Collart and Oliviero, 1993]. The protocol was modified in order to increase the yield of RNA and I precipitated the RNA in 100%

ethanol (Merck Millipore) at -20 °C overnight, followed by a second precipitation in 100% ethanol at -80 °C for 2-4 h. As a quality check for total RNA extraction, I performed agarose gel electrophoresis (1% agarose gel, run 30 min at 100 V) to check for the presence of the 25s, 18s and 5.8s ribosomal RNA bands. Lastly, I measured the concentration and purity of the RNA samples with a spectrophotometer (Thermo Fisher Scientific, NanoDrop 2000) at 260 nm and 280 nm.

RT-qPCR

To generate cDNA from the obtained RNA via reverse-transcription, I transcribed 800 ng total RNA in a PCR cycler (Applied Biosystems, ProFlex PCR system 3x32-well) using random primers and a high-capacity cDNA reverse transcription kit following the included protocol (Thermo Fisher Scientific).

The qPCR measurements were then carried out on a LightCycler 480 Multiwell Plate 96 (Roche) using a DNA-binding fluorescent dye (BioRad, SsoAdvanced Universal SYBR Green Supermix) and mRNA sequence specific primers (Sigma-Aldrich). For the genes *mCitrine*, *HHO1*, *HTB2* and *mCitrine*, I performed the qPCR using 2 μ L of a 1:10 dilution of the cDNA, for all other genes, I used a 1:100 dilution.

After completion of the qPCR, I analysed the melting curve data to verify primer specificity. I measured each sample in technical duplicates and used the mean value C_P^{Gene} for further analyses if $\sigma_{C_P^{Gene}} < 0.5$. To calculate relative concentrations, I normalized the results of each measured gene, C_P^{Gene} , on the reference gene *RDN18*, encoding for ribosomal RNA, using equation 2.5.

For each condition measured, I performed the RT-qPCR experiments at least three times on different days.

2.4.2 Test for qPCR primer specificity

In order to be sure that the primers used to quantify mRNA concentrations during the qPCR are specific to the genes of interest, a lab member, Daniela Bureik, tested their specificity. In order to do so, she analysed deletion strains, where possible, for their

respective deleted gene to check for unspecific primer binding.

For example, she performed a qPCR measurement with the *HHO1* primers on a *hho1Δ* strain and compared the obtained C_P values with the C_P values obtained in the reference strain MS63-1 (Table C.1). Deletion strains with viable colonies and without dramatic growth defects were obtained for the following genes : *HHO1*, *HTB2*, *HHF1*, *HHF2*, *HHT1* and *HHT2*. RNA was extracted using the same protocol as described above, and she used 1 μ g of total RNA to reverse-transcribe into cDNA, using the above mentioned high capacity cDNA synthesis kit. She performed the qPCR with 2 μ L of a 1:10 dilution of each cDNA sample, and measured the samples in 3 or 6 technical replicates. To verify the primer specificity, she analysed C_P values and melting curve data. Results are shown in Table C.1, a list of all qPCR primers used during this work can be found in Table C.2, and the deletion strains used are listed in Table D.1.

2.5 Flow cytometry

Flow cytometry (FC) allows the analysis of cell populations with a high through-put, by measuring hundreds or thousands of cells in liquid suspension per second [Picot et al., 2012]. For this reason, I decided to perform experiments with this technique in addition to live-cell fluorescence microscopy in order to analyse a wide range of different cell populations in relatively short time. The principle of FC is similar to fluorescence microscopy, in that it allows measuring the fluorescence intensities of tagged proteins or stained compartments of the cells, after exciting them with laser-light of the appropriate wavelength. It does, however, not image the cells but quantifies the emitted fluorescence and other optical properties, such as the side-scattered light (SSC) and the forward-scattered light (FSC) of each measured particle. FSC and SSC can give insight on the volume and morphology of the measured cells [Picot et al., 2012].

Similar to the microscopy experiments, I measured the fluorescent amount of *mCitrine* when expressed from additional promoters, integrated in the genome of the yeast cells. I also performed cell cycle analysis experiments by staining the nuclear DNA of cells and measuring the fluorescent amount of the nuclear stain.

This chapter will give an overview on the experimental procedure I followed for the FC experiments, as well as describe the analyses performed to gather information on total mCitrine fluorescence concentrations in dependence on the mean cell volume of budding yeast cell populations. Additionally, this chapter will also give insights on how I determined the distributions of cell cycle phases in cell populations.

2.5.1 Experimental procedure

Fixation of cells for experiments to determine fluorescent concentrations of mCitrine

First, I grew liquid cultures of budding yeast cells (2 mL – 5 mL) in YPD for at least 6 h in a shaking incubator (30 °C, 250 rpm), then washed and transferred them to SCGE. After that, I let them grown for at least 16 h and added appropriate β -estradiol concentrations to inducible cells (0 nM and 30 nM for haploids or 50 nM for diploids). Those cultures then grew for at least 24 h in a final volume of 3 mL – 5 mL. I made sure to maintain $OD_{600} < 1.3$ during cell growth through appropriate dilutions.

Before fixing the cells, I took 1 mL out of each sample, sonicated them for 5 s, and measured the cell volume distributions of the populations with a Coulter counter. I then took another 900 μ L of each cell culture and fixed the cells by adding 100 μ L of a 37% formaldehyde solution (Sigma-Aldrich) in order to achieve a final formaldehyde concentration of 3.7%. I incubated the cultures at room temperature on a rotator (VWR International, Tube Rotator) for 15 min, then spun them down at 10k g-force for 3 min and subsequently washed and resuspended them in 100mM potassium phosphate (pH 7.5). Depending on the optical density of the cell populations, measured before starting the protocol, I suspended the cells in 100 μ L - 1000 μ L potassium phosphate, using lower volumes for cultures with a low optical density. I then stored the samples on ice until using them for flow cytometry.

Fixation and staining of cells for experiments to determine cell cycle phases

First, I grew liquid cell cultures (5 mL) in YPD for at least 6 h in a shaking incubator (30 °C, 250 rpm), before washing and transferring them to SCGE; where I added appropriate β -estradiol concentrations (10 nM or 30 nM for haploid cells, 50 nM for diploid cells). The cultures then grew for at least 24 h, a time span during which I assured $OD_{600} < 1.3$ through appropriate dilutions. I measured the cell volume distributions of the cultures with a Coulter counter after sonication for 5 s. To fixate the cells and subsequently stain the DNA, I followed an already established protocol [Örd et al., 2019]. Specifically, I pipetted 1 mL of each cell culture into 9 mL of cold 80% ethanol and incubated them at 4 °C on a rotator overnight. I then spun down the cultures at 4000 rpm for 2 min and washed them twice in 50 mM Tris-HCl (pH = 8.0). Then, I first treated the cells with a 1 mg/mL RNase A (Thermo Fisher Scientific) solution for 40 min at 37 °C, and then a 20 mg/mL Proteinase K (Promega) solution for 1 h at 37 °C. Finally, to stain the nuclear DNA, I incubated the cells with a 10x SYBR Green I (Sigma-Aldrich) solution for 1 h at room temperature. Between each treatment, I washed the cells twice with 50 mM Tris-HCl and resuspended them in 50 mM Tris-HCl. After the last treatment, I sonicated the cells for 5 s and stored the samples on ice until using them for flow cytometry.

FC measurements

I performed the FC measurements at the HMGU-Immunoanalytics-Core Facility in Großhadern, kindly introduced to the equipment and the best way to measure my samples by Thomas Hofer.

For the experiments, I used a benchtop flow cytometer with octagon and trigon detector arrays (BD Biosciences, LSR II, software installed: BD FACSDiva 8.0.1). To excite either the fluorescent protein mCitrine or the nuclear stain SYBR Green I, I selected a 488 nm coherent sapphire solid-state laser paired with a 530/30 nm filter set. I set the side-scatter voltage to 220 V for all measurements, and adjusted the voltages for forward-scatter and photomultiplier tubes depending on the type of experiment: measuring only haploid or diploid cells, or both. However, I used identical settings for replicate experiments. Af-

ter removing obvious outliers or potential doublets through standard gating strategies, I measured at least 10.000 cells in the final stopping gate. For experiments during which I measured yeast strains expressing *mCitrine*, I also measured cells not expressing *mCitrine* in order to determine the cell-volume-dependent autofluorescence background. I performed those experiments at least three times on different days. I performed experiments during which I measured cells with stained nuclear DNA twice on different days.

2.5.2 Calculation of fluorescent concentrations

In order to calculate the concentration of mCitrine fluorescence in the cell populations, I determined the mean cell volumes from the cell volume distributions measured with the Coulter counter. I subtracted the volume-dependent autofluorescence background from the mean fluorescent amount of each sample measured and quantified with FC. Then, I calculated the mean fluorescence concentration by dividing the mean fluorescent amount of the population by its mean cell volume. This allowed me to analyse mCitrine fluorescence concentrations as a function of cell volume.

2.5.3 Analysis of cell cycle phases

To estimate cell-cycle fractions, I analysed the imaged DNA content frequency histograms. I expected the histograms to show a sharp bimodal distribution with one peak representing the cells with 1N DNA content (G1 cells) and the second peak representing the cells with 2N DNA content (G2/M cells) [Haase and Reed, 2002]. S-phase cells should lead to a plateau between the two peaks. Using Watson modelling [Watson et al., 1987] in FlowJoTM Software, those two peaks and the plateau in between can be fitted and the fraction of cells in each cell cycle quantified.

However, I noticed that for cell populations with large cell volumes (i.e. high β -estradiol concentrations), the DNA content distributions showed pronounced tails at large cell volumes. I speculate that this tail represents an increased mitochondrial DNA content in large cells [Rafelski et al., 2012, Seel et al., 2022]. The fact that this tail is not properly fit by the model suggests that a fraction of G1 cells would be wrongly identified as S-

phase. Thus, I decided to limit the analysis to classifying cells as either G1/S-phase or G2/M-phase.

2.6 Single-molecule fluorescence *in situ* hybridization

Single-molecule *in situ* hybridization (smFISH) allows the detection and quantification of individual mRNA molecules within thin layers of cells using wide-field fluorescence microscopy [Orjalo and Johannsson, 2016]. The principle of the technique is to use fluorescently labeled oligonucleotide probes that can bind to specific sequences of the mRNA [Raj et al., 2008]. Multiple of those probes (up to 48 oligos), targeting different sequences of the mRNA, can bind to one single molecule of mRNA. When exciting those probes with light of the appropriate wavelength, the fluorescence intensity emitted by multiple bound probes is then sufficient to allow the detection and quantification of single mRNA molecules. Additionally, in order to gather supplementary information, for example determine the cell cycle phases of measured cells, the nuclear DNA can be stained with a fluorescent dye. In that case, it is important to make sure there is no strong overlap between excitation and emission spectra of the DNA dye and the fluorophore of the oligonucleotides.

The smFISH experiments were carried out by a lab member, Dimitra Chatzitheodoridou, who established the method in the lab. The analysis of the experimental data was carried out by myself. This chapter will give an overview of the experimental procedure she used to perform the smFISH experiments. Additionally, this chapter will also describe the analyses I performed to quantify mRNA spots in budding yeast cells and how I classified cells into different cell cycle stages.

2.6.1 Experimental procedure

We used commercially available Stellaris® FISH probes and designed a custom probe set for the coding sequence of *mCitrine* using the Stellaris® FISH Probe Designer (Biosearch

Technologies, available online at www.biosearchtech.com/stellarisdesigner). The probe set consisted of 27 probes, each 18 nucleotides long and labeled with the fluorophore Quasar®-670 (Biosearch Technologies).

The smFISH experiments were carried out according to the Stellaris® RNA FISH Protocol for *Saccharomyces cerevisiae*, available online at www.biosearchtech.com/stellarisprotocols. To start, Dimitra Chatzitheodoridou grew liquid cell cultures (5 mL) in YPD for at least 6 h in a shaking incubator (30 °C, 250 rpm) before washing them and transferring them to SCGE. She then grew those cultures overnight to let them reach $OD_{600} \approx 0.25 - 0.4$ and fixed them the next morning. Fixation was achieved by adding 5 mL of 37% formaldehyde to 45 mL of cell culture (final concentration 3.7%) and incubating at room temperature for 45 minutes. Then, she washed the cells twice with ice-cold fixation buffer (1.2 M sorbitol (Sigma-Aldrich), 0.1 M K₂HPO₄ (Sigma-Aldrich), pH 7.5), and digested them at 30 °C in 1 mL of a fixation buffer containing 6.25 µg zymolyase (Biomol). She monitored the progression of cell digestion visually by using bright-field microscopy and continued the digestion until most of the cells appeared dark, which was mostly the case after 55 min of incubation. She then washed the digested cells with ice-cold fixation buffer and stored them at 4°C in 70% EtOH overnight.

For the hybridization process, she centrifuged 300 µL of digested cells and resuspended them in 100 µL hybridization buffer (Stellaris® RNA FISH Hybridization Buffer (Biosearch Technologies) with 10% v/v formamide (VWR International)) with a final Stellaris® FISH probe concentration of 125 nM and hybridized them overnight at 30 °C. Afterwards, she washed the cells with wash buffer A (Stellaris® RNA FISH 1X wash buffer A (Biosearch Technologies) with 10% v/v formamide), then incubated them in 1 mL of a DAPI solution (5 ng/mL DAPI in wash buffer A) at 30 °C for 30 min to stain the nuclear DNA and finally washed them with Stellaris® RNA FISH wash buffer B.

For image acquisition, she mounted the cell samples between glass microscope slides (Thermo Fisher Scientific, Superfrost plus, 25x75x1 mm) and cover slides (VWR International, 18x18 mm No. 1) using Vectashield® Mounting Medium (Vector Laboratories) and allowed them to settle overnight. The image acquisition was carried out on a Zeiss

LSM 800 microscope with additional epifluorescence setup using a 63x/1.4 oil immersion objective and an axiocam 506 camera. To cover the entire depth of cells, she measured stacks composed of 20 z-slices with a 0.24 μm step size. For each condition, she took multiple images per experiment and measured at least two independent biological replicates on different days.

Before the above mentioned microscope maintenance service, she took images to quantify *mCitrine* mRNAs using the Colibri 630 LED module at 55% power and set an exposure time of 5 s. For DAPI images, she used the Colibri 385 LED module at 30% power and set an exposure time of 130 ms. After the microscope maintenance, she changed the *mCitrine* settings to 30% power and an exposure time of 5 s to roughly match the intensities in the images taken before. For DAPI images, she changed the settings to 20% power and an exposure time of 80 ms. For the bright-field images, she set the illumination voltage to 3 V and the exposure time to 100 ms, which remained unaffected by the microscope maintenance service.

2.6.2 Quantification of mRNA spots

To analyse the smFISH images and quantify single mRNA spots, I used FISH-quant v3 [Mueller et al., 2013]. Briefly, with the help of the measured bright-field and DAPI images, I first manually segmented the cells in the FISH-quant interface by tracing their outlines and the outlines of the nuclei. In order to calculate cell volumes from those traced cell outlines, I then used the same method as described above (ch. 2.3.2): I aligned the cells along their major axis, dividing them into slices perpendicular to their major axis, each 1 pixel in width, and then assumed rotational symmetry of each of those slices around their middle axis parallel to the cell's major axis. I then obtained the total cell volume by summing up the volumes of each slice.

In order to then quantify single mRNA spots in the imaged cells, I used the batch processing tool of FISH-quant. First, I defined the ideal image filtering settings, resulting in images with little background and bright, localized spots, for each experiment by applying a Laplacian of Gaussian filter on one example image of each experimental condition. I

confirmed the quality of the filtered image by visual inspection. Second, I performed a pre-detection of mRNA spots in this filtered example image to define the best intensity thresholds to use for the spot detection in the batch processing. I aimed to use example images containing at least one S-phase cell (with high number of mRNA spots). Finally, I analysed all images belonging to the same experimental condition via the FISH-quant batch processing.

The mRNA spots were detected and then fit with a 3D Gaussian on the raw, unfiltered images, allowing me to set different maximum thresholds for the spot sizes in xy and z , as well as a minimum threshold for the amplitude and intensity of the detected spots in order to differentiate background spots from real mRNA spots. Using this approach, I was able to exclude most spots detected in a wild-type strain carrying no *mCitrine* allele, and I thus neglected the contribution of background in the mRNA *mCitrine* concentration for further analyses.

I estimated the total *mCitrine* mRNA concentration as the total number of mRNA spots detected with FISH-quant in the whole cell, including the bud, divided by the total cell volume, including the bud.

2.6.3 Classification of cell cycle phases

Lastly, to classify cells in G1-, S-, or G2/M-phase, I used the cell and nucleus segmentations performed with the help of the bright-field and DAPI images. I classified cells with nuclear signal but no bud as G1-phase cells, and cells with a nuclear signal and a bud without nuclear signal as S-phase cells. However, if the ratio of bud area divided by mother area was greater than 0.3, I classified those cells as G2/M-phase cells instead. I ensured that cells with nuclear signal and a bud that also had nuclear signal were still in G2/M-phase (rather than two separate G1 cells) by inspecting the bright-field and DAPI images.

Chapter 3

Results

This chapter will focus on the experimental results I obtained during this thesis and their interpretations. First, it will explain why and how I used a system of inducible-Whi5 to tune the cell volume of budding yeast cells for the scope of this work, as well as demonstrate that the growth behaviour of yeast cells is only weakly influenced by using this system (ch. 3.1). Second, this chapter will show that concentrations of histone proteins and mRNAs are decreasing with increasing cell volume and increasing with gene copy number (chs. 3.2 & 3.3), and that this regulation is achieved by the histone promoters alone (ch. 3.4). Then, it will describe a mathematical model developed in order to explain the behaviour of histone concentrations with cell volume and ploidy (ch. 3.5). This model correctly predicts the behaviour of histone promoters and most other promoters: depending on the parameters chosen to describe the promoter, the model shows a decrease of transcript concentrations with cell volume, or constant transcript concentrations over cell volume. The main prediction of this model is that the behaviour of a histone promoter can be changed towards the behaviour of most other promoters, solely by tuning its binding affinity to the transcriptional machinery. Thus, this chapter will also show how I tested and confirmed this theoretical prediction experimentally (chs. 3.6 & 3.7). Finally, this chapter will highlight the remaining limitations of the model and its interpretation. Transcriptional degradation and feedback mechanisms might have to be taken into account for the full understanding of histone regulation with cell volume and genome content (ch. 3.8), something that is not yet incorporated into the model.

3.1 Characterisation of inducible-Whi5 strains

3.1.1 Inducible-Whi5 strains allow tuning of cell volume

The base of this study, investigating and quantitatively assessing the behaviour of histone concentrations in relation to cell volume, is the ability to measure a wide range of budding yeast cell volumes. For single cell measurements it allows for the increase of the observable cell volume range. For bulk measurements it is even more essential, since increasing the range of budding yeast cells allows the creation of yeast populations with different mean cell volumes. This makes it possible to measure properties of bulk populations as a function of the mean cell volumes of the populations. As discussed in chapter 1, experimental methods commonly used to change the size of yeast cells include cell cycle block-and-release methods [Futcher, 1999], or the use of strains bearing mutations that result in smaller or larger than normal yeast cells [Jorgensen et al., 2002, Zhang et al., 2002]. However, using such methods means heavily interfering into the cell cycle and growth dynamics of yeast cells, potentially resulting in artefacts. Moreover, most of the mutants resulting in high changes in cell volume usually display very slow growth rates compared to wild-type strains. For this reason, I decided to use a different method to increase the range of observable yeast cell volumes during my experiments.

WHI5 is a known budding yeast cell cycle regulator [Jorgensen et al., 2002] and over-expression leads to an increase of cell volumes [Schmoller et al., 2015]. Hence, for my experiments, I used a β -estradiol-inducible-Whi5 system (ch. 1.2.3, Fig. 1.2). Briefly, this system employs a β -estradiol-dependent transcription factor and an inducible promoter that drives the expression of *WHI5*. This promoter construct is introduced into the genome of the yeast cells, and addition of β -estradiol leads to increased *WHI5* expression which should result in bigger cells. Indeed, Fig. 3.1a shows that the addition of β -estradiol to the media of growing cells leads to an increase of cell volume. Concretely, the mean cell volumes of steady-state exponentially growing populations of haploid and diploid cells, measured in bulk cell populations (ch. 2.2.3) and in single cells (ch. 2.3.1), increased by up to three-fold upon addition of β -estradiol. This result affirms the choice of using

strains with this inducible-Whi5 system during this study in order to be able to measure a wide range of yeast cell volumes.

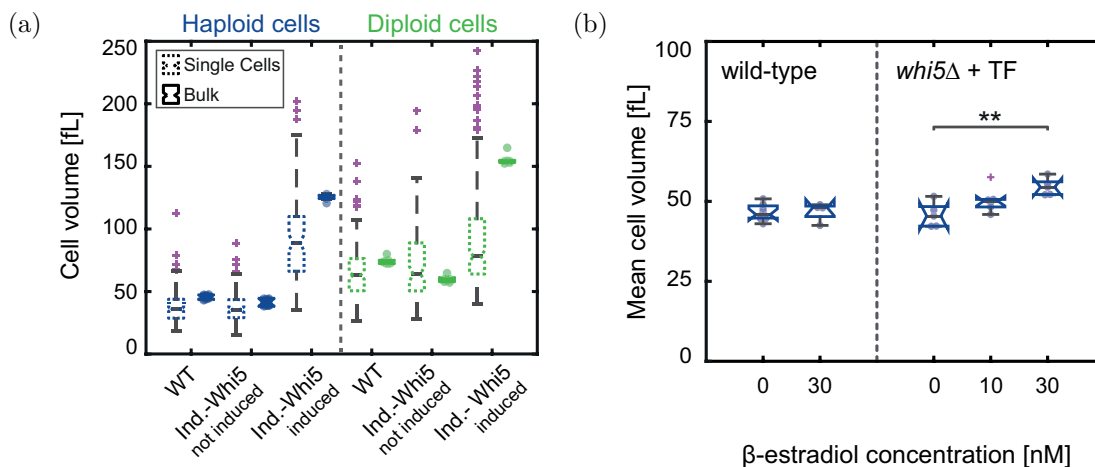


Figure 3.1: **Distribution of cell volumes for non-inducible-Whi5 and inducible-Whi5 strains.** (a) Distribution of cell volumes for non-inducible-Whi5 (WT) and inducible-Whi5 haploids (blue) and diploids (green) measured in *HTB2-mCitrine* single cells with live-cell fluorescence microscopy, or mean cell volumes in exponentially growing bulk populations of cells with untagged *HTB2* measured with a Coulter counter. Black, horizontal lines indicate the median between single cells for single cell measurements ($n_{haploid}^{WT} = 185, n_{haploid}^{not\ ind.} = 120, n_{haploid}^{ind.} = 108, n_{diploid}^{WT} = 170, n_{diploid}^{not\ ind.} = 99, n_{diploid}^{ind.} = 243$) or the median of population means across $n = 7$ biological replicates for bulk measurements. Haploid cells were induced with 30 nM β -estradiol, diploid cells with 50 nM. (b) Distribution of mean cell volumes in exponentially growing bulk cell populations measured with a Coulter counter are shown as a function of β -estradiol concentrations for non-inducible-Whi5 (WT) haploid cells and *whi5Δ* haploid cells with an additional β -estradiol-dependent transcription factor (TF). Black, horizontal lines indicate the median of population means, which are shown as blue circles. Significance was tested using a two-tailed, two-sample t-test at a confidence level $\alpha = 0.05$, $**p < 0.01$.

In all box-plots the coloured boxes highlight the 25- and 75-percentiles, whiskers extend to $\pm 2.7\sigma$ of the distributions and coloured crosses highlight outliers. Notches indicate the 95% confidence interval of the median.

However, the increase in cell volume could solely be due to the addition of β -estradiol to the yeast cultures. Explicitly, adding β -estradiol to wild-type cells, not carrying the inducible-Whi5 system, may also lead to an increase in cell volume. To ensure that the addition of β -estradiol has no such effect, I investigated the mean cell volumes of exponentially growing cell populations of a non-inducible-Whi5 wild-type haploid strain and of a haploid *whi5* Δ strain, containing the artificial β -estradiol-dependent transcription factor (ch. 1.2.3), but no copies of inducible *WHI5*. All yeast cultures were grown with and without β -estradiol addition and I compared the mean cell volumes after at least 24 h of growth in the specific hormone concentration. I could not identify any significant deviation in population means between cell populations with and without the addition of β -estradiol for the non-inducible-Whi5 wild-type haploid strain (Fig. 3.1b). For the haploid *whi5* Δ strain, additionally containing the artificial β -estradiol-dependent transcription factor, I observed no significant increase in mean cell volume when grown in 10nM β -estradiol, and a significant but only small increase in mean cell volumes when grown in 30 nM β -estradiol.

In summary, those results show that for yeast strains carrying the inducible-Whi5 system, the drastic increase in mean cell volume upon addition of β -estradiol (Fig. 1.2) is not a side-effect of β -estradiol addition by itself.

3.1.2 Inducible-Whi5 system does not impair on cell growth

Before basing my experiments on the use of this inducible-Whi5 promoter system, however, I wanted to check whether using this system in yeast strains does not drastically affect cell growth, i.e. doubling times and cell cycle distributions.

Fig. 3.2a shows the doubling times calculated from growth curves (ch. 2.2.1) of exponentially growing yeast cultures of haploid and diploid cells. For inducible-Whi5 haploids, induced and non-induced cells exhibited slower growth when compared to non-inducible-Whi5 wild-type cells. This coincides with a decrease in the budding index (ch. 2.2.2) calculated for similar cell populations (Fig. 3.2b): for populations of induced haploid cells, a smaller fraction of cells was in the process of budding, indicating a smaller frac-

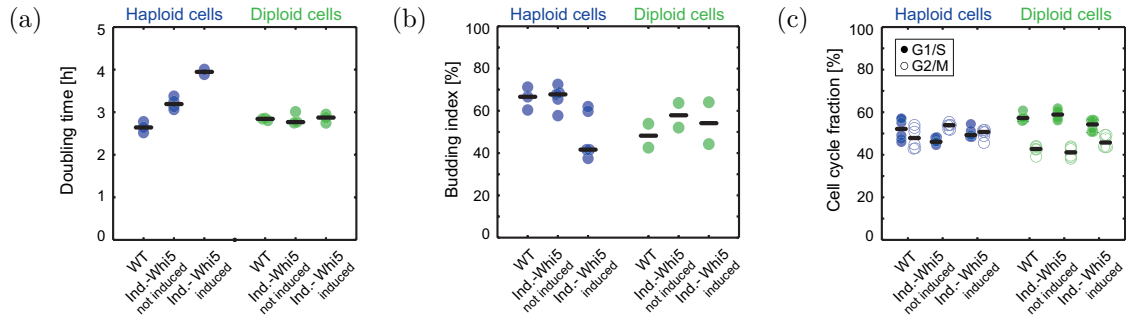


Figure 3.2: **Control experiments on inducible-Whi5 strains.** In all panels, haploid cells (blue circles) were induced with 30 nM β -estradiol and diploid cells (green circles) with 50 nM. Black, horizontal lines indicate the median of the distributions. (a) Doubling times calculated from growth curves of exponentially growing cell populations for inducible-Whi5 and non-inducible-Whi5 (WT) haploids and diploids. (b) Budding index (percentage of budded cells), calculated by counting of budded and non-budded cells in exponentially growing cell populations using an optical microscope, for inducible-Whi5 and non-inducible-Whi5 (WT) haploids and diploids. (c) Cell cycle distributions (percentage of cells in G1/S-phases (filled circles), or in G2/M-phases (open circles)) of inducible-Whi5 and non-inducible-Whi5 (WT) haploid and diploid cells, calculated from population distributions obtained through SYBR Green I staining of the DNA and flow cytometry.

tion of cells in S or G2/M-phase and thus a bigger fraction of cells in G1-phase. I did not find a similar result for diploid cells, where both the doubling time and the budding index remained the same for wild-type, induced and non-induced cells. One possible explanation could be that too high a concentration of β -estradiol in the growth medium might have possible toxic effects on inducible-Whi5 cells, and that these effects only start to become problematic for haploid cells. However, it could also be that the relative volume increase itself, which is larger for haploid cells than for diploid cells (Fig. 3.1a), has a negative effect on growth. As a compromise between not affecting cell growth too much and still inducing cells to a larger cell volume, I decided to not use a higher concentration than 30 nM on haploid cells and than 50 nM on diploid cells. Additionally, I performed most of the experiments in both haploid and diploid cells so that I could compare results.

Lastly, I wanted to gain further insights into the distributions of cell cycle fractions in

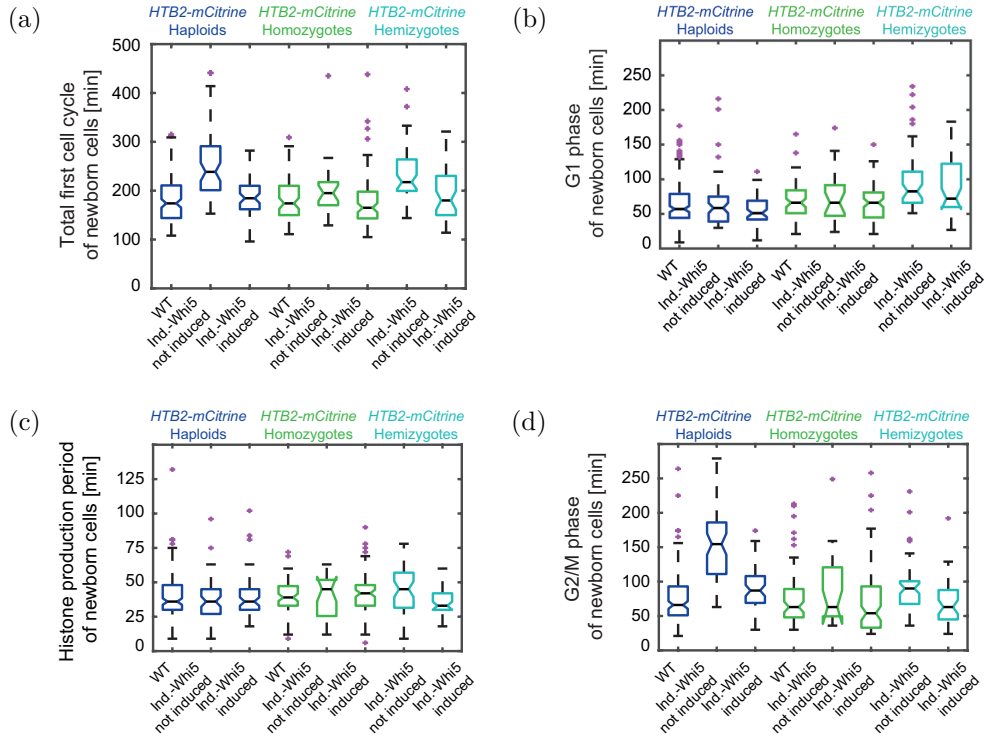


Figure 3.3: **Cell cycle phases of newborn cells in microscopy experiments.** (a) Total first cell cycles of new-born cells as well as individual (b) G1-phases, (c) histone production periods and (d) G2/M-phases of new-born cells for inducible-*Whi5* and non-inducible-*Whi5* (WT) *HTB2-mCitrine* haploids (blue), *HTB2-mCitrine* homozygous diploids (green) and *HTB2-mCitrine/htb2Δ* hemizygous diploids calculated from single cell fluorescent traces, measured with live cell fluorescence microscopy. G1-phases are defined as the time from birth to the first budding, histone production phases as the time between the first point of increase in fluorescent signal and the last point of increase, G2/M-phases as the time from end of histone production phase to the separation of the cell from its bud. Black, horizontal lines indicate the median between single cells, with notches indicating the 95% confidence interval ($n_{haploid}^{WT} = 145, n_{haploid}^{not\ ind.} = 58, n_{haploid}^{ind.} = 58, n_{homozy}^{WT} = 71, n_{homozy}^{not\ ind.} = 21, n_{homozy}^{ind.} = 85, n_{hemiz}^{not\ ind.} = 48, n_{hemiz}^{ind.} = 43$). Coloured boxes highlight the 25- and 75-percentiles, whiskers extend to $\pm 2.7\sigma$ of the distribution and coloured crosses highlight outliers.

populations of growing cells, investigate the duration of those cell cycle phases, and determine whether the addition of β -estradiol has any effect on them. First, I quantified the cell cycle fractions with flow cytometry by staining the nuclear DNA of cells (ch. 2.5.3).

I find that the total amount of yeast cells in G1/S- or G2/M-phase in populations of haploid or diploid cells remained unchanged when comparing wild-type and inducible-Whi5 cells (Fig. 3.2c). To calculate the duration of cell cycle phases, I fluorescently tagged *HTB2* with *mCitrine* and used live-cell fluorescence microscopy to measure the fluorescence amounts of *HTB2-mCitrine* over time. Since histones are only expressed during S-phase [Eriksson et al., 2012], this allowed me to calculate the duration of the different cell cycle phases (ch. 2.3.3). The length of cell cycle phases in newborn single cells calculated for haploid and diploid cells remained mostly unaltered upon induction with β -estradiol and in comparison to non-inducible-Whi5 wild-type cells (Fig. 3.3).

In summary, those results show that using this inducible-Whi5 system, I am able to significantly increase the range of observable cell volumes in yeast cells (Fig. 1.2), without drastically affecting growth (Fig. 3.2a), budding indices (figure 3.2b), cell cycle distributions (Fig. 3.2c) and lengths (Fig. 3.3). Thus, I decided to use this system for my experiments, in order to quantitatively investigate the behaviour of histones with cell volume.

3.2 Histone protein concentrations depend on cell volume & gene copy number

3.2.1 Histone protein amounts stay constant over cell volume and increase with ploidy

As established in chapter 1, the production of most proteins within a cell is coupled to cell volume, leading to an increase in amounts with increasing cell volume [Zhurinsky et al., 2010, Marguerat and Bähler, 2012, Padovan-Merhar et al., 2015, Sun et al., 2020, Williamson and Scopes, 1961, Crissman and Steinkamp, 1973, Wu and Pollard, 2005]. Generally, this coupling of protein production to cell volume makes sense, since cells need to maintain constant protein concentrations with increasing cell volume in order to maintain cellular fitness. For histones, the building blocks of nucleosomes [Cox et al.,

2005], however, this regulation might not be the ideal scenario, since they are likely needed in a constant ratio to the genomic DNA content of the cell. Thus, in contrast to most proteins, histone amounts might be regulated with genomic DNA content, rather than with cell volume.

To verify whether this is the case, I decided to measure the amounts of two histone proteins as a function of cell volume using live-cell fluorescence microscopy. I chose Htb1 and Htb2, the two H2B proteins in budding yeast, since *HTB1* and *HTB2* can be fluorescently tagged without drastic effects on cell growth and overall fitness. Thus, I endogenously tagged either of those genes with the fluorescent protein *mCitrine*, both in haploid and in diploid cells, and measured their fluorescence intensities in living cells with a microfluidics-based approach (ch. 2.3, Fig. 3.4a). This allowed me to track the fluorescent amounts of Htb1-mCitrine and Htb2-mCitrine over time on a single-cell level. Fig. 3.4b shows the development of the fluorescent amount of Htb2-mCitrine over time in single cells of a non-inducible-Whi5 yeast strain. As expected since histone production is limited to S-phase [Eriksson et al., 2012], the fluorescent amount, a metric for the histone amounts within the cell, stays constant over time in G1-phase and starts increasing when cells enter S-phase. The amount doubles over the duration of S-phase and reaches a second plateau just before cytokinesis, when the daughter cell detaches from the mother cell.

I decided to quantify the histone amounts of daughter cells born during the experiment, at cell birth just after cytokinesis, and put them in relation with their cell volume at birth, which was determined from the phase-contrast images taken together with the fluorescence images (ch. 2.3.2). Fig. 3.4c & 3.4d show the amounts of Htb2-mCitrine and Htb1-mCitrine, respectively, as a function of cell volume at birth, both in haploid and in diploid cells. The histone amounts for both Htb2-mCitrine and Htb1-mCitrine stay largely constant with cell volume. Additionally, the histone amounts in diploid cells, where both alleles of the respective gene were tagged with *mCitrine*, are roughly twice as high compared to haploid cells of similar volume. Those results indicate that the histone amounts might indeed be coupled to DNA content and are largely independent of cell volume.

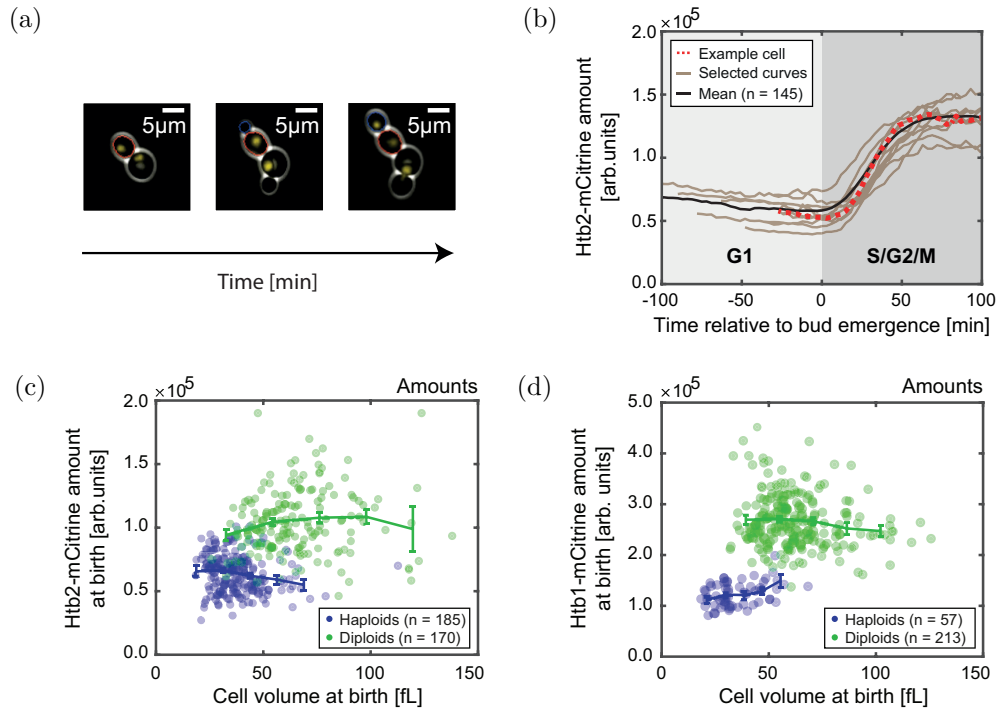


Figure 3.4: **Htb1/2-mCitrine amounts stay constant over cell volume and increase with ploidy.** (a) Example live-cell fluorescence microscopy images of a non-inducible-Whi5 haploid cell with *HTB2* fluorescently tagged with *mCitrine*. For visualisation purposes, the phase-contrast and the fluorescence images are merged together. The red outline depicts the growing mother cell, the blue outline depicts its daughter cell. The Htb2-mCitrine signal (shown in yellow) is only expressed in the nucleus. The phase-contrast images allow the calculation of cell volumes. (b) Fluorescence traces of Htb2-mCitrine over time. Brown lines show selected curves, red dashed line shows the fluorescent amount over time of the mother cell in the example images, and the black line shows the mean of all single cell traces. (c) Htb2-mCitrine and (d) Htb1-mCitrine fluorescence amounts over cell volume at birth for non-inducible-Whi5 haploid (blue) and diploid (green) cells. Bold lines show the connection between binned means, with error bars indicating respective standard errors.

3.2.2 Histone protein concentrations decrease with increasing cell volume and increase with ploidy

In order to increase the range of overlapping cell volumes between haploid and diploid cells even further and more accurately quantify and compare the amounts of histones between them, I included the inducible-Whi5 strains in the experiments. I decided to focus on Htb2 and, again, endogenously tagged all alleles of *HTB2* with *mCitrine* in inducible-Whi5 haploid and diploid cells.

Fig. 3.5a shows the Htb2-mCitrine amounts of newborn inducible-Whi5 and non-inducible-Whi5 cells as a function of their cell volume at birth. Clearly, the range of observable and overlapping cell volumes between haploid and diploid cells is widely increased compared to Fig. 3.4c (also ch. 3.1). Again, I find that the Htb2-mCitrine amounts stay constant as a function of cell volume and are doubling when comparing diploid to haploid cells of similar volume.

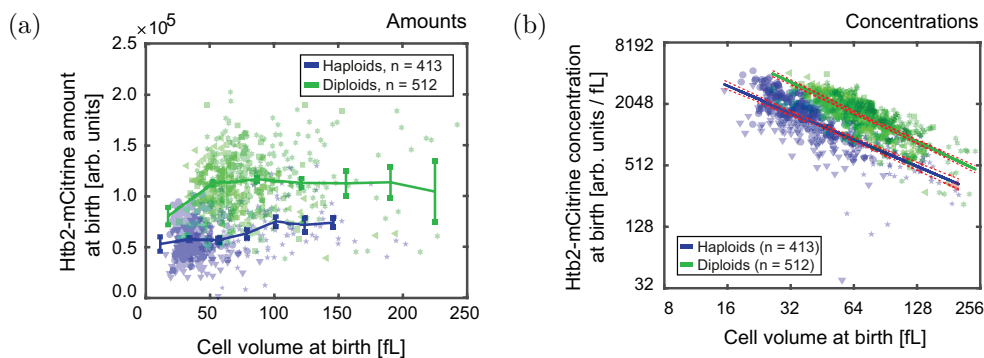


Figure 3.5: **Htb2-mCitrine concentrations decrease with increasing cell volume and increase with ploidy.** (a) Htb2-mCitrine amounts over cell volume at birth for non-inducible-Whi5 and inducible-Whi5 haploid (blue) and diploid (green) cells. Bold lines show the connection between binned means, with error bars indicating respective standard errors. (b) Htb2-mCitrine concentrations over cell volume at birth for non-inducible-Whi5 and inducible-Whi5 haploid (blue) and diploid (green) cells, shown in a double logarithmic plot. Bold lines show the linear fit through the double logarithmic data, with red dashed lines indicating the 95% confidence intervals of the fit.

Volume Dependence Parameter VDP

To better analyse the dependence of histones on cell volume, and also have a way to quantitatively compare this dependence with that of other proteins, I decided to include a quantitative measure. For this purpose, I calculated the concentration of Htb2-mCitrine within each single cell by dividing the Htb2-mCitrine amount with the cell volume at birth. I then plotted the concentration in dependence of the cell volume at birth in a double logarithmic plot, as shown in Fig. 3.5b. Since the Htb2-mCitrine amounts are roughly constant, the concentrations decrease with increasing cell volume. To quantify this decrease, I performed a linear regression on the double logarithmic data and defined the slope of the fit as the Volume Dependence Parameter (VDP):

$$\log_2(c) = \log_2(c_0) + VDP \cdot \log_2(V) \quad (3.1)$$

The VDP now gives us a quantitative measure for the decrease of protein concentrations with cell volume: a negative VDP indicates a decrease of concentration with increasing cell volume. The special case of $VDP = -1$ corresponds to a decrease of concentration with $c \approx 1/V$, and therefore signifies a constant amount of proteins with increasing cell volume. A positive VDP indicates an increase of concentration with increasing cell volume, and $VDP = 0$ corresponds to a constant concentration c_0 .

For Htb2-mCitrine, the observed VDP s of -0.87 ± 0.04 for haploid cells, and -0.97 ± 0.03 for diploid cells, are very close to the value of -1. Thus, those results reinforce the hypothesis that histone production is coupled to the genomic DNA content, and not to the cell volume.

3.2.3 Htb2 protein concentrations depend on *HTB2* gene copy number

Accurate histone homeostasis is crucial for the proper functioning of cells [Amodeo et al., 2015, Joseph et al., 2017, Hauer et al., 2017, Chari et al., 2019], and histone concentrations in budding yeast are known to be tightly regulated at several layers, including

transcription, translation and degradation [Eriksson et al., 2012, Kurat et al., 2014b, Gunjan and Verreault, 2003]. Particularly, as described in chapter 1, the *HTA1-HTB1* gene pair is known to exhibit dosage compensation at the transcript level [Norris and Osley, 1987, Moran et al., 1990, Cross and Smith, 1988]. When deleting *HTB2*, the other gene encoding for the histone H2B, *HTB1*, will compensate with increased expression. However, this compensation only works when deleting *HTB2*, not the other way around [Moran et al., 1990]. Additionally, as another level of regulation in budding yeast cells, excess histones are also known to be degraded [Gunjan and Verreault, 2003]. It would be possible that coupling histone amounts to genomic DNA content is achieved through such feedback mechanisms: Large cells could be producing proportionally too many histones, but then degrade the excess. As an alternative, it would also be possible that cells sense the amounts of histones present in the cell and directly regulate histone transcription depending on those amounts. Such a direct feedback mechanism could ensure that cells produce histones until their amounts match the genome content of the cell.

To investigate whether this type of direct feedback mechanism on transcription, translation or degradation is necessary to couple the production of histones to genomic DNA content, I decided to perform the same live-cell fluorescence microscopy experiments on a *HTB2-mCitrine/htb2Δ* hemizygous diploid and compare the results to the previously measured *HTB2-mCitrine* homozygous diploid (Fig. 3.6a).

To construct a *HTB2-mCitrine* hemizygote, I deleted one of the two *HTB2* alleles in an inducible-Whi5 diploid strain. At the same time, the other *HTB2* allele is tagged with *mCitrine*. In theory, if some type of feedback mechanism were responsible for coupling the amounts of Htb2 to genome content, the remaining *HTB2-mCitrine* allele should compensate for the deleted *HTB2* allele at least to some extent (Fig. 3.6a). However, the *HTB2-mCitrine* concentration in the hemizygote shows a clear decrease compared to the homozygote (Fig. 3.6b). Comparing the *HTB2-mCitrine* concentration of the previously measured haploid and homozygote to the hemizygote at the same cell volume shows that the concentrations for the hemizygote and the haploid are roughly the same, while the concentration in the homozygote is twice as much (Fig. 3.6c). This suggests the absence

of any direct feedback mechanism to couple histone amounts to genomic DNA content.

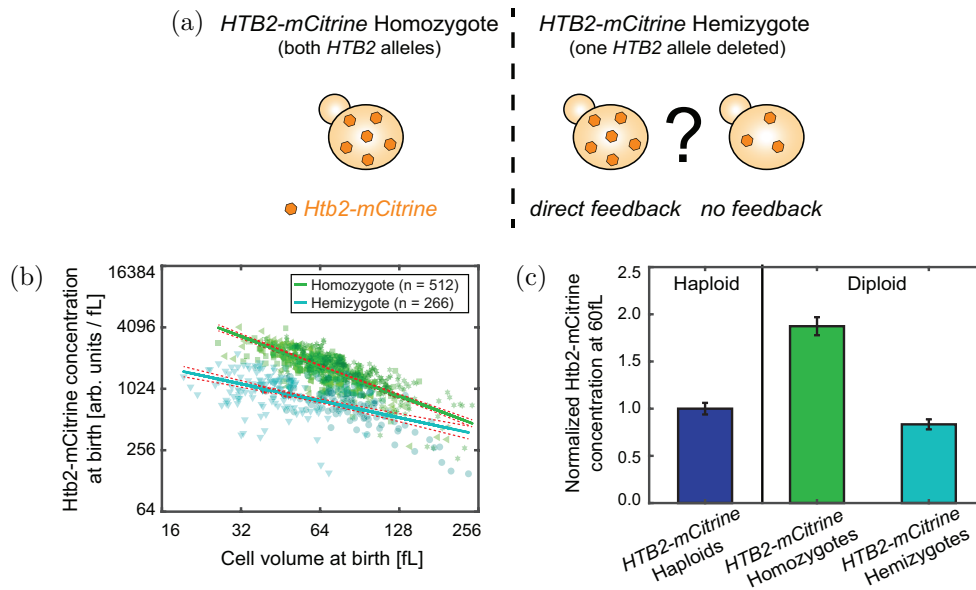


Figure 3.6: **Htb2-mCitrine concentrations depend on *HTB2* gene copy number.**

(a) Illustration of the impact of potential feedback mechanisms on the concentration of Htb2-mCitrine concentration in a *HTB2-mCitrine/htb2Δ* hemizygous diploid compared to a *HTB2-mCitrine* homozygous diploid. (b) Htb2-mCitrine concentrations over cell volume at birth for non-inducible-Whi5 and inducible-Whi5 *HTB2-mCitrine* homozygous diploids (green) and *HTB2-mCitrine/htb2Δ* hemizygous diploids (teal), shown in a double logarithmic plot. Bold lines show the linear fit through the double logarithmic data, with red dashed lines indicating the 95% confidence intervals of the fit. (c) Htb2-mCitrine concentrations at 60 fL, estimated from the linear fit to the double logarithmic dependence of concentration on cell volume, for haploids (blue), *HTB2-mCitrine* homozygous diploids (green), and *HTB2-mCitrine/htb2Δ* hemizygous diploids (teal), normalised on the concentration at 60 fL in haploids. Error bars are derived by error propagation of the 95% confidence interval of the linear fit at 60 fL.

In summary, this section shows that the amounts of the histone proteins Htb1 and Htb2 are not coupled to cell volume, and are increasing with cell ploidy (Figs. 3.4 & 3.5). Additionally, at least for *HTB2*, the results suggests that the Htb2-mCitrine concentration depends on the copy number of the gene, and not overall genome content (Fig. 3.6). Moreover, no direct feedback mechanism seems to be necessary for this regulation. This

suggests that for histone protein production in general, the whole genomic DNA content does not seem to be of importance. Rather, the copy number of the gene encoding for the specific histone protein seems to set the histone protein amounts in the cell, which are independent of cell volume. Since diploid cells generally have two alleles of each gene, this leads to an increase of histone protein amounts with cell ploidy.

3.3 Histone mRNA concentrations depend on cell volume & gene copy number

3.3.1 Histone mRNA concentrations decrease with increasing cell volume

So far, I have shown that histone Htb1 and Htb2 protein amounts roughly stay constant with cell volume (Fig. 3.4), resulting in a decrease of protein concentrations with increasing cell volume (Fig. 3.5). In addition, the Htb2 protein concentrations are coupled to the *HTB2* gene copy number (Fig. 3.6). Since no direct feedback mechanism seems to be necessary for this coupling, the regulation of histone concentrations might already be established at the transcript level. In order to test this hypothesis, I performed reverse-transcription quantitative PCR (RT-qPCR) on growing haploid yeast cell populations, after extracting total RNA (ch. 2.4). This allowed me to determine the mean transcript concentrations of specific genes in the measured cell population. To put those transcript concentrations in relation to the mean cell volume of the cell populations, I also measured cell volume distributions using a Coulter Counter (ch. 2.2.3). To be able to quantitatively assess the behaviour of transcript concentration as a function of cell volume, I needed to measure a wide range of mean cell volumes. Thus, I again worked with non-inducible-Whi5 wild-type strains as well as inducible-Whi5 strains (ch. 1.2.3 and Fig. 3.1). I grew cells without hormone addition and with a concentration of 10 nM and 30 nM β -estradiol. Total RNA was extracted after letting the cells grow on the respective hormone condition for at least 24h.

As a first step, I measured the behaviour of ribosomal RNA *RDN18* concentration relative to total RNA. Fig. 3.7a shows that with a *VPD* of 0.08 ± 0.12 , the *RDN18* concentration clearly stays constant with increasing cell volume. This is consistent with the fact that a large portion of total RNA consists of ribosomal RNA [von der Haar, 2008], and that total RNA concentrations should stay constant with cell volume [Williamson and Scopes, 1961]. Since I found the *RDN18* concentration to be constant, I normalised all other RT-qPCR measurements on *RDN18*.

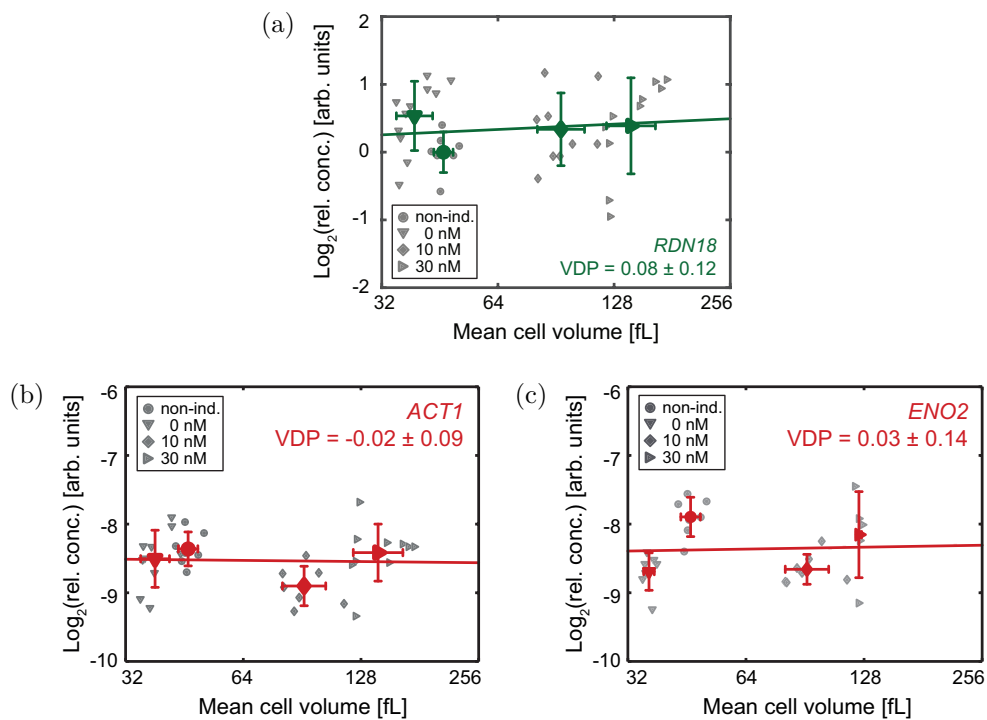


Figure 3.7: **mRNA concentrations of *RDN18* and housekeeping genes stay constant with cell volume.** (a - c) Relative *RDN18* (a), *ACT1* (b) or *ENO2* (c) mRNA concentrations for non-inducible-Whi5 and inducible-Whi5 haploid cells over mean cell volume, shown in a double logarithmic plot. For *RDN18* mRNA concentrations are normalised on the mean mRNA concentration of non-inducible-Whi5 cells (green circle). For *ACT1* and *ENO2* mRNA concentrations are normalised on *RDN18*. Individual data points for the different β -estradiol concentrations are shown in grey. Coloured symbols indicate the mean of the different conditions with error bars indicating the standard deviations. Lines show linear fits to the double logarithmic data, with volume-dependence parameters (*VDPs*) determined as the slope of the fit.

Then, I measured the mRNA concentrations of two housekeeping genes, *ACT1* and *ENO2*. Since global transcription increases with cell volume [Marguerat and Bähler, 2012, Zhurinsky et al., 2010, Padovan-Merhar et al., 2015, Sun et al., 2020], I would expect those genes to be expressed in such a way that their mRNA concentrations stay constant. The calculated *VDPs* for both *ACT1* and *ENO2* are close to and not significantly different from 0 (Figs. 3.7b, 3.7c & 3.8). This means that the mRNA concentrations indeed stay constant as a function of cell volume.

Additionally, I also measured the mRNA concentrations of *RPB1* and *RPB3*, two genes encoding for large subunits of the RNA polymerase II. Interestingly, the *VDPs* calculated for both genes are slightly negative and significantly different from 0 (Fig. 3.8). This indicates a modest decrease of transcript concentrations with increasing cell volume, which is in accordance with findings of other studies [Mena et al., 2017, Lanz et al., 2021].

Finally, I determined the mRNA concentration of all the core histone genes and the H1-like linker histone, and put them in relation to the mean cell volume of the measured yeast populations. As described in chapter 1, each of the core histone genes in budding yeast is expressed from two gene variants [Eriksson et al., 2012], which show high sequence similarity. Thus, a colleague (Daniela Bureik) performed tests on deletion strains, where possible, to ensure the specificity of the histone qPCR primer (ch. 2.4.2, Table C.1 & C.2). That way, we could make sure that we were able to distinguish between the transcripts of the individual gene variants when performing the RT-qPCR measurements.

The *VDPs* calculated for all histone genes are negative and significantly different from 0, and most of them are close to -1 (Fig. 3.8), which is equivalent to a decrease of concentration with $c \approx 1/V$. Interestingly, the *VDP* of *HHT2* is closer to 0 than the *VDPs* of all other histone genes, which is consistent with a similar finding in another recent study [Swaffer et al., 2021a]. This means that all histone transcript concentrations decrease with increasing cell volume, and most of them stay at constant amounts. In contrast, global transcription increases with cell volume and leads to constant concentrations of most mRNAs.

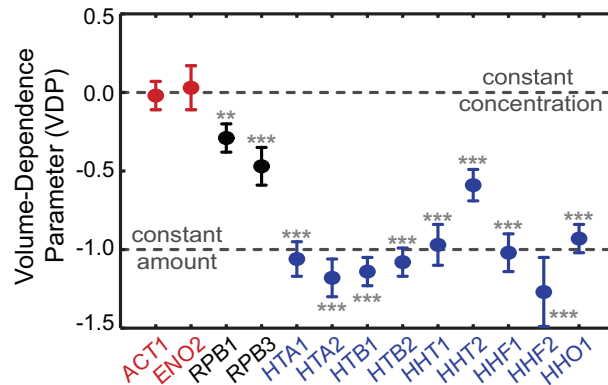


Figure 3.8: **Histone mRNA concentrations decrease with cell volume.** Summary of the VDP s for all measured genes with error bars indicating the standard error. Significance that the VDP is different from 0 was tested using linear regressions; ** $p < 0.01$, *** $p < 0.001$

In addition, I wanted to investigate whether the decrease of histone mRNA concentrations is an artefactual result, induced by the addition of β -estradiol. Therefore, I performed the same RT-qPCR measurements on cell populations of a non-inducible-Whi5 wild-type haploid strain and of a haploid *whi5* Δ strain, containing the artificial β -estradiol-dependent transcription factor, but no copies of inducible *WHI5* (strain referred to as MS62-1).

The control experiments in chapter 3.1 showed no drastic increase of mean cell volume upon addition of β -estradiol in bulk populations of those yeast strains (Fig. 3.1b). For all the genes measured, I could not identify any significant decrease of mRNA concentration as a function of the β -estradiol concentration, both for the wild-type strain (Fig. 3.9a) and the MS62-1 strain (Fig. 3.9b). This confirms that the observed decrease of histone mRNA concentrations is specific to the increase of mean cell volumes of the measured populations, and not a side-effect of β -estradiol addition.

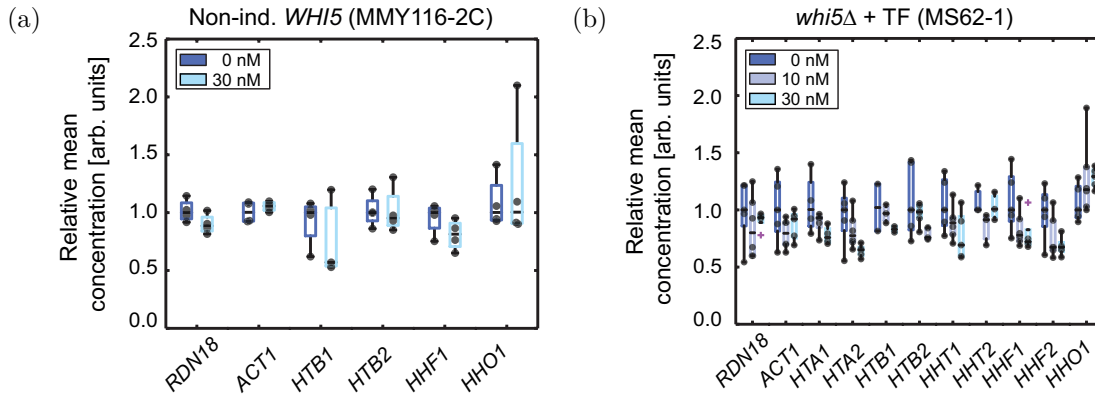


Figure 3.9: **Decrease of histone transcript concentrations is specific to the increase of cell volume.** Relative mean mRNA concentrations (grey circles) of exponentially growing haploid cell populations with and without β -estradiol addition. (a) Non-inducible-Whi5 cells, and (b) *whi5* Δ cells with artificial β -estradiol-dependent transcription factor. For each gene, values are normalised on the mean mRNA concentration of the cell populations without β -estradiol addition (0 nM). Black horizontal lines indicate the median of the distribution, grey circles indicate biological replicates. Grey boxes highlight the 25- and 75-percentiles, whiskers extend to $\pm 2.7\sigma$ of the distribution, magenta crosses highlight outliers.

3.3.2 *HTB2* mRNA concentrations depend on *HTB2* gene copy number

When comparing the dependence of histone transcript concentrations (Fig. 3.8) and histone protein concentrations on cell volume (Fig. 3.5b), it becomes clear that they behave very similarly. Thus, it might be the case that the coupling of histone protein concentrations to gene copy number (Fig. 3.6c) is already established at the mRNA level, and that histone mRNA concentrations themselves are also dependent on gene copy number. To test whether this is the case, I performed RT-qPCR measurements on bulk populations of inducible-Whi5 diploid strains, which were either homozygous or hemizygous for *HTB2*.

First, I measured the dependence of selected histone transcript concentrations as a function of the mean cell volume of the population and calculated the *VDPs*. Similar to the

VDPs in haploid cells (Fig. 3.8), I find that the *VDPs* for all histone genes investigated are close to -1 , and I could not find any significant deviation between the respective *VDPs* of the homozygote and the hemizygote (Fig. 3.10a).

Then, I compared the *HTB2* transcript concentration at a characteristic cell volume between the homozygote and the hemizygote. Similar to the findings for Htb2 protein concentrations (Fig. 3.6c), the *HTB2* transcript concentration in the hemizygote is greatly reduced compared to the homozygote. Since *HTB1* is known to compensate for missing *HTB2* alleles [Moran et al., 1990], I expected to see an overexpression of *HTB1* transcript concentrations in the hemizygote. However, I do not observe such an overexpression (Fig. 3.10b).

As a control, I performed similar experiments in haploid cells, and compared the *HTB1* transcript concentrations between a wild-type strain and a *htb2* Δ strain. There, as expected, I see a roughly 50% overexpression of *HTB1* in the *htb2* Δ cells (Fig. 3.10c). Interestingly, I also find a 50% overexpression of *HTA1* (Fig. 3.10c). Since diploid cells have two alleles of each gene, I would expect a 25% overexpression of *HTB1* in the hemizygote, because only one allele of *HTB2* was deleted. Thus, I suspect that I might not be able to resolve this weaker overexpression of *HTB1* in the hemizygous strain.

In summary, I showed that histone mRNA concentrations decrease with increasing cell volume (Fig. 3.8) and that *HTB2* mRNA concentrations depend on the *HTB2* gene copy number (Fig. 3.10). Together with the results obtained for histone proteins (ch. 3.2), this highlights that histone production is not coupled to cell volume but to gene copy numbers instead. This results in an increase of histone protein concentrations with ploidy, but a decrease with cell volume. This regulation is already established at the transcript level, and no direct feedback mechanisms seem to be necessary.

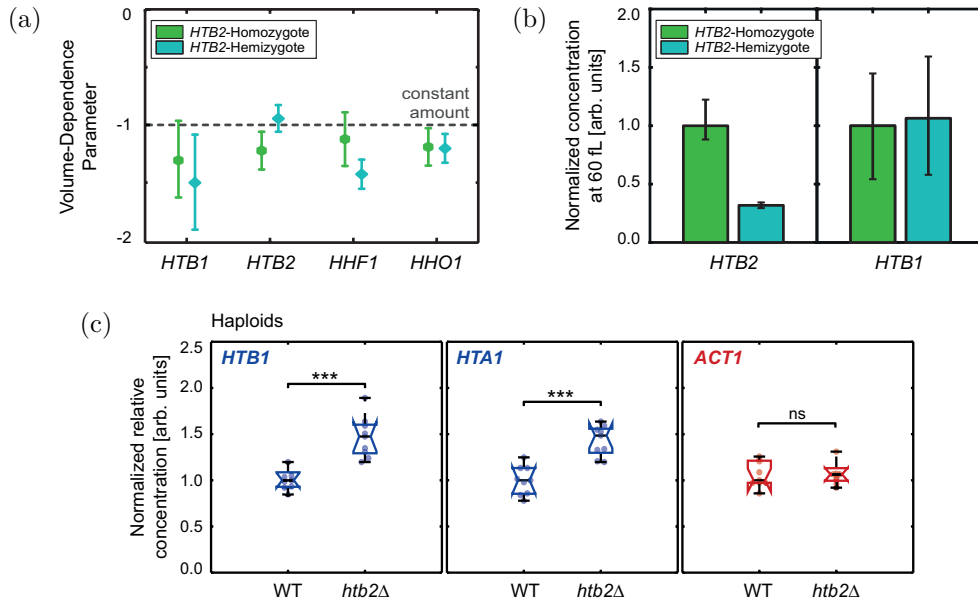


Figure 3.10: ***HTB2* mRNA concentrations increase with gene copy number.** (a) Summary of the *VDPs* for non-inducible-Whi5 and inducible-Whi5 *HTB2* homozygous (green circles) and a *HTB2/htb2Δ* hemizygous (teal diamonds) diploids, determined by RT-qPCR. *VDPs* were determined as the slopes of the linear fits to the double logarithmic dependence of concentration on cell volume (fit through $n^{HTB1, HTB2} = 18$, $n^{HHF1, HHO1} = 12$). Error bars indicate the standard error of the slope. (b) Median mRNA concentrations at 60 fL, estimated from the linear fit to the double logarithmic dependence of concentration on cell volume, for *HTB2* (left) and *HTB1* (right) in *HTB2* homozygous (green) and *HTB2/htb2Δ* hemizygous (teal) cells, normalised on the respective median concentration of the *HTB2* homozygous cells. Error bars indicate the 2.5- and 97.5-percentiles around the median concentration ratio, determined from 10000 bootstrap samples. (c) Relative *HTB1*, *HTA1* and *ACT1* mRNA concentrations (normalised on *RDN18*) for a wild-type haploid strain and a *htb2Δ* in the same background, measured by RT-qPCR. Concentrations are normalised on the respective median concentration in the wild-type. Biological replicates are represented as coloured circles. Black, horizontal lines indicate the median, and notches indicate the 95% confidence interval. Coloured boxes highlight the 25- and 75-percentiles, whiskers extend to $\pm 2.7\sigma$ of the distributions. Significance was tested using a two-tailed, two-sample t-test at a confidence level $\alpha = 0.05$; *** $p < 0.001$.

3.4 Histone promoters regulate histone concentrations with cell volume and gene copy number

3.4.1 Histone promoters determine the dependence of transcripts on cell volume

So far, I have established that histone protein and mRNA concentrations are not coupled to cell volume but to gene copy numbers instead (ch. 3.2 & 3.3). This regulation does not seem to require any type of direct feedback mechanism on transcription, translation or degradation. Thus, the next step was to investigate whether the histone promoters alone are sufficient to establish the specific regulation of histone concentrations with cell volume and gene copy number. For this purpose, I worked with non-inducible-Whi5 and inducible-Whi5 haploid and diploid yeast strains, each having an additional copy of a promoter of interest integrated into their genome (Fig. 3.11).

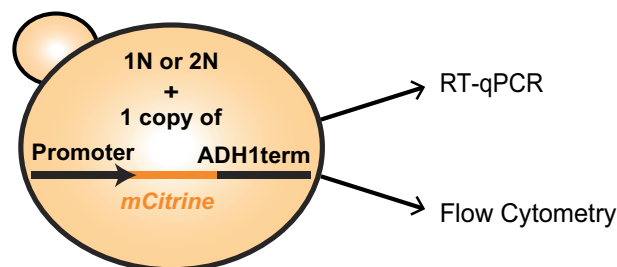


Figure 3.11: **Illustration of the promoter experiments.** Haploid (1N) or diploid (2N) strains carry a single additional copy of a promoter of interest, driving the expression of the fluorescent reporter *mCitrine* regulated by the *ADH1* terminator. The expression of the fluorescent reporter was analysed using RT-qPCR or flow cytometry.

Each gene promoter was defined as the 1000 bp preceding the start codon of the respective gene, where possible. If using the full 1000 bp as the promoter would conflict with the preceding gene, then the promoter was defined as a shorter sequence. Each of those additional promoters drove the expression of the fluorescent protein *mCitrine*, and all promoter constructs were regulated by the same *ADH1* terminator. I focused the experiments on the promoters of the histone genes *HTB1*, *HTB2* and *HHF1*, and included the

ACT1 promoter as a control. To investigate the behaviour of *mCitrine* transcripts driven by those additional promoter copies, I performed RT-qPCR (ch. 2.4) or flow cytometry (ch. 2.5) on bulk cell populations. I then quantified the mean transcript concentrations (RT-qPCR), or the mean expression of the fluorescent protein mCitrine (flow cytometry) and put them in relation with the mean cell volume of the cell populations in order to calculate the *VDPs*.

First, using RT-qPCR, I made sure that this additional promoter construct does not have a drastic influence on the *VDP* of the endogenous histone genes. To do so, I compared the calculated *VDPs* in haploid cells to the ones previously obtained for haploid strains carrying no additional promoter copy (Fig. 3.12 & 3.8).

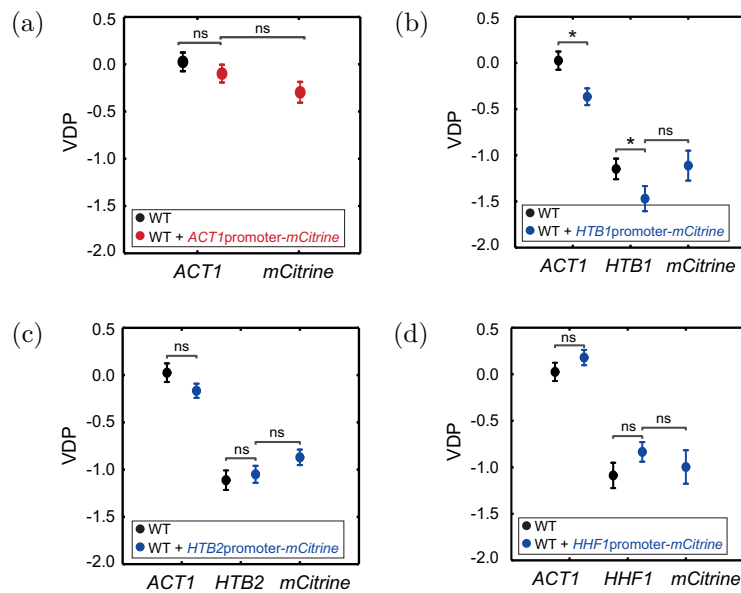


Figure 3.12: **Histone promoters are sufficient for cell volume dependence of transcript concentrations, as shown by RT-qPCR.** (a - d) *VDPs* determined with RT-qPCR for the genes *ACT1*, *mCitrine*, and *HTB1*, *HTB2*, or *HHF1* for non-inducible-Whi5 and inducible-Whi5 haploid strains carrying an additional *ACT1* promoter (a), and strains carrying an additional *HTB1* (b), *HTB2* (c), or *HHF1* (d) promoter in comparison to wild-type strains carrying no additional promoter (black circles). *VDPs* were determined as the slope of the linear fit to the double logarithmic dependence of concentration on cell volume, with error bars indicating the standard error of the *VDPs*. Significant *VDP* deviation between two genes was tested using linear regressions; * $p < 0.05$

For all promoter constructs investigated, except for the *HTB1* promoter, the additional promoter copy does not have a significant influence on the *VDP* of the endogenous gene. For the *HTB1* promoter, the calculated *VDPs* of both *ACT1* and endogenous *HTB1* are consistently slightly more negative than the *VDPs* determined for cells carrying no additional promoter. However, the qualitative difference of transcript regulation with cell volume between the endogenous *ACT1* and the endogenous *HTB1* gene is still observable. In addition, I also find that the regulation of *mCitrine* transcript concentrations with cell volume depends on the promoter which is driving its expression. If *mCitrine* is driven by the *ACT1* promoter, the *VDP* of *mCitrine* is similar to the *VDP* of endogenous *ACT1* (Fig. 3.12a). The same holds true for the histone promoters: When driven by either the *HTB1*, *HTB2*, or *HHF1* promoter, the *VDP* of *mCitrine* is similar to the *VDP* of endogenous *HTB1*, *HTB2*, or *HHF1*, respectively (Figs. 3.12b, 3.12c, & 3.12d). Thus, the histone promoter alone is sufficient to establish the decrease of histone transcript concentrations with increasing cell volume.

3.4.2 Histone promoters determine the dependence of transcripts on gene copy number

As described above, I also performed similar experiments to the RT-qPCR measurements using flow cytometry (Fig. 3.11), which enables a fast experimental read out of the fluorescent amounts of mCitrine. Thus, I was able to measure both haploid and diploid cells carrying those additional promoter constructs relatively fast. First, I quantified the mean mCitrine fluorescence driven by the additional promoter of interest, and calculated the respective *VDPs*. Similar to the RT-qPCR measurements, all *VDPs* determined for the additional histone promoters are significantly negative, both for haploid and diploid cells. In contrast, the *VDPs* determined for *mCitrine* driven by the *ACT1* promoter are closer to 0 (Figs. 3.13 & 3.14a). Thus, this confirms that flow cytometry can be used to qualitatively distinguish the different cell volume dependencies of histone promoters and other promoters.

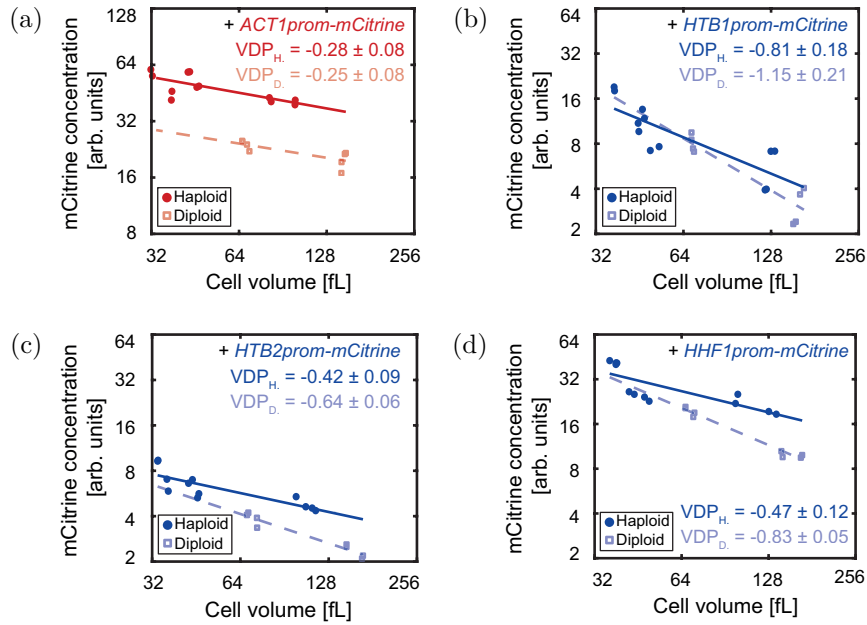


Figure 3.13: **Histone promoters are sufficient for cell volume- and ploidy-dependence of transcript concentrations, as shown by flow cytometry.** (a - d) *mCitrine* concentration, driven by an additional copy of the *mCitrine* (a), *HTB1* (b), *HTB2* (c) or *HHF1* (d) promoter in non-inducible-Whi5 and inducible-Whi5 haploid (filled circles) and diploid (open squares) cells, shown as a function of cell volume in a double logarithmic plot. Lines show linear fits to the double logarithmic data with volume-dependence parameters (*VDPs*) determined as the slope of the fit, with respective standard error.

As established in chapters 3.2 & 3.3, histone protein and mRNA concentration are not just maintained at constant amounts over cell volume, resulting in a decrease of concentration with cell volume. Their amounts, and thus concentrations, also increase with gene copy number, and therefore with cell ploidy. This type of regulation is in contrast with the regulation of most other proteins, which are kept at constant concentrations as a function of cell volume. Moreover, the concentrations most proteins are kept at, are usually independent of ploidy, meaning that haploid and diploid cells of similar volumes have similar concentrations of proteins [Wu et al., 2010].

In order to test whether the histone promoters alone are sufficient to also couple the transcript concentrations to gene copy number, I quantified the mCitrine fluorescence in

haploid and diploid cells of similar volume. Here, I want to remind that both haploids and diploids only carry one additional copy of the additional promoter construct. Thus, for *mCitrine* driven by one additional *ACT1* promoter, the concentration in the diploid should be halved when compared to the concentration in the haploid [Schmoller and Skotheim, 2015]. In a homozygous diploid, with two *ACT1* promoters driving the *mCitrine* expression, this would lead to the same concentration than in a haploid of similar volume. As expected, the calculated concentration of mCitrine driven by the single *ACT1* promoter at a characteristic cell volume is indeed halved when compared to the concentration in haploids carrying one additional *ACT1* promoter (Figs. 3.13a & 3.14b).

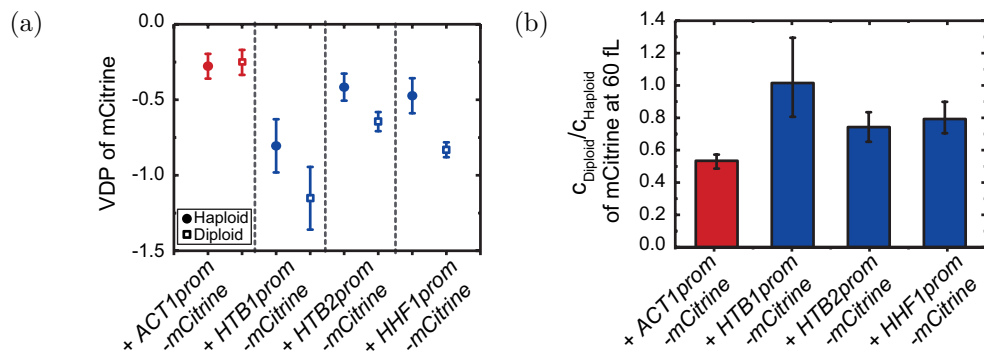


Figure 3.14: **Summarising cell volume- and ploidy-dependence of transcripts driven by histone promoters.** (a) Summary of *VDPs* determined with flow cytometry for different strains in non-inducible-Whi5 and inducible-Whi5 haploid (filled circles) and diploid (open squares) cells. *VDPs* were determined as the slope of the linear fit to the double logarithmic dependence of concentration on cell volume, with error bars indicating the standard error of the *VDPs*. (b) Median concentration of mCitrine, estimated from the linear fit to the double logarithmic dependence of concentration on cell volume, in diploid cells compared to the median concentration in haploid cells at 60 fL. Error bars indicate the 2.5- and 97.5-percentiles around the median concentration ratio, determined from 10000 bootstrap samples.

In contrast, for the histone promoters, I would expect a different behaviour, since the transcript concentrations need to be coupled to gene copy numbers. The concentration in a diploid carrying only one additional promoter driving *mCitrine* expression should

be the same as in a haploid carrying only one additional promoter. For a homozygous diploid, with two histone promoters driving the *mCitrine* expression, this would lead to a doubling in concentration, when compared to a haploid of similar volume. Indeed, the calculated mCitrine concentration at a characteristic cell volume in diploids carrying one additional histone promoter is nearly the same concentration as in haploids for all histone promoters investigated (Figs. 3.13b, 3.13c, 3.13d & 3.14b).

In summary, those results highlight that the histone promoters are sufficient to drive the regulation of histone transcript concentrations with cell volume (Figs. 3.12, 3.13). In addition, they are also sufficient to couple histone transcript concentrations to gene copy numbers, and thus to the ploidy of the cell (Fig. 3.14).

3.5 Model for the dependence of transcription rate on cell volume and ploidy

3.5.1 Introducing the model

The experimental results obtained up to this point strongly suggest that the regulation of histones with cell volume and cell ploidy is different than for most proteins. In fact, most genes are transcribed in proportion to cell volume [Marguerat and Bähler, 2012, Zhurinsky et al., 2010, Padovan-Merhar et al., 2015, Sun et al., 2020] and thus, constant protein concentrations are maintained, which are independent of cell ploidy [Wu et al., 2010]. In contrast, histone promoters express transcripts at a cell volume independent rate, leading to a decrease of transcript concentrations with increasing cell volume (ch. 3.4.1). Moreover, the transcript concentrations are coupled to the copy number of the histone promoter driving their expression (ch. 3.4.2). Generally, this leads to an increase of histone transcripts and proteins with cell ploidy (chs. 3.3 & 3.2).

Since histone promoters are sufficient to drive the decrease of histone concentrations with cell volume and the increase with copy number, I speculate that this regulation is mediated by the synthesis of histone proteins. Thus, I focused on the dependence of

transcription rates on cell volume and ploidy. In order to gain deeper insights into the possible ways the transcription rates of promoters can be coupled to cell volume or cell ploidy, I used mathematical modelling. Together with Prof. Abhyudai Singh from the University of Delaware, we rethought a mathematical model that was previously proposed by Heldt et al. [Heldt et al., 2018]. However, in order to simplify their model, we did not explicitly model the growth rates of cells as a function of time. As has been discussed in the literature for several years [Zhurinsky et al., 2010, Marguerat et al., 2012, Padovan-Merhar et al., 2015, Lin and Amir, 2018, Heldt et al., 2018, Sun et al., 2020], we suppose that transcription is limited by one component of the transcriptional machinery, which we denote as TM . That limiting component could potentially be a subunit of the RNA polymerase.

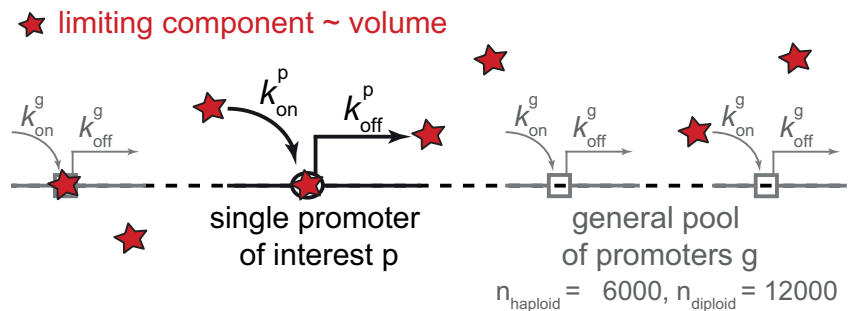


Figure 3.15: **Illustration of the minimal model for the dependence of transcription rate of one specific promoter of interest on cell volume and ploidy.** The model includes two classes of promoters: the general pool of promoters g , and the specific promoter of interest p , with their respective initiation rates k_{on}^g or k_{on}^p , describing the binding of the limiting machinery, and off-rates k_{off}^g or k_{off}^p , summarising all other steps of transcription.

We consider two classes of promoters, a specific promoter of interest, p , present as a single copy, and a general pool of promoters, g , which are present as $n_h \approx 6000$ copies in haploids and $n_d \approx 12000$ in diploids (Fig. 3.15). Each promoter is competing for a finite number of the limiting component of the transcriptional machinery, and is modelled as one single binding site for TM . The number of TM bound to general promoters is denoted as R^g . Whether TM is bound to the single promoter of interest is described by R^p , which can

assume values between 0 (not bound) and 1 (bound). Moreover, R^f denotes the number of free TM .

We assume that the total number of TM (free and bound) scales proportionally to cell volume, V , and is given by

$$R^g + R^p + R^f = c_{TM} \cdot V \quad (3.2)$$

with c_{TM} being the total TM concentration. In other words, the concentration of the limiting component of the transcriptional machinery c_{TM} stays constant with cell volume. Initiation, i.e. binding of the machinery, occurs at a rate k_{on}^p for the promoter of interest, and at a rate k_{on}^g for the general pool of promoters. Furthermore, we assume that all other steps of transcription can be summarised in a single rate-limiting step, occurring at a rate k_{off}^p and k_{off}^g , respectively. In addition, we assume transcript degradation to be the same for all transcripts, and set the corresponding degradation rate $k_{deg} = 1$, i.e., all other rates are normalised with respect to k_{deg} . I want to note that in the case of stable transcripts, k_{deg} describes the dilution of transcripts by cell growth.

Assuming that the arrival of TM at promoters is proportional to the concentration of free TM , the change in number of bound general promoters over time is given by following equation:

$$\frac{dR^g}{dt} = k_{on}^g \cdot (n_{h/d} - R^g) \cdot \frac{R^f}{V} - k_{off}^g \cdot R^g \quad (3.3)$$

where $(n_{h/d} - R^g)$ are the number of general promoters not bound to TM in haploids or diploids, respectively.

Similarly, the change in binding of TM to the single promoter of interest over time is given by:

$$\frac{dR^p}{dt} = k_{on}^p \cdot (1 - R^p) \cdot \frac{R^f}{V} - k_{off}^p \cdot R^p \quad (3.4)$$

Solving (3.3) and (3.4) at steady-state, $\frac{dR^g}{dt} = \frac{dR^p}{dt} = 0$, constraints the number of bound TM s via the following nonlinear equations

$$k_{on}^g \cdot (n_{h/d} - R^g) \cdot \frac{R^f}{V} = k_{off}^g \cdot R^g \quad (3.5)$$

$$k_{on}^p \cdot (1 - R^p) \cdot \frac{R^f}{V} = k_{off}^p \cdot R^p \quad (3.6)$$

Finally, the steady-state concentration of transcripts produced from the single promoter of interest, c_p , is given by

$$c_p = \frac{k_{off}^p \cdot R^p}{V} \quad (3.7)$$

Now, with a fixed set of parameters c_{TM} , k_{on}^g , k_{off}^g , k_{on}^p , k_{off}^p , numerically solving equations (3.2), (3.5) and (3.6) allows to calculate the transcript concentration, c_p , generated by the single promoter of interest as a function of cell volume V . The parameter sets I chose for this work are described in Appendix A.

3.5.2 Model predictions for the behaviour of transcript concentrations

The minimal model can predict different types of behaviour for the regulation of transcript concentrations with cell volume and cell ploidy. Those different predictions depend on the parameters chosen to describe the promoter of interest (Fig. 3.16 & 3.17).

First, the model accurately predicts the behaviour of most transcript concentrations as a function of cell volume and cell ploidy (red curves in Figs. 3.16 & 3.17). As of now, this behaviour will be referred to as actin-like behaviour. For a given k_{off}^p of the promoter of interest, this behaviour takes place for a moderate initiation rate k_{on}^p , when compared to the initiation rate of the general pool of promoters ($k_{on}^p \approx k_{on}^g$). In other words, both the promoter of interest and the general pool of promoters have similar binding affinities to the limiting component of the transcriptional machinery. They thus equally compete for that component, and the transcription rate of the promoter of interest increases with increasing availability of the limiting component, i.e. cell volume. This leads to constant transcript concentrations as a function of cell volume. In diploid cells, the promoter of interest competes with twice as many general promoters than in haploid cells. Thus, the concentration of transcripts expressed through this promoter of interest is halved, when compared to the concentration in haploids of similar volume. For a homozygous diploid

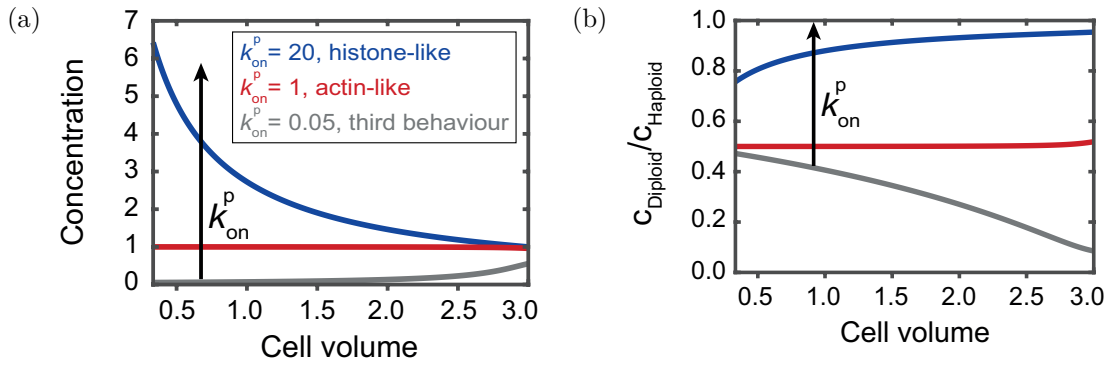


Figure 3.16: **Predictions of the minimal model for the behaviour of transcript concentrations with cell volume and ploidy.** The model predicts three different types

of behaviours, depending on the initiation rate k_{on}^p of the specific promoter of interest.

(a) Concentration of transcripts expressed through the specific promoter of interest, as a function of cell volume. (b) Ratio of transcript concentrations in diploids compared to the concentration in haploids of same size, as a function of cell volume. Red curves depict actin-like behaviour, blue curves depict histone-like behaviour and grey curves depict the third type of behaviour.

carrying two of those promoters, this leads to the same concentration than in a haploid with one promoter, as expected from the literature [Wu et al., 2010].

Secondly, the model also correctly predicts the behaviour of transcript concentrations that are expressed through histone promoters (blue curves in Figs. 3.16 & 3.17). For this behaviour to take place, the initiation rate k_{on}^p of the promoter of interest must be relatively higher than the initiation rate of the general pool of promoters ($k_{on}^p \gg k_{on}^g$). In other words, in comparison with the general pool of promoters, the binding affinity to the limiting component of the transcriptional machinery is much higher for the promoter of interest. Thus, the promoter is already saturated with transcriptional machinery, even at very small cell volumes. Cell growth, and thus increased availability of the transcriptional machinery, does therefore not lead to a higher occupancy of the promoter with transcriptional machinery. Thus, the transcription rate stays constant as a function of cell volume, resulting in a decrease of transcript concentrations with increasing cell volume. For a diploid cell, the amount of general promoters doubles, but the binding

affinity of the promoter of interest is much higher than the binding affinity of the general pool of promoters. Thus, the occupancy of the promoter of interest with transcriptional machinery does not get affected. Hence, the transcription rate of the promoter of interest in a diploid is the same as the transcription rate in a haploid. For a homozygous diploid carrying two of those promoters of interest, this will therefore lead to a doubling in transcript concentrations, when compared to a haploid of similar volume.

Lastly, the model also predicts a third type of behaviour when the initiation rate k_{on}^p of the promoter of interest is much lower than the initiation rate of the general pool of promoters ($k_{on}^p \ll k_{on}^g$, grey curves in Figs. 3.16 & 3.17). In this regime, the transcript concentrations first stay constant at very small concentration values, and only start to increase at higher cell volumes. Simultaneously, the ratio of transcript concentrations in a diploid compared to the transcript concentrations in a haploid decreases with cell volume. This behaviour can be understood as follows: since the binding affinity of the promoter of interest is so low, when compared to the general pool, the transcriptional machinery rarely binds the promoter of interest. Hence, the transcription rate is very low, leading to barely any production of transcripts. At bigger cell volumes, when there is an abundance of transcriptional machinery, the machinery also becomes available for the promoter of interest. This then leads to a non-linear increase of transcription rate with cell volume. In a diploid, there are double as many general promoters compared to a haploid. Thus, in a diploid, the transcription rate of the promoter of interest only increases at even bigger cell volumes, in comparison to a haploid. As a consequence, for the computed cell volume range, the transcript concentration ratio decreases as a function of cell volume.

To sum up the findings so far, depending on the parameters chosen, the model can predict histone-like behaviour or actin-like behaviour. This means that when all other parameters are fixed, tuning the initiation rate k_{on}^p - or the off-rate k_{off}^p , describing all other steps of transcription - can change the behaviour of the promoter of interest from a histone-like promoter to that of an actin-like promoter, or vice-versa (Fig. 3.17).

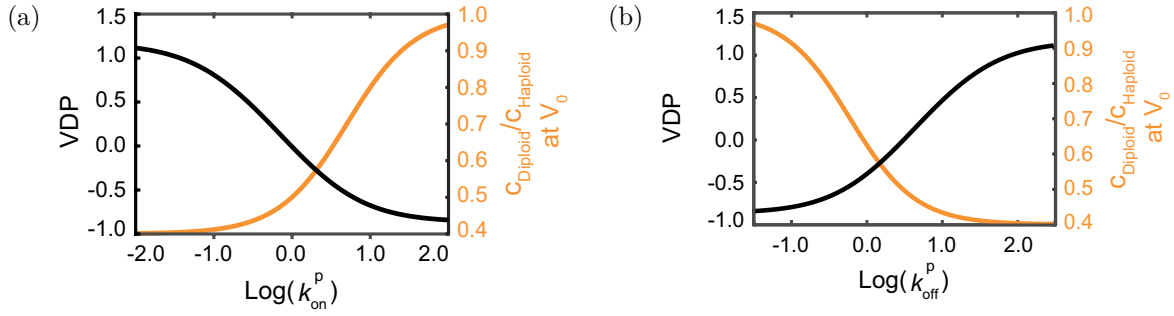


Figure 3.17: **Tuning k_{on}^p or k_{off}^p can change the behaviour of the promoter of interest.** The model predicts that tuning k_{on}^p (a), or k_{off}^p (b), while keeping all other parameters fixed results in a qualitative change in the dependence of transcript concentrations on cell volume (black curves), as well as a change in the ratio between the concentration in diploid cells and the concentration in haploid cells (orange curves).

3.6 Change behaviour of histone promoters experimentally

3.6.1 Create histone promoter truncations

The minimal model described in ch. 3.5 predicts that one specific promoter of interest can exhibit different behaviours, depending on the parameters chosen to describe the promoter. For example, the promoter can behave like an actin promoter (constant transcript concentrations over cell volume, $VDP \approx 0$, but ploidy dependent, $\frac{c_{diploid}}{c_{haploid}} \approx 0.5$) or like a histone promoter (decrease of transcript concentrations with increasing cell volume, $VDP \approx -1$, but independent of ploidy, $\frac{c_{diploid}}{c_{haploid}} \approx 1$). One of the key predictions of this model is that the behaviour of a histone-like promoter can be changed to that of an actin-like promoter, solely by tuning its initiation rate k_{on}^p , and leaving all other parameters fixed (Fig. 3.17a).

In order to test this theoretical prediction experimentally, I focused on the *HTB1* and *HHF1* promoters. To decrease their initiation rates, I worked with increasingly shorter truncations of those promoters (Fig. 3.18).

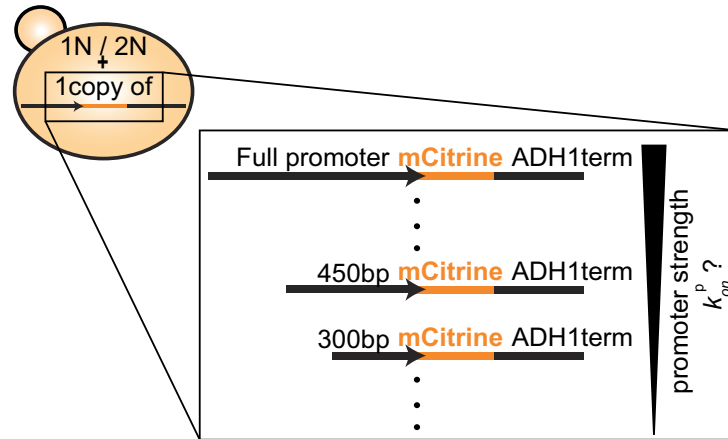


Figure 3.18: **Illustration of the experiments on histone promoter truncations.** Series of haploid and diploid strains carry a single additional copy of increasingly shorter fragments of histone promoters driving *mCitrine* expression, each truncated from the 5'-end. *mCitrine* fluorescence is then quantified by flow cytometry. Additionally, for some promoter truncations, *mCitrine* expression is measured with RT-qPCR.

Those truncations were created by shortening the full promoters from the 5' end in sections of 150 bp. Similar to the full promoter constructs described in chapter 3.4, each promoter truncation drove the expression of the fluorescent protein *mCitrine*. Again, all promoter constructs were regulated by the same *ADH1* terminator, and one single copy of each construct was incorporated into the genome of non-inducible-Whi5 and inducible-Whi5 haploid and diploid cells.

I then quantified the mean *mCitrine* fluorescence of cell populations by flow cytometry (ch. 2.5), or the mean *mCitrine* expression by RT-qPCR (ch. 2.4). To determine the dependence of *mCitrine* fluorescence or *mCitrine* transcript concentrations on cell volume, I performed the experiments on cell populations of different mean cell volumes, and measured the cell volume distributions with a Coulter Counter (ch. 2.2.3).

3.6.2 Histone promoter truncations change the dependence of transcript concentrations on cell volume

As a first step, I analysed the *mCitrine* expression driven by those additional promoter truncation constructs in haploid cells, using flow cytometry. I quantified the *mCitrine*

fluorescent concentrations at a characteristic cell volume (Fig. 3.19a), and determined the VDP s of mCitrine concentrations (Fig. 3.19b) for each of the investigated promoter truncations. For both the *HTB1* and the *HHF1* promoter, I observe a drastic drop in mCitrine concentration between the 450 bp and the 300 bp truncation. This drop in promoter expression also coincides with a change of the VDP towards 0.

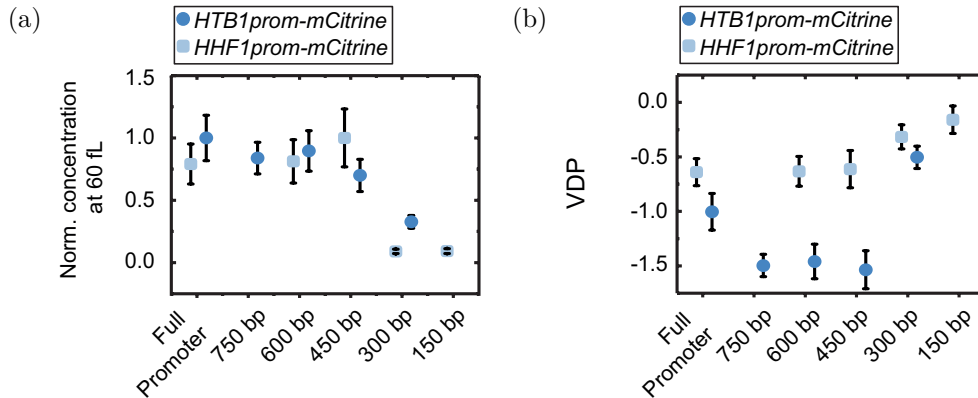


Figure 3.19: **Reducing the strength of the histone promoter changes its VDP , as shown by flow cytometry in haploid cells.** (a) mCitrine concentration at 60 fL, normalised on the maximum concentration, for promoter truncations of the *HTB1* promoter (dark blue circles) and the *HHF1* promoter (light blue squares), respectively. Concentrations were estimated from the linear fit to the dependence of concentration on cell volume. Error bars are derived by error propagation of the 95% confidence interval of the linear fit at 60 fL. (b) VDP of mCitrine for the respective promoter truncations of the *HTB1* promoter (dark blue circles) and the *HHF1* promoter (light blue squares). VDP s were determined as the slope of the linear fit to the dependence of concentration on cell volume. Error bars show the standard error of the VDP s. In both panels, the linear fit was performed through $n = 15$ biological replicates, except for the full *HTB1* and *HHF1* promoter, where the fit was performed through $n = 12$ biological replicates.

As discussed in chapter 1, all major core histone promoters in budding yeast include upstream activating sequence (UAS) elements [Osley, 1991, Eriksson et al., 2005]. These UAS elements act as binding sites for the transcription factor Spt10, which is known to activate histone transcription during S-phase [Eriksson et al., 2011]. For the *HTB1* and *HHF1* promoters, part of those UAS elements get lost between the 450 bp and the 300

bp truncation (Fig. 3.20), which is when the drop of concentration and the change in VDP is happening. Thus, it is plausible that this partial loss of UAS elements causes the observed reduction in promoter strength.

In the minimal model introduced in chapter 3.5, this reduction in promoter strength is described as a reduction in initiation rate k_{on}^p of the promoter of interest. The model predicts that reducing k_{on}^p shifts the VDP of a histone-like promoter ($VDP \approx -1$) towards the VDP expected for an actin-like promoter ($VDP \approx 0$). Experimentally, I observe this switch for both the *HTB1* and the *HHF1* promoter between the 450 bp and 300 bp truncations.

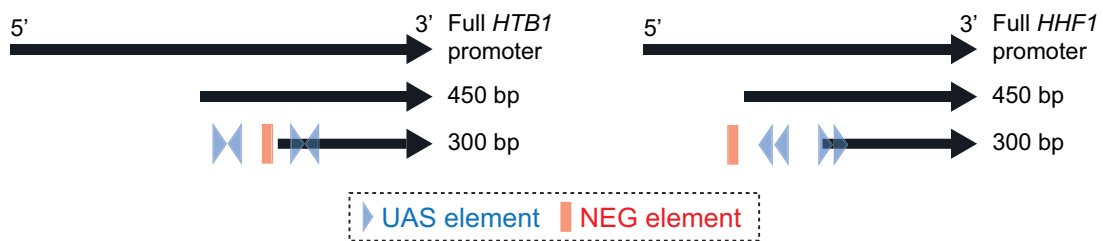


Figure 3.20: **Illustration of the full *HHF1* and *HTB1* promoter, as well as the 450 bp and 300 bp truncations.** Blue arrowheads show the location of the upstream activating sequences (UAS) elements [Osley et al., 1986], red boxes show the location of the NEG elements [Osley, 1991, Mariño-Ramírez et al., 2006].

3.6.3 Histone promoter truncations lead to switch from histone-like to actin-like behaviour

The model also predicts that the ploidy dependence of transcript concentrations expressed through a histone-like promoter ($\frac{c_{diploid}}{c_{haploid}} \approx 1$) should change when reducing its initiation rate k_{on}^p . Thus, as a next step, I performed similar flow cytometry experiments not only on haploid cells, but on both haploid and diploid cells. This allowed me to calculate the ratio of mCitrine concentration between diploid and haploid cells, at a chosen cell volume of 60 fL. In haploid cell, I observe the change in VDP between the 450 bp and 300 bp truncation of both promoters. Thus, I decided to focus the rest of my experiments on those truncations and their corresponding full promoters (Fig. 3.21).

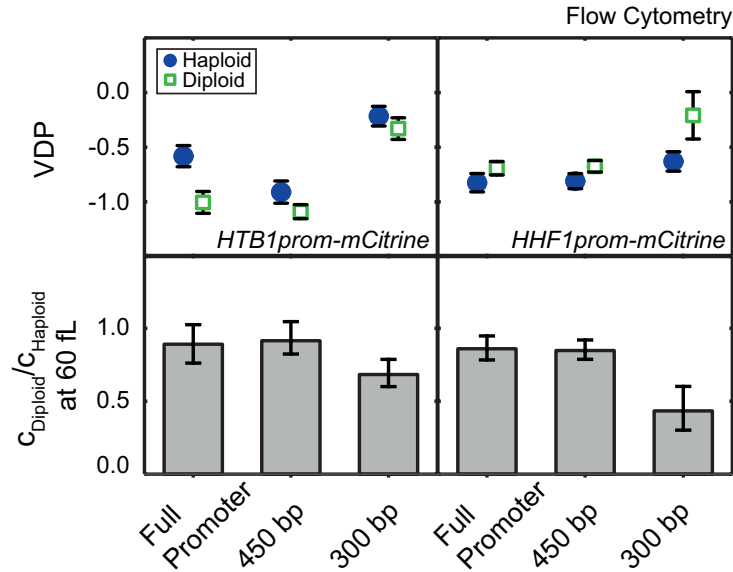


Figure 3.21: **Reducing the strength of a histone promoter shifts its behaviour from histone-like to actin-like, as shown by flow cytometry in haploid and diploid cells.** VDP of mCitrine in non-inducible-Whi5 and inducible-Whi5 haploid (blue filled circles) and diploid (green open squares) cells (upper panel) and mCitrine concentration at 60 fL in diploids compared to the concentration in haploids (bottom panel). Left shows results for the *HTB1* promoter truncations, right shows results for the *HHF1* promoter truncations. Concentrations were estimated from the linear fit to the dependence of concentration on cell volume, VDP s were determined as the slope of the linear fit. Error bars in the upper panels show the standard error of the VDP s. In the bottom panel, error bars indicate the 2.5- and 97.5-percentiles around the median concentration ratio, determined from 10000 bootstrap samples. Linear fits were performed through $n = 27$ biological replicates, except for the full *HTB1* and *HHF1* promoter in diploid cells, where the fit was performed through $n = 18$ biological replicates. For the diploid 450 bp *HHF1* promoter $n = 18$, and for the diploid 300 bp *HHF1* promoter $n = 17$.

Again, for both the *HTB1* and the *HHF1* promoter, the VDP in haploid and in diploid cells changes towards 0 for the 300 bp truncation (Fig. 3.21, upper panel). In addition, the ratio of mCitrine concentration at a characteristic volume decreases from close to 1 towards 0.5 (Fig. 3.21, lower panel). This is in full accordance with the predictions of the minimal model. Thus, those results highlight that for both the *HHF1* and the *HTB1*

promoter it is indeed possible to change the behaviour from a histone-like promoter to that of an actin-like promoter, experimentally.

While I consistently observe this same trend in the flow cytometry measurements, I realised that the exact VDP s measured with flow cytometry depended on the flow cytometry settings. Depending on the cell volume range I wanted to measure (only haploid cells or both diploid and haploid cells at the same time), I needed to adjust those settings, which could lead to quantitatively different VDP s, without changing the qualitative trend of changing the promoter's behaviour. However, in order to quantitatively confirm the flow cytometry results, I repeated the experiments for the 450 bp and 300 bp truncations of the *HTB1* and *HHF1* promoters using RT-qPCR (Fig. 3.22).

Again, I see a change in the VDP towards 0, and a decrease of the ratio of the *mCitrine* concentration between diploid and haploid cells from close to 1 to close to 0.5. It is worth noting though that, especially for the diploid 450 bp *HHF1* truncations, the RT-qPCR measurements were subject to a lot of experimental noise, resulting in large error bars for the VDP and the ratio in concentration. Even though I decided to perform the RT-qPCR measurements in order to get more quantitative measures, again, the qualitative trend is the main result from those experiments.

To summarise, I was able to observe a qualitative change of the *HHF1* and the *HTB1* promoter from histone-like to actin-like, both with flow cytometry (Figs. 3.19 & 3.21) and with RT-qPCR (Fig. 3.22), two independent experimental methods. Those results confirm the predictions of the minimal model (Fig. 3.17), namely that reducing the initiation rate k_{on}^p of the promoter of interest will eventually shift its behaviour from histone-like towards actin-like. This reinforces the hypothesis that the coupling of histone mRNA and protein concentrations to gene copy number is an inherent property of the histone promoters.

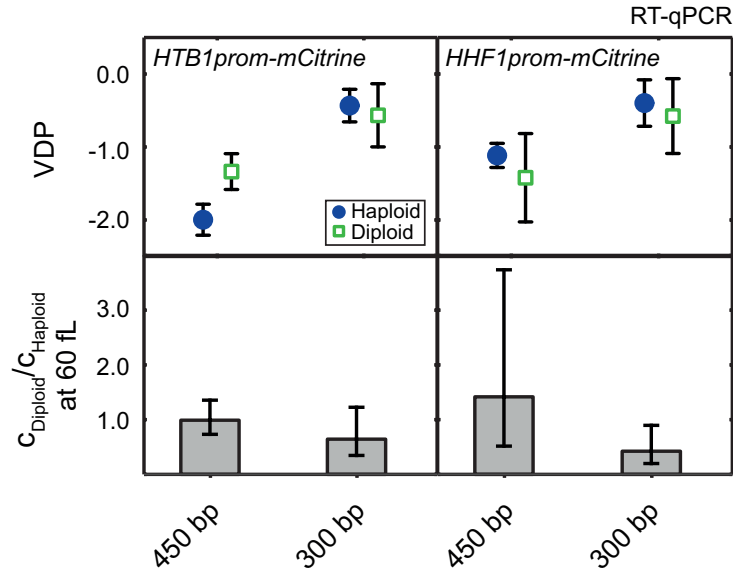


Figure 3.22: **Reducing the strength of a histone promoter shifts its behaviour from histone-like to actin-like, as shown by RT-qPCR in haploid and diploid cells.** *VDP* of *mCitrine* in non-inducible-Whi5 and inducible-Whi5 haploid (blue filled circles) and diploid (green open squares) cells (upper panel) and *mCitrine* mRNA concentration at 60 fL in diploids compared to the concentration in haploids (bottom panel) for *HTB1* and *HHF1* promoter truncations driving *mCitrine* expression. Concentrations were estimated from the linear fit to the dependence of concentration on cell volume, *VDPs* were determined as the slope of the linear fit. Error bars in the upper panel show the standard error of the *VDP*. Error bars in the bottom panel indicate the 2.5- and 97.5-percentiles around the median concentration ratio, determined from 10000 bootstrap samples. Linear fits were performed through the following numbers of biological replicates: $n_{300bp, diploid}^{HTB1prom} = n_{450bp, haploid}^{HHF1prom} = n_{450bp, diploid}^{HHF1prom} = n_{300bp, diploid}^{HHF1prom} = 12$, $n_{300bp, haploid}^{HTB1prom} = 16$, $n_{450bp, haploid}^{HTB1prom} = 15$, $n_{300bp, haploid}^{HHF1prom} = 11$.

3.7 Cell cycle dependent production of histone transcripts

3.7.1 S-phase duration does not decrease for larger cells

So far, the experiments performed show that for *mCitrine* transcripts expressed from histone promoters, mean concentrations in asynchronous bulk populations decrease with mean cell volume and increase with cell ploidy (ch. 3.4). Additionally, they also confirm the model predictions (ch. 3.5) by showing that it is possible to change this behaviour through reduction of the promoter strength and make the histone promoters behave like an actin promoter (ch. 3.6).

Up to this point, I considered this to be solely due to the inherent property of histone promoters to synthesise transcripts at a constant and cell volume independent rate. However, it is known that the production of histones in budding yeast is linked to DNA replication, and is not uniform during the cell cycle. In fact, the production of histones is restricted to the late G1- and S-phase of the cell cycle [Eriksson et al., 2012]. It has also been shown that the histone promoters alone are sufficient to increase the expression of histone transcripts during S-phase [Osley et al., 1986, Eriksson et al., 2011]. Thus, the observed decrease of mean *mCitrine* transcript concentrations with mean cell volume could have two possible explanations:

The first possibility would be that the duration of S-phase is not affected by cell volume, i.e. that smaller and bigger cells express histones for the same amount of time. If histone promoters synthesised transcripts at a constant and cell volume independent rate, this would indeed lead to decreasing transcript concentrations with increasing cell volume.

However, a second possibility would be that the duration of S-phase is affected by cell volume, and that bigger cells express histones for a shorter time period. In bulk populations this would lead to a decrease in the fraction of *mCitrine* expressing cells as a function of cell volume. Again assuming a constant and cell volume independent transcription rate, this would also result in a decrease of mean *mCitrine* concentration with increasing mean cell volume.

In order to determine which of those possible explanations applies, I performed live-cell fluorescence microscopy (ch. 2.3) on all full histone promoter constructs investigated so far. In detail, I measured the mCitrine fluorescence expressed from either the *HTB1*, *HTB2* or *HHF1* promoter as a function of time in inducible-Whi5 diploid single cells. This allowed me to quantify the synthesis of mCitrine as a function of time (ch. 2.3.5) in single cells. First, I observe that the synthesis of mCitrine exhibits a peak in production, right after bud emergence (Fig 3.23). This roughly corresponds to S-phase and confirms that the *HTB1*, *HTB2* and *HHF1* promoter restrict the production of *mCitrine* to this period.

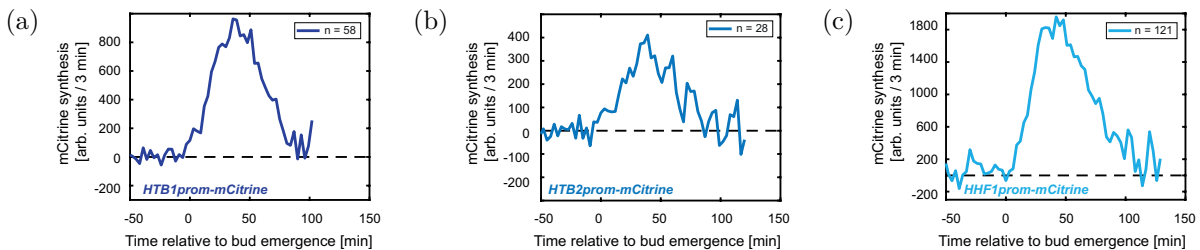


Figure 3.23: **Additional histone promoters express *mCitrine* in a cell cycle dependent manner, as shown by live-cell fluorescence microscopy.** (a -c) mCitrine synthesis rate measured during the first cell cycle of new-born inducible-Whi5 diploid cells, when expressed from an additional *HTB1* (a), *HTB2* (b) or *HHF1* (c) promoter. Traces represent the mean of the moving averages over 3 frames of the single cell traces and are shown for the time span during which at least 10 single cell traces were included in the average. All traces are aligned at the time of first bud emergence ($t = 0$).

In addition, I quantified the cell volume of single cells from the phase contrast images (ch. 2.3.2), and the duration of the *mCitrine* production period (ch. 2.3.3). For all three promoters investigated, I do not observe a relevant decrease in the duration of the *mCitrine* production period as a function of cell volume (Fig. 3.24).

Those results highlight that the observed decrease of mean transcript concentrations with increasing mean cell volume of asynchronous bulk populations is not a result of a decrease in S-phase duration in larger cells. Rather, they support the idea that the decrease of transcript concentrations is already established during S-phase, as a result of cell volume

independent transcription rates.

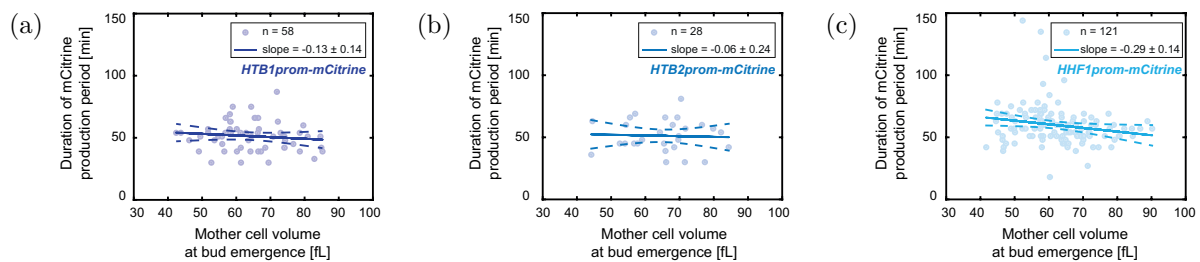


Figure 3.24: **Duration of S-phase expression of additional histone promoters remain unchanged over cell volume.** (a - c) Duration of mCitrine production period, determined by live-cell fluorescence microscopy, shown as a function of the cell volume at bud emergence for an inducible-Whi5 diploid strain carrying an additional *HTB1* (a), *HTB2* (b) or *HHF1* (c) promoter driving *mCitrine* expression. Solid lines show linear fits to the data, dashed lines represent the 95% confidence intervals of the fit. Slopes of the fit are stated with respective standard error.

3.7.2 Decrease of histone-promoter-mediated transcript concentrations is achieved during S-phase

As a next step I wanted to verify whether the decrease of transcript concentrations with increasing cell volume is indeed already achieved during S-phase. In other words, I wanted to confirm whether I observe a decrease of transcript concentration as a function of cell volume, when focusing only at cells in S-phase.

To do this, I asked the help of a colleague (Dimitra Chatzitheodoridou), who performed single-molecule fluorescence in situ hybridization (smFISH, ch. 2.6) on inducible-Whi5 diploid cells carrying one additional *HTB1*, *HTB2*, or *HHF1* promoter driving *mCitrine* expression. As a comparison, she also investigated cells carrying an additional *ACT1* promoter driving *mCitrine* expression. This way, smFISH allows counting of *mCitrine* mRNA molecules expressed by either the histone promoter or the *ACT1* promoter in single cells (Fig. 3.25a). At the same time, bright-field microscopy can be used to determine the cell volume. Additionally, staining the nuclear DNA with DAPI in order to visualise the nucleus allowed me to classify cells into G1, S, or G2/M-phase. Thus, I could put the

mCitrine mRNA concentrations within the cells in relation to their volume, and focus on S-phase cells.

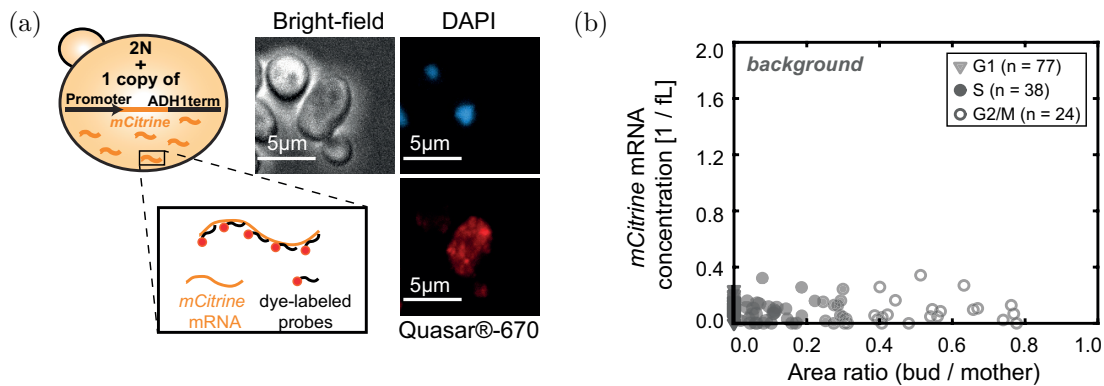


Figure 3.25: **Illustration of the smFISH experiments.** (a) Quasar®-670-labelled probes were used to count *mCitrine* mRNA spots in inducible-Whi5 diploid cells carrying an additional promoter driving *mCitrine* expression. DAPI-staining of nuclear DNA and bright-field microscopy were used to classify cells as G1, S, or G2/M-phase and to estimate cell volumes. Multiple images were taken per condition and at least two independent biological replicates were measured on different days. Example images show maximum intensity z-projections of diploid cells carrying an additional *HTB1* promoter; contrast was adjusted for visualisation. (b) Results of control experiments on inducible-Whi5 diploid cells carrying no additional promoter driving *mCitrine* expression. mRNA concentration, estimated as the number of spots detected with smFISH in the whole cell including the bud and divided by the cell volume, shown as a function of the cell area ratio (cell area of the bud divided by the cell area of the mother cell).

First, I made sure that this experimental design indeed allowed me to specifically count *mCitrine* mRNA molecules, by performing the experiments on cells of a wild-type strain not carrying any additional promoter driving *mCitrine* expression. Fig. 3.25b shows that some minimal background signal is present in the cells, resulting in a small background concentration. However, this concentration was much smaller than for cells carrying a promoter driving the expression of *mCitrine*. Thus, I decided to neglect the weak background signal for further experiments.

Then, I analysed the cell cycle dependent expression of *mCitrine* transcripts driven by

the histone promoters by visualising the *mCitrine* concentrations in cells in dependence of the cell cycle stage of the cell (Fig. 3.26).

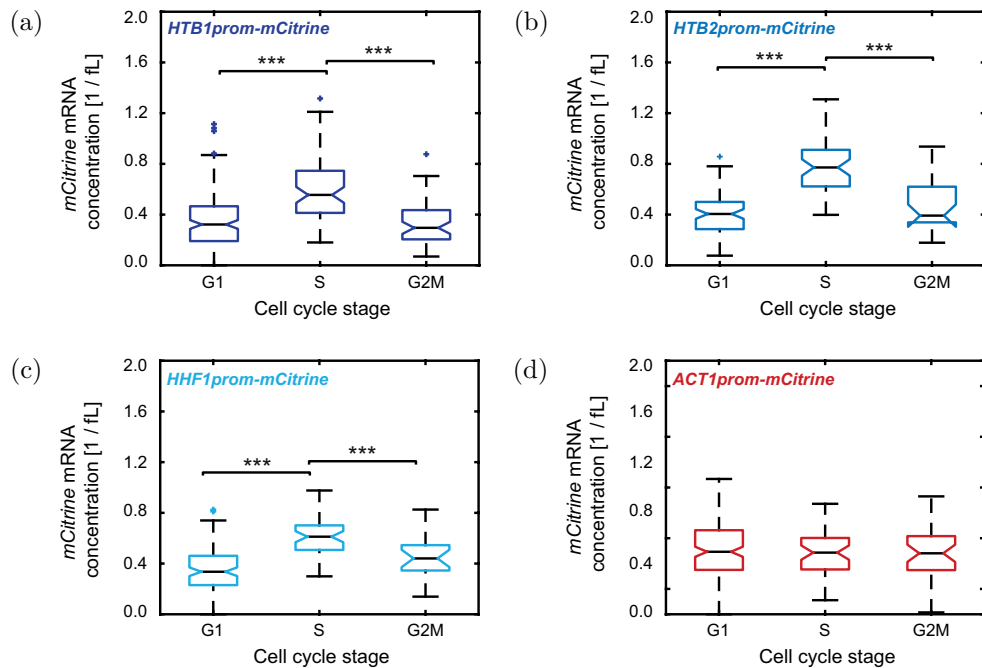


Figure 3.26: **Additional histone promoters express *mCitrine* in a cell cycle dependent manner, as shown by smFISH.** (a - d) *mCitrine* mRNA concentration in G1-, S- or G2/M-phases, estimated as the number of mRNA spots detected with smFISH in the whole cell including the bud and divided by the cell volume, for inducible-Whi5 diploid cells expressing *mCitrine* from an additional *HTB1* (a), *HTB2* (b), *HHF1* (c) or *ACT1* (d) promoter. Coloured boxes highlight the 25- and 75-percentiles, whiskers extend to $\pm 2.7\sigma$ of the distributions, and coloured crosses highlight outliers. Black, horizontal lines indicate the median between single cells for $n_{G1} = 158$, $n_S = 69$, $n_{G2M} = 57$ (a), $n_{G1} = 77$, $n_S = 49$, $n_{G2M} = 25$ (b), $n_{G1} = 113$, $n_S = 48$, $n_{G2M} = 21$ (c), and $n_{G1} = 151$, $n_S = 48$, $n_{G2M} = 38$ (d), with notches indicating the 95% confidence interval. Significance was tested using a two-tailed, two-sample t-test at a confidence level $\alpha = 0.05$, where applicable (between G1- and S-phase cells for (b), between all populations for (c) & (d)), or a Kruskal-Wallis test at a confidence level $\alpha = 0.05$ otherwise; *** $p < 0.001$

Consistent with the results obtained from live-cell fluorescence microscopy, I observe a peak of *mCitrine* concentration in S-phase cells, for all three histone promoters investigated (3.26a, 3.26b & 3.26c). In contrast, for the *ACT1* promoter driving *mCitrine*

expression, I do not observe such a peak in *mCitrine* concentration (Fig. 3.26d), which is expected for a housekeeping gene such as *ACT1*. Again, this confirms that the histone promoters are sufficient to drive the cell cycle dependent synthesis of transcripts.

Lastly, I determined the behaviour of *mCitrine* mRNA concentrations as a function of cell volume, focusing only on cells in S-phase. All three histone promoters investigated (*HTB1*, *HTB2*, and *HHF1* promoter) lead to a significant decrease of *mCitrine* mRNA concentrations with increasing cell volume (Figs. 3.27a, 3.27b & 3.27c). In contrast, when *mCitrine* is driven by the *ACT1* promoter, the *mCitrine* concentration stays constant as a function of cell volume (Fig. 3.27d), as expected.

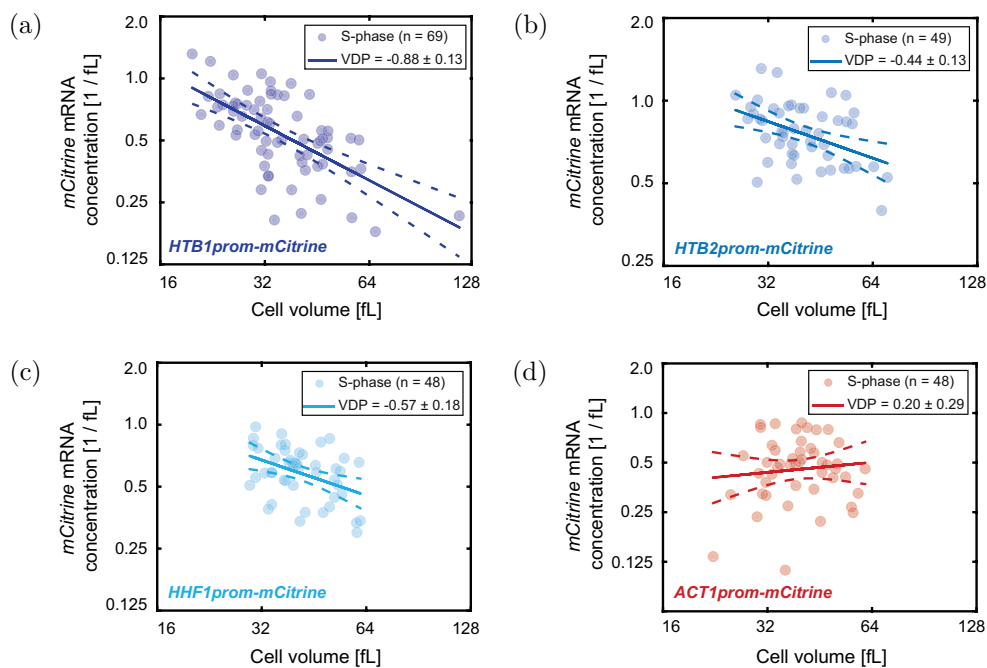


Figure 3.27: **Cell-cycle-dependence of histone promoter does not account for the cell volume dependence of transcript concentrations, as shown by single-molecule FISH.** (a - d) *mCitrine* mRNA concentration in S-phase cells of inducible-Whi5 diploid strains, expressed from an additional *HTB1* (a), *HTB2* (b), *HHF1* (c), or *mCitrine* (d) promoter, shown as a function of cell volume in a double logarithmic plot. Solid lines show linear fits to the double logarithmic data, dashed lines represent the 95% confidence intervals of the fit. *VDPs* were determined as the slope of the fit, with respective standard error.

In summary, those results confirm that the histone promoters are sufficient to drive the

cell cycle dependent regulation of transcripts by limiting their expression to S-phase. In addition, the results also highlight that the distinct regulation of histone transcripts with cell volume is established by the histone promoters during S-phase. Again, this reinforces the hypothesis that the coupling of histone transcript to gene copy number, and not to cell volume, is an intrinsic property of the histone promoters themselves.

3.7.3 Cell cycle dependent regulation is not disrupted in histone promoter truncations

As described in chapter 3.6, it is possible to change the behaviour of a histone promoter towards that of an actin-like promoter by reducing the strength of the promoter. Experimentally, I achieved this by truncating the *HTB1* and *HHF1* promoters from the 5' end into increasingly shorter fragments. The observed switch in histone promoter behaviour coincides with the partial loss of the UAS elements within the promoters (Fig. 3.20). As discussed in chapter 1, those UAS elements are binding sites for Spt10, which activates histone expression in S-phase [Eriksson et al., 2011]. It is plausible that the shortening of histone promoters and the partial loss of the UAS elements lead to a disruption in the cell cycle dependent expression of the histone promoter truncations. Therefore, the observed switch in histone promoter behaviour could be a direct effect of such a possible disruption, and not a result of the reduction in promoter strength.

In order to test whether such a disruption is indeed responsible for the switch in histone promoter behaviour, I performed live-cell fluorescence microscopy experiments on inducible-Whi5 diploid cells carrying the additional *HTB1* and *HHF1* promoter truncations. Again, this allowed me to quantify the mCitrine synthesis as a function of time, and to determine the duration of *mCitrine* production period on a single cell level. As expected from the results obtained with flow cytometry (Fig. 3.19), the total mCitrine intensity is strongly reduced in the 300 bp truncations, both for the *HTB1* and the *HHF1* promoter. But, when compared to the respective full promoter and 450 bp truncation, both *HTB1* and *HHF1* 300 bp truncations still show a clear peak in mCitrine synthesis (Figs. 3.28a & 3.28d). Additionally, for all histone promoter truncations investigated, the

duration of S-phase is not affected by cell volume (Figs. 3.28b, 3.28c & 3.28e, 3.28f).

The 300 bp truncations of the *HTB1* and the *HHF1* promoters seem to have a small effect on the level and the exact timing of *mCitrine* expression. However, the qualitative cell cycle dependence still remains intact. Thus, this suggests that the observed switch in histone promoter behaviour (ch. 3.6) is indeed a result of reducing the strength of the promoter, and not an effect caused by a disruption in the cell cycle regulation.

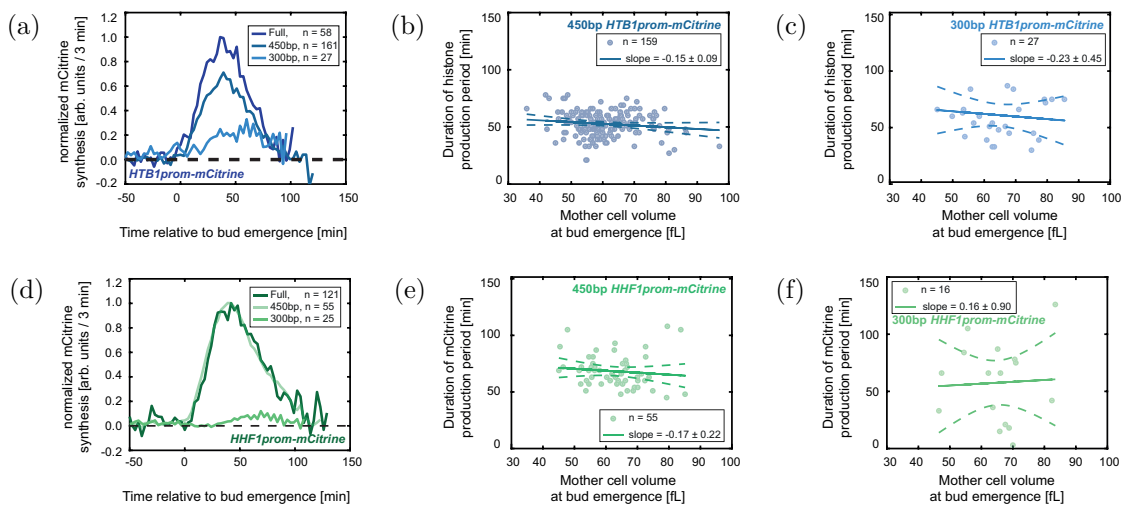


Figure 3.28: Change in behaviour of truncated histone promoter is not due to a disruption of the cell cycle dependence, as shown by live-cell fluorescence microscopy. (a & d) mCitrine synthesis rate measured during the first cell cycle of newborn inducible-Whi5 diploid cells, when expressed from *HTB1* (a) or *HHF1* (d) promoter truncations. Traces represent the mean of the moving averages over 3 frames of the single cell traces and are shown for the time span during which at least 10 single cell traces were included in the average. All traces are aligned at the time of first bud emergence ($t = 0$) and normalised to the maximum mean value of mCitrine synthesis for the full promoter. (b - c & e - f) Duration of mCitrine production period shown as a function of the cell volume at bud emergence for an inducible-Whi5 diploid strain carrying an additional 450 bp *HTB1* (b) or 300 bp *HTB1* (c), and an additional 450 bp *HHF1* (e) or 300 bp *HHF1* (f) promoter truncation driving *mCitrine* expression. Solid lines show linear fits to the data, dashed lines represent the 95% confidence intervals of the fit. Slopes of the fit are stated with respective standard error.

In order to further confirm that the switch in promoter behaviour is indeed caused by a change in expression during S-phase rather than a change in the cell cycle dependence, I included smFISH measurements and focused on the 450 bp and 300 bp truncations of the *HTB1* promoter. Again, I asked Dimitra Chatzitheodoridou for help and she performed the smFISH experiments. This allowed me to quantify the *mCitrine* concentrations as a function of cell volume in S-phase cells.

I find that both promoter truncations show a peak of *mCitrine* expression during S-phase (3.29a & 3.29c), which is consistent with the results obtained by live-cell fluorescence microscopy (Fig. 3.28). Again, this shows that the histone promoter truncations do not drastically impact on the cell cycle dependent expression of transcripts driven by the histone promoters. Additionally, I also find that the *mCitrine* concentration significantly decreases with cell volume for the 450 bp *HTB1* promoter truncation (Fig. 3.29b). However, I do not find such a significant decrease in *mCitrine* concentration for the 300 bp truncation (Fig. 3.29d). This confirms a switch in the histone promoter behaviour towards an actin-like behaviour.

To summarise, I found that the histone promoter truncations might have a small impact on the exact timing of the cell cycle dependent regulation of transcript concentrations (Fig. 3.28). However, the cell cycle dependence is clearly not disrupted for any of the investigated histone promoter truncations. In addition, I was able to confirm the switch of the *HTB1* promoter from a histone-like behaviour towards an actin-like behaviour with smFISH (Fig. 3.29). Thus, while the exact cell cycle regulation of histone transcripts might play a role in the coupling of histone concentrations to gene copy number, and not to cell volume, it is likely not the main regulatory mechanism.

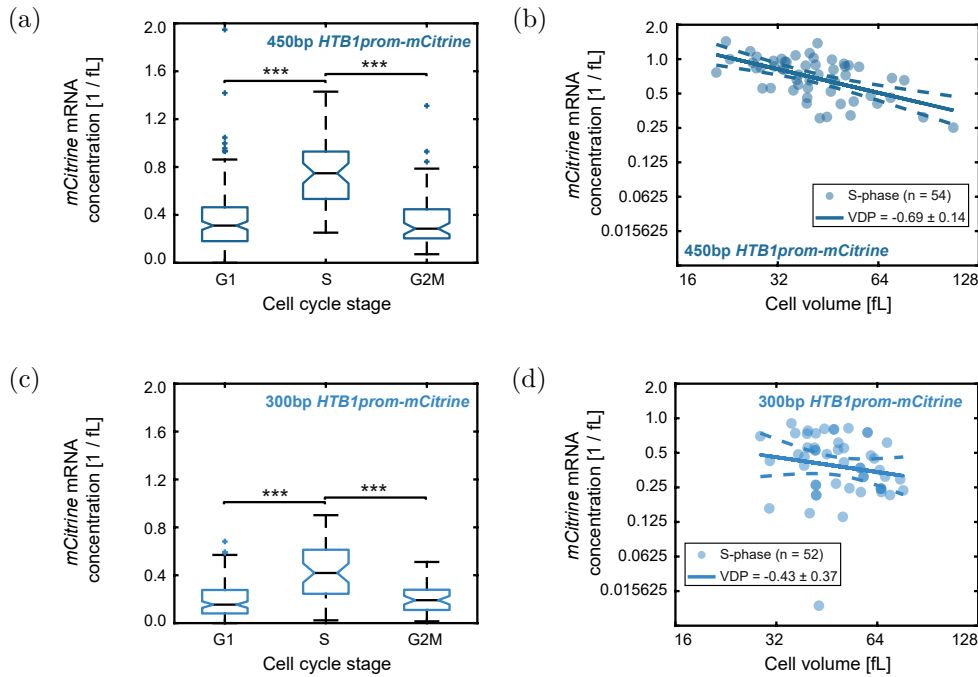


Figure 3.29: **Change in behaviour of truncated histone promoters is not due to a disruption of the cell cycle dependence, as shown by smFISH(a & c) *mCitrine* mRNA concentration in G1-, S- or G2/M-phases, estimated as the number of mRNA spots detected with smFISH in the whole cell including the bud and divided by the cell volume, measured for inducible-Whi5 diploid cells expressing *mCitrine* from an additional 450 bp (a) or 300 bp (c) *HTB1* promoter truncation. Coloured boxes highlight the 25- and 75-percentiles, whiskers extend to $\pm 2.7\sigma$ of the distributions and coloured crosses highlight outliers. Black, horizontal lines indicate the median between single cells for $n_{G1} = 160$, $n_S = 54$, $n_{G2M} = 66$ (a), and $n_{G1} = 131$, $n_S = 52$, $n_{G2M} = 55$ (c), with notches indicating the 95% confidence interval. Significance was tested using a Kruskal-Wallis test at a confidence level $\alpha = 0.05$; $***p < 0.001$. (b & d) *mCitrine* mRNA concentration in S-phase cells, expressed from an additional 450 bp (b) or 300 bp (d) *HTB1* promoter truncation, shown as a function of cell volume in a double logarithmic plot. Solid lines show linear fits to the double logarithmic data, dashed lines represent the 95% confidence intervals of the fit. *VDPs* were determined as the slope of the fit, with respective standard error.**

3.8 Taking a closer look at degradation and transcriptional feedback

3.8.1 Degradation of mRNA through the nuclear exosome might play a role for the accurate cell volume dependence of histone transcript concentrations

Up to now, I have assumed that the regulation of transcript concentrations through the histone promoter is solely given by a constant transcription rate which is independent of cell volume or ploidy. I considered this to be an inherent property of the histone promoters and did not take possible regulations through transcript or protein degradation into account. In ch. 3.2 and 3.3, I showed that in diploid cells with only one *HTB2* allele, the concentrations of *HTB2* transcripts and proteins are reduced compared to wild-type diploid cells. This highlighted the absence of direct feedback mechanisms sensing and controlling the concentration of Htb2 with cell volume and was part of the reason I neglected the possible effects of transcriptional feedback mechanisms or degradation.

However, as described in chapter 1 histones are subject to various layers of regulation in order to ensure appropriate histone homeostasis within cells. For example, histone accumulation in *rad53* Δ budding yeast cells is known to be lethal [Gunjan and Verreault, 2003]. Thus, excess histones are actively degraded by the proteasome and this degradation process is likely mediated by Rad53, a DNA damage response kinase. Another mechanism that could possibly be involved in the regulation of histone transcript concentrations with cell volume is the degradation of mRNA through the nuclear exosome. In budding yeast, *RRP6* encodes for a component of the nuclear exosome exonuclease [Canavan and Bond, 2007, Beggs et al., 2012]. Thus, in order to test whether degradation from the 3' end through the nuclear exosome is important for the regulation of histone transcript concentrations, I worked with *rrp6* Δ strains.

I performed RT-qPCR measurements (ch. 2.4) on bulk cell populations of non-inducible-Whi5 and inducible-Whi5 *rrp6* Δ strains, and induced the cell populations with 10 nM

and 30 nM β -estradiol. At the same time, I measured the cell volume distributions using a Coulter Counter (ch. 2.2.3). This allowed me to calculate the mean mRNA concentrations of representative histone genes (*HTB1*, *HTB2*, *HHF1*, *HHO1*) as a function of mean cell volume of the populations. As described in chapter 3.3, I normalised all mRNA concentrations on *RDN18*, and I also included the housekeeping gene *ACT1* as a comparison. I then determined the *VDP* of each gene and compared it to the *VDP* measured earlier (Fig. 3.8) in wild-type strains carrying no deletion (Fig. 3.30).

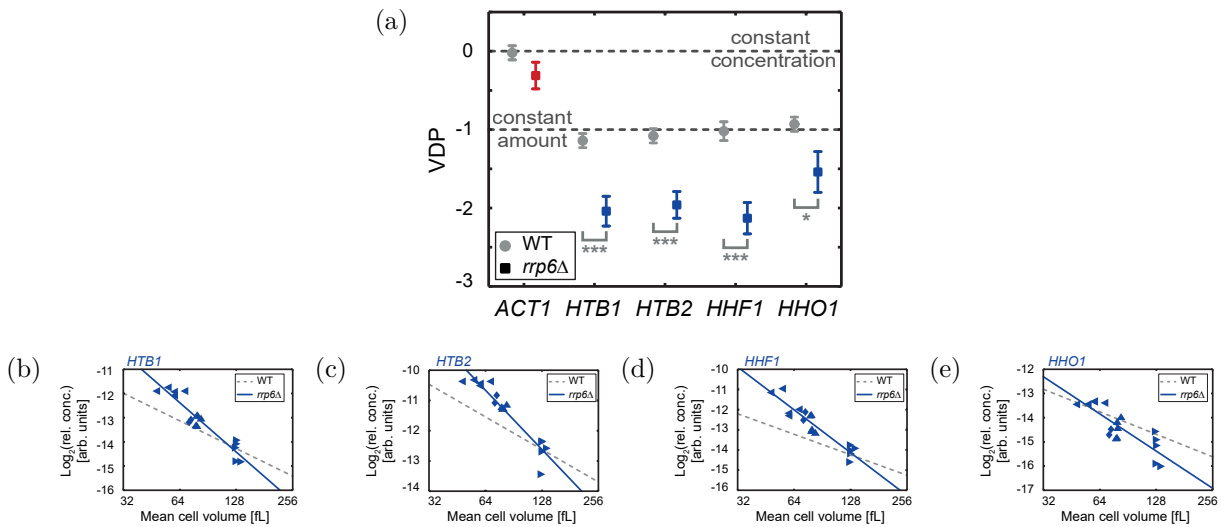


Figure 3.30: **Summary of *VDP*s for *rrp6Δ* strain.** (a) *VDP*s were determined as the slopes of the linear fits to the double logarithmic dependence of concentration on cell volume (fit through $n_{ACT1}^{rrp6\Delta} = n_{HTB1}^{rrp6\Delta} = n_{HTB2}^{rrp6\Delta} = n_{HHF1}^{rrp6\Delta} = n_{HHO1}^{rrp6\Delta} = 17$ biological replicates). Error bars indicate the standard error of the *VDP*s. Significant *VDP* deviation from the wild-type *VDP* (carrying no deletion) was tested using linear regressions; *** $p < 0.001$. (b - e) Relative mRNA concentrations (normalized on *RDN18*) for inducible-Whi5 and non-inducible-Whi5 haploid cells over mean cell volume, shown in double logarithmic plots. Data corresponding to the *rrp6Δ* cells are highlighted in blue for the different conditions (diamonds for non-inducible, left-pointing triangles for 0 nM, up-pointing triangles for 10 nM, and right-pointing triangles for 30 nM). Lines show the linear fits to the double logarithmic data. Grey dashed lines correspond to the linear fit for the wild-type cells, carrying no deletion.

First, I find that the *VDP* of *ACT1* is not affected by the deletion of *RRP6*. Additionally,

all measured histone genes still display a negative VDP in the *rrp6Δ* cells. However, for all measured histone genes, the VDP significantly differs from the wild-type VDP and is comparably more negative. In fact, most of the histone genes have a VDP of around -2 in the *rrp6Δ* cells, meaning that the decrease of histone transcript concentration with cell volume is much stronger when deleting *RRP6*. Interestingly, histone transcript concentrations in *rrp6Δ* cells are mostly increased when compared to wild-type concentrations, but only at smaller cell volumes (Fig. 3.30b - 3.30e).

Thus, those results highlight that mRNA degradation through the nuclear exosome is probably not needed for the decrease of histone transcript concentrations with increasing cell volume. However, it might play a role in order to achieve the correct dependence on cell volume and keep constant amounts as a function of cell volume. In addition, the results suggest that the degradation rate of mRNA might not be the same in small and big cells, and could possibly be dependent on cell volume. This has also been suggested in other recent studies [Mena et al., 2017, Swaffer et al., 2021b].

3.8.2 Transcriptional feedback involving HIR complex is not necessary for cell volume dependence of histone transcript concentrations

As mentioned above, excess histones are not only subject to active degradation. Other mechanisms of regulation also make sure that histone genes are expressed at the right time during the cell cycle. Specifically, upon replication stress, all core histone gene pairs, excluding the *HTA2-HTB2* pair, are subject to negative feedback regulation on the transcript level [Eriksson et al., 2012, Libuda and Winston, 2010]. As suggested by various studies, this negative feedback regulation is likely mediated by the HIR complex and depends on *HIR1* and *RTT106* [Fillingham et al., 2009, Feser et al., 2010, Zunder and Rine, 2012]. Thus, I wanted to investigate whether any feedback mechanisms involving the HIR complex might play a role in the decrease of histone transcript concentrations with increasing cell volume.

Similarly to the measurements described above, I performed RT-qPCR (ch. 2.4) on popu-

lations of *hir1* Δ and *rtt106* Δ cells, determined the mean mRNA concentrations of selected histone genes (*HTB1*, *HTB2*, *HHF1*, *HHO1*) and *ACT1*, and measured cell volume distributions with a Coulter Counter (ch. 2.2.3). Again, this allowed me to determine the *VDP* of each gene and compared it to the *VDP* measured earlier (Fig. 3.8) in wild-type strains carrying no deletion (Fig. 3.31).

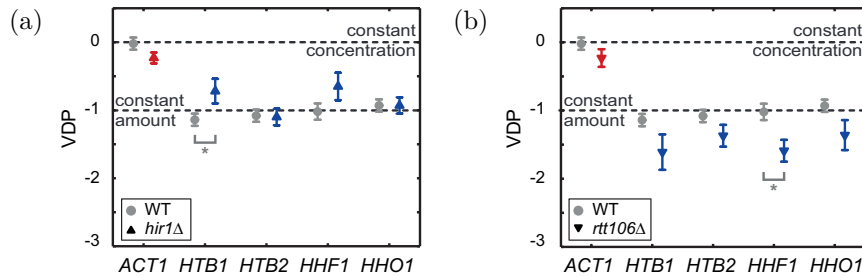


Figure 3.31: **Summary of *VDPs* for deletion strains.** *VDP* of *hir1* Δ (a) and *rtt106* Δ (b) deletion strains. *VDPs* were determined as the slopes of the linear fits to the double logarithmic dependence of concentration on cell volume (fit through $n_{ACT1}^{hir1\Delta} = n_{HTB2}^{hir1\Delta} = n_{HHF1}^{hir1\Delta} = n_{HHO1}^{hir1\Delta} = 30$, $n_{HTB1}^{hir1\Delta} = 28$ (a), and $n_{ACT1}^{rtt106\Delta} = n_{HTB1}^{rtt106\Delta} = n_{HTB2}^{rtt106\Delta} = n_{HHF1}^{rtt106\Delta} = 12$, $n_{HHO1}^{rtt106\Delta} = 11$ (b) biological replicates). Error bars indicate the standard error of the *VDPs*. Significant *VDP* deviation from the "wild-type" (carrying no deletion) *VDP* was tested using linear regressions; * $p < 0.05$

The *VDP* of *ACT1* remains unaffected by both the deletion of *HIR1* and *RTT106*. In addition, all histone genes investigated in both the *hir1* Δ and the *rtt106* Δ cells still have negative *VDPs* of around -1 , and are not significantly different than the wild-type *VDPs*. Only the *VDP* of *HTB1* in the *hir1* Δ is significantly less negative, and the *VDP* of *HHF1* in the *rtt106* Δ is significantly more negative.

This means that the histone transcript concentrations still decrease as a function of cell volume, even when deleting *HIR1* or *RTT106*. For most of the histone genes investigated, this decrease in concentration with $c \approx 1/V$ still corresponds to keeping constant amounts as a function of cell volume. Thus, in general, neither *Hir1* nor *Rtt106* seem to play an essential role in the regulation of histone transcript concentrations with cell volume. In fact, those results support the idea that the coupling of histone concentrations to gene copy number, and not to cell volume, is an intrinsic property of the histone promoters,

not requiring HIR-dependent feedback mechanisms on the transcript level.

3.8.3 Transcriptional feedback might contribute to the cell volume dependent regulation by the *HTB1* promoter

Those additional experiments, and all experiments performed so far, suggest that histone promoters achieve a coupling of histones to genome content by a constant transcription rate, which is independent of cell volume and gene copy number. However, during the analyses of the experiments one additional question opened up. In ch. 3.6, I have shown that decreasing the promoter strength of either the *HTB1* or the *HHF1* promoter can shift their behaviour ($VDP \approx -1$, $\frac{C_{diploid}}{C_{haploid}} \approx 1$) towards an actin-like behaviour ($VDP \approx 0$, $\frac{C_{diploid}}{C_{haploid}} \approx 0.5$), as was predicted by the minimal model (ch. 3.5). For both promoters, this shift in behaviour happens between the 450 bp and 350 bp truncation, coinciding with the partial loss of the upstream activating sequences (UAS). In the case of the *HTB1* promoter though, the section lost for the 300 bp truncation also includes the NEG element [Osley, 1991, Mariño-Ramírez et al., 2006] (Fig. 3.20, left). For the *HHF1* promoter, the NEG element is already lost in the 450 bp truncation (Fig. 3.20, right). As described in chapter 1, the NEG element is necessary for the HIR-complex-dependent negative feedback mechanism on transcription [Osley and Lycan, 1987].

The results obtained on the *HTB1* promoter with live-cell fluorescence microscopy and smFISH (ch. 3.7) suggest that the decrease of transcript concentrations is not due to a change in the duration of S-phase as a function of cell volume. However, if some kind of transcriptional feedback mechanism sensing the amount of histone proteins acts uniformly throughout S-phase, it could still play a role in the regulation of histone concentrations with cell volume. Even though the experiments described above (ch. 3.8.2) suggest that HIR-complex-mediated feedback is not necessary for the regulation of histone transcript concentrations, the VDP calculated for *HTB1* in *hir1Δ* cells was the only one significantly changed towards 0, when compared to the VDP in wild-type strains (Fig. 3.31a). Some kind of HIR-complex-mediated feedback might have a stronger effect on the promoter alone. Thus, the loss of the NEG element in the 300 bp truncation of the *HTB1* promoter

could lead to the disruption of a possible negative feedback regulation. This might be the reason for the observed switch to actin-like behaviour, and not the reduction in promoter strength.

In order to investigate whether the NEG element is important for the regulation of transcripts through the *HTB1* promoter, I deleted *HIR1* in non-inducible-Whi5 and inducible-Whi5 haploid strains already carrying the additional *HTB1* promoter driving the expression of *mCitrine*. As a control, I also deleted *HIR1* in haploid strains carrying the additional *HTB2* promoter. Since the *HTB2* promoter does not include an NEG element, *HTB2* is likely not subject to a HIR-complex-dependent regulation. Again, I performed RT-qPCR (ch. 2.4) measurements on cell populations of different mean cell volumes and determined the *VDP* of selected genes (*ACT1*, *HTB1*, *HTB2*, *mCitrine*, and *HTA1* for the *HTB1* promoter or *HTA2* for the *HTB2* promoter). Then, I compared the *VDP*s obtained in the *hir1* Δ cells to the *VDP*s obtained in cells carrying the additional promoters but where *HIR1* was not deleted (Fig. 3.32).

Similar to the results obtained previously (Fig. 3.31a), the *VDP* of endogenous *HTB1* is again significantly shifted to less negative values upon deletion of *HIR1* (Fig. 3.32a). In addition, the *VDP* of *mCitrine*, driven by the additional *HTB1* promoter, is drastically shifted towards 0, when compared to the "wild-type" cells only carrying the additional *HTB1* promoter without deleting *HIR1*. Thus, deleting *HIR1* seems to have a stronger effect on the *VDP* of transcripts driven by the *HTB1* promoter than on the *VDP* of the complete endogenous *HTB1* gene.

However, I also observe a significant shift towards 0 in the *VDP* of *mCitrine* driven by the *HTB2* promoter (Fig. 3.32b). Because of the lack of an NEG element in the *HTB2* promoter, I would have expected that the deletion of *HIR1* does not have an impact on the *VDP* of *mCitrine* driven by the *HTB2* promoter. Thus, the observed effect on the *HTB1* promoter could indeed mean that some kind of HIR-complex-mediated feedback mechanism does play a role in the regulation of *HTB1* transcript concentrations. Then, the switch of histone-like to actin-like behaviour observed for the 300 bp *HTB1* promoter truncation (ch. 3.6) could be due to the loss of the NEG element. But, I can not exclude

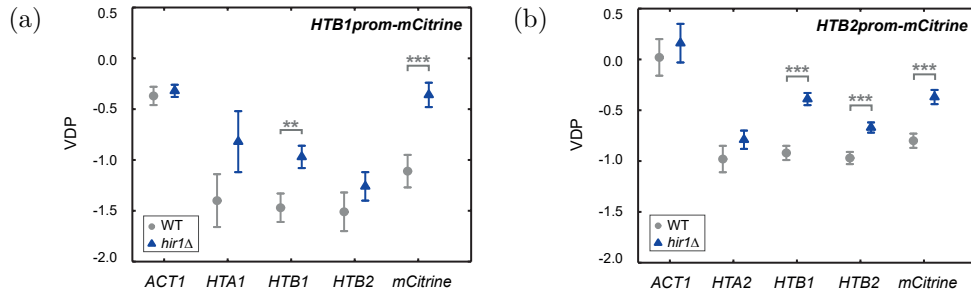


Figure 3.32: ***HIR1*-dependent regulation on the transcript level might contribute to the cell volume dependence of histone expression.** (a & b) Summary of *VDPs* for non-inducible-Whi5 and inducible-Whi5 haploid strains carrying an additional *HTB1* promoter (a) or an additional *HTB2* promoter (b) driving *mCitrine* expression (grey circles), and *hir1Δ* cells (blue triangles) in the same background, determined by RT-qPCR for *mCitrine*, *HTA1/HTA2*, *HTB1*, *HTB2* and *mCitrine*. *VDPs* were determined as the slope of the linear fit to the double logarithmic dependence of concentration on cell volume (fit through $n_{ACT1}^{hir1Δ} = n_{HTB1}^{hir1Δ} = n_{mCitrine}^{hir1Δ} = n_{ACT1}^{WT} = n_{mCitrine}^{WT} = 18$, $n_{HTA1}^{hir1Δ} = n_{HTB2}^{hir1Δ} = n_{HTA1}^{WT} = n_{HTB2}^{WT} = 12$, $n_{HTB1}^{WT} = 17$ (a), and $n = 18$ (b) biological replicates). Error bars indicate the standard error of the slope. Deviation of the *VDP* from that of the ‘wild-type’ (carrying no deletion) was tested using linear regressions; ** $p < 0.01$, *** $p < 0.001$.

that the observed behaviour of the *HTB1* and *HTB2* promoter upon deletion of *HIR1* are a result of some indirect effect due to the deletion. In addition, if the loss of the NEG element were responsible for the switch of behaviour in the *HTB1* promoter, it could still not explain the switch in the *HHF1* promoter. There, the NEG element is already lost in the 450 bp truncation, which still exhibits histone-like behaviour.

In summary, it seems that the exact regulation of histones with cell volume and gene copy number might be achieved by a combination of constant transcription rate and possible layers of transcriptional feedback sensing and degradation. However, those exact mechanisms might differ for each promoter since the NEG element, for example, is not part of all histone promoters. Different histones being subject to different mechanisms of regulation would not be that surprising, as for example dosage compensation is also only

known to happen for the *HTA1-HTB1* gene pair [Norris and Osley, 1987, Moran et al., 1990, Cross and Smith, 1988].

3.8.4 *HTB1* promoter does not show dosage compensation upon deletion of *HTB2*

As a last and additional experiment, I wanted to investigate whether the *HTB1* promoter alone is already sufficient to drive the dosage compensation when deleting *HTB2*, as observed earlier for the endogenous *HTB1* (Fig. 3.10c). In an older study, it has been reported that a *HTB1* promoter construct containing the N-terminus of the *HTB1* open reading frame (ORF) was enough to exhibit dosage compensation upon deletion of the full *HTA2-HTB2* locus [Moran et al., 1990]. Here, however, the *HTB1* promoter construct does not include the N-terminus of the ORF, and I only deleted *HTB2* in the non-inducible Whi5 haploid strain carrying the additional *HTB1* promoter driving *mCitrine* expression. I then performed RT-qPCR (ch. 2.4) and quantified the mean mRNA concentrations of *HTB1* and *mCitrine* in "wild-type" cells carrying the additional *HTB1* promoter and in *htb2* Δ cells in the same background (Fig. 3.33).

Again, I find that the concentration of endogenous *HTB1* is significantly increased upon deletion of *HTB2* (Fig. 3.33a). Surprisingly, and in contrast to what has been observed in the study by Moran et. al. [Moran et al., 1990], I do not observe a significant increase of *mCitrine* transcript concentration (Fig. 3.33b). This might be due to the fact that the *HTB1* N-terminus of the ORF is needed in order to drive dosage compensation through the promoter. Or, maybe the deletion of *HTB2* alone is not sufficient, and the whole *HTA2-HTB2* locus needs to be deleted in order to induce dosage compensation through the *HTB1* promoter.

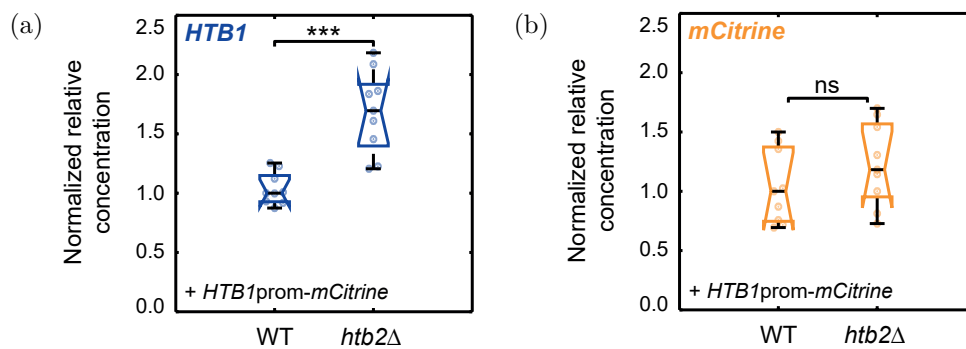


Figure 3.33: Relative *HTB1* (a) and *mCitrine* (b) mRNA concentrations (normalised on *RDN18*) for a "wild-type" non-inducible-Whi5 haploid strain carrying an additional *HTB1* promoter driving *mCitrine* expression, and a *htb2Δ* in the same background, measured by RT-qPCR. Concentrations are normalised on the respective median concentration in the "wild-type". Biological replicates are represented as coloured data points, coloured boxes highlight the 25- and 75-percentiles and whiskers extend to the minimum and the maximum of the distributions. Black, horizontal lines indicate the median of the biological replicates, notches indicate the 95% confidence interval. Significance was tested using a two-tailed, two-sample t-test at a confidence level $\alpha = 0.05$; *** $p < 0.001$.

Chapter 4

Discussion and Outlook

4.1 Overall discussion

4.1.1 Histone protein and mRNA concentrations decrease with increasing cell volume, and increase with gene copy number

This thesis started with the question of how cells could achieve to uncouple the production of histones from cell volume, and couple it to genomic DNA instead, even though the global biosynthesis of cells increases with cell volume. Thus, the aim of this thesis was to investigate the regulation of histones with cell volume and genome content, and gain insights into the molecular mechanisms involved in this regulation.

Using budding yeast as a model organism, I showed that histone protein concentrations decrease with increasing cell volume and are coupled to their gene copy number (ch. 3.2). Additionally, I showed that this regulation is already achieved at the transcript level (ch. 3.3). This finding has recently been confirmed by another study on budding yeast by RNA-seq analysis of cell populations with different mean cell volumes [Swaffer et al., 2021a]. In that study, the different mean cell volumes of the populations were achieved by first using centrifugal elutriation in order to recover cells in G1-phase. Then, cells were arrested in G1-phase, and subsequently released after increasing amounts of time spent in the G1 arrest. Thus, using another experimental technique and a different strategy to obtain cell populations of different mean cell volumes, the authors confirm one of the

central findings of this thesis, namely, that histone mRNA concentrations decrease with increasing cell volume. Moreover, another recent study on human lung fibroblasts also shows similar results [Lanz et al., 2021]. By performing triple-SILAC proteomics and determining the cell volume dependent behaviour of protein concentrations, the authors find that the concentrations of all 17 histone variants of humans decrease with increasing cell volume. This suggests that the regulation of histone concentrations with cell volume is conserved in human cells, and thus might be conserved across most eukaryotic cells.

4.1.2 Histone promoters are sufficient for regulation of histone concentrations

Having established how histone proteins and mRNA concentrations behave in relation to cell volume and gene copy number, I then showed that the histone promoters alone are sufficient to drive this regulation of their transcripts (ch. 3.4). I also showed that this regulation is not a result of the cell cycle dependent production of histones (ch. 3.7), and that transcriptional feedback and degradation mechanisms are likely not needed for it (ch. 3.8). This indicates that the decrease of histone concentrations with cell volume and increase with gene copy number is probably an intrinsic property of the histone promoters themselves.

4.1.3 Mathematical model for the dependence of transcription rates on cell volume and ploidy

In order to understand the general increase of cellular biosynthesis with cell volume, the literature has been discussing the idea of a limiting factor of the transcriptional machinery modulating genome wide transcription [Zhurinsky et al., 2010, Marguerat and Bähler, 2012, Padovan-Merhar et al., 2015, Lin and Amir, 2018, Heldt et al., 2018, Sun et al., 2020]. The general understanding is that the availability of the transcriptional machinery is limited by one single component, and that it's being titrated against the genome. This means that the transcriptional machinery gets distributed over all available

gene promoters within the genome, depending on its availability. Since the amount of transcriptional machinery increases with cell volume [Marguerat and Bähler, 2012], larger cells will therefore be able to produce more mRNA transcripts. This allows cells to keep constant concentrations of most transcripts with increasing cell volume. However, since every promoter has to compete for this limiting component, increasing the total number of promoters will result in a decrease of produced mRNA transcripts per promoter. This is in accordance with the fact that most protein concentrations are similar in diploid and haploid cells of same volume [Wu et al., 2010, Lin and Amir, 2018, Sun et al., 2020]: The produced mRNA transcript concentration per promoter is reduced in diploids, but since each gene promoter is present as two copies, the total mRNA transcript concentration is similar to the one in haploids, where each gene promoter is only present as one copy.

Following the general idea, and to better understand the different behaviour of histone promoters, I introduced a minimal mathematical model (ch. 3.5), similar to other models proposed in the literature [Heldt et al., 2018, Sun et al., 2020]. It describes promoters as single binding sites for the transcriptional machinery, and distinguishes between the general pool of promoters and a promoter of interest. This simple model, which is not taking potential transcriptional feedback or degradation into account, is sufficient to predict the behaviour of histone promoters and other promoters. For promoters having a higher initiation rate than the general pool (higher binding affinity to the transcriptional machinery), it predicts a decrease of transcript concentrations with increasing cell volume and an increase of concentration with ploidy. This describes the behaviour of transcripts driven by histone promoters, as demonstrated in this thesis (ch. 3.4), and is achieved by a constant cell-volume- and ploidy-independent transcription rate. On the other hand, the model also correctly describes the behaviour of most other promoters, and predicts that the behaviour of a histone promoter could be changed to that of most promoters by decreasing its initiation rate. In order to test this theoretical prediction, I tried to experimentally reduce the initiation rate of histone promoters by truncating them from the 5'-end, and then determined the behaviour of transcripts driven by those promoter truncations (ch. 3.6). Indeed, I was able to confirm the theoretical prediction, and change the

behaviour of two histone promoters towards the behaviour expected for most promoters.

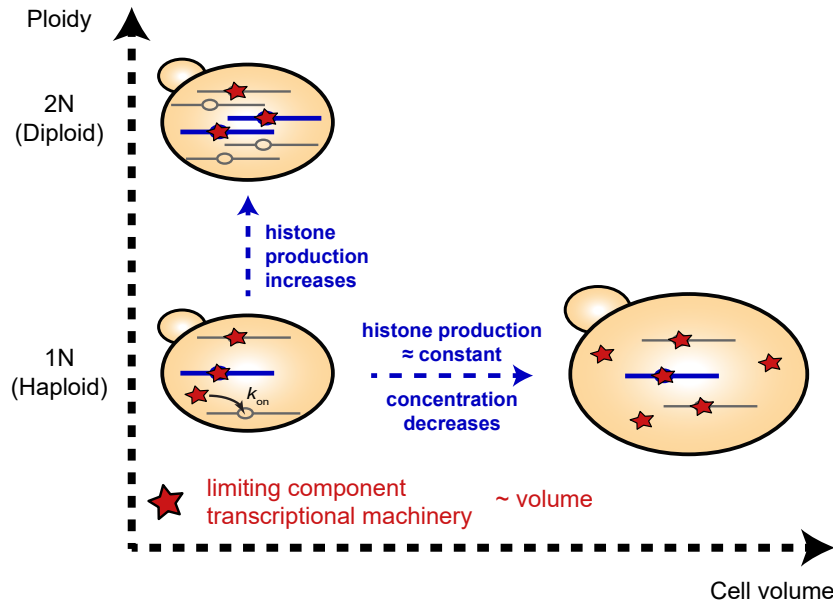


Figure 4.1: **Graphical summary.** Histone promoters produce histone transcripts at a constant rate, independent of cell volume or ploidy. Thus, even though the total biosynthetic capacity is linked to cell volume, the concentration of histone proteins decreases with increasing cell volume, but increases with ploidy.

In summary, I propose a novel mechanism that allows cells to couple the production of some proteins to cell volume, and the production of other proteins to genome content (fig. 4.1). This mechanism is an intrinsic property of the gene promoters themselves and is driven by the competition for a limiting component of the transcriptional machinery.

4.2 Outlook

4.2.1 Limitations of the current minimal model

The mathematical model describing the dependence of transcription rates on cell volume and ploidy introduced during this thesis assumes that some component of the transcriptional machinery is limiting. Strikingly, a recent study investigated potential limiting components of the transcriptional machinery and identifies the limiting component as the RNA polymerase II itself [Swaffer et al., 2021b]. However, in contrast to the general un-

derstanding until now, the authors also introduce a new mechanism that could regulate genome wide transcription with cell volume. They describe a dynamic equilibrium model, where the binding of the RNA polymerase II is determined by mass action kinetics and where RNA polymerase II is not titrated against the genome. This is consistent with their findings showing that a non-negligible percentage of the polymerase remains unbound, and that the amounts of bound RNA polymerase II are not increasing in direct proportion to cell volume. This would result in a decrease of transcript concentration with increasing cell volume. Thus, in order to maintain constant concentrations of transcripts, cells need to increase the mRNA stability with increasing cell volume. Consistent with this idea it had previously been proposed that mRNA degradation in budding yeast might be dependent on cell volume [Mena et al., 2017]. Indeed, Swaffer et. al., find that the mRNA decay rates of *MET* and *GAL* genes decrease with increasing cell volume [Swaffer et al., 2021b].

Even though the simple mechanism I propose is sufficient to explain the behaviour of histone promoters and most other promoters, it does not take mRNA degradation rates into account. For histones, transcriptional degradation controlled from the 5' UTR of the genes seems to not be responsible for the decrease of concentration with cell volume. Those regions are part of all promoter truncations investigated, and I still see a switch in promoter behaviour between the respective truncations (ch. 3.6).

However, it could still be possible that the untranscribed regions of the histone promoters have an indirect effect on transcriptional degradation through an "imprinting" mechanism, as has been suggested in a recent study [Catala and Abou Elela, 2019]. I also showed that degradation through the nuclear exosome exonuclease is not necessary for the decrease of histone mRNA concentrations (ch. 3.8). But, the minimal model can not explain why the decrease of histone mRNA concentrations is actually stronger in *rrp6Δ* cells. In addition, my results also suggest that mRNA degradation might indeed be dependent on cell volume.

Lastly, I also demonstrated that direct feedback mechanisms or HIR-mediated feedback does not seem to be of importance in order to couple histone concentrations to gene copy

number instead of cell volume (chs. 3.2, 3.3, & 3.8). However, my results on the *HTB1* promoter (ch. 3.8) also suggest that some type of transcriptional feedback regulation could be contributing to the exact regulation of *HTB1* transcript concentrations. Thus, it could well be the case that the exact type of regulation depends on the individual histone gene, and that degradation mechanisms need to be considered in order to fully understand how cells can couple histone proteins to genome content, and most other proteins to cell volume.

4.2.2 Possible further experiments

To gain more insights, it would be of interest to measure the degradation rates of histone transcripts as a function of cell volume. mRNA synthesis and degradation rates have previously been measured by using 4-Thiouracil (4tU) metabolic labelling [Miller et al., 2011, Schulz et al., 2013]. Performing metabolic labelling experiments on cell populations of different mean cell volumes could help answer whether the degradation of histone transcripts is dependent on cell volume or not. Additionally, using a combination of metabolic labelling and RNA-seq could give insights into the cell volume dependence of genome wide degradation rates.

In order to better understand the regulation of histone concentrations with cell volume and gene copy number, it will also be of importance to investigate the molecular mechanisms involved. For example, revealing which transcription factors or other molecules bind on the histone promoters, and investigating whether the occupancy is dependent on cell volume might help to better understand the regulation of histones. A technique developed by Hamperl, et. al. for budding yeast [Hamperl et al., 2014a, Hamperl et al., 2014b] could be employed in order to do this. Briefly, this technique is based on site-specific recombination of DNA and therefore allows for the purification of selected chromosomal domains. Combining this technique with mass spectrometry would allow identifying which molecules bind on the histone promoters. Again, performing experiments on cell populations of different mean cell volumes might also answer whether the occupancy of histone promoters are dependent on cell volume or not.

4.2.3 Cells need a general mechanism for the regulation of all protein subsets

To summarise, in order to understand the differential behaviour of histone concentrations with cell volume and ploidy, I introduced a mathematical model, only taking binding affinity to the transcriptional machinery into account. This minimal model is enough to explain how cells can achieve to couple the production of most proteins to cell volume, and the production of other proteins, such as histones, to genome content instead. However, the exact regulation of each individual histone gene seems to be more complex than this model can explain. Possible degradation mechanisms will likely have to be taken into account in order to fully understand genome wide regulation of proteins with cell volume and genome content.

In this thesis, I focused on the regulation of histones in budding yeast, since they are a good model to study a different regulation with cell volume and genome content than the regulation of most other genes. However, the concentration of other proteins, like the cell cycle regulators Whi5 in budding yeast or Rb in mammalian cells, have also been shown to decrease as a function of cell volume [[Schmoller et al., 2015](#), [Zatulovskiy et al., 2020](#)]. Another recent study also suggests that this is the case for a variety of cell cycle regulators [[Chen et al., 2020](#)]. In general, I speculate that the production of most DNA binding proteins might be decoupled from cell volume, and coupled to genome content instead, which is in accordance with findings of recent studies [[Swaffer et al., 2021a](#), [Lanz et al., 2021](#)]. In addition, proteins associated with the cell surface are likely also not produced in direct proportion to cell volume, since the surface area of cells does not increase in direct proportion to cell volume [[Galitski, 1999](#), [Wu et al., 2010](#), [Marguerat and Bähler, 2012](#)]. Thus, even though the concentration of the majority of proteins might stay constant as a function of cell volumes, many different protein subgroups might show a different regulation. It has indeed been shown in a recent study that some protein subsets exhibit sub-scaling behaviour (decrease of concentration with cell volume) and others super-scaling (increase of concentration with cell volume) behaviour [[Lanz et al., 2021](#)].

In general, keeping accurate protein concentrations as a function of cell volume or ploidy is of crucial importance for the survival of cells [Alberts et al., 2002]. Especially when subject to drastic changes in cell growth due to environmental changes, differentiation or development [Conrad et al., 2014, Aiken et al., 2004, Tsihlaki and FitzHarris, 2016], cells still need to be able to maintain correct protein concentrations. Thus, fully understanding how cells regulate the production of different subsets of proteins depending on cell volume or ploidy is a key biological question.

The minimal model introduced in this thesis allows the modulation of promoter behaviours not only by tuning their initiation rates, but also their elongation rates. Thus, the regulation of synthesised transcripts with cell volume and ploidy can be decoupled from the expression level of the promoters. In addition, by either tuning the initiation rate or the elongation rate, a variety of different cell-volume- and ploidy-dependent regulations of transcript concentrations can be achieved. Like most fundamental processes, the regulation of protein subsets with cell volume and ploidy is likely conserved across most eukaryotes. Thus, this minimal model lays a foundation for the deeper understanding of protein homeostasis with cell volume and ploidy.

Appendix A

Parameter sets for the minimal model

To calculate the behaviour of transcript concentrations, c_p , predicted by the minimal model, I set $c_{TM} = 2000$, $k_{on}^g = 1$, $k_{off}^g = k_{off}^p = 3$ and calculated the steady-state concentration both in haploids ($n_h = 6000$) and in diploids ($n_d = 12000$) over cell volume for $k_{on}^p = [0.01, 100]$.

In order to determine the VDP as a function of k_{on}^p , or k_{off}^p , I calculated the concentration for each value of k_{on}^p , or k_{off}^p , over a cell volume range of $V = [\frac{1}{3}, 3]$ and performed a linear regression fit on the logarithm of the concentration as a function of the logarithm of the cell volume, with cell volumes being equally spaced on the log scale. The VDP was then determined as the slope of the linear fit.

In order to determine the concentration ratio between diploids and haploids as a function of k_{on}^p , or k_{off}^p , I calculated the concentration at a characteristic volume V_0 both in haploids and in diploids for each value of k_{on}^p , or k_{off}^p . Then, I calculated the ratio of the concentration in diploids compared to the concentration in haploids.

Appendix B

Statistical analyses and error estimations

B.1 Testing significance of the Volume-Dependence-Parameter

To test for a significant deviation of the VDP from 0, I performed two-tailed one-sample t-tests on the regression coefficients of the linear fit at a confidence level of $\alpha = 0.05$. The null hypothesis H_0 assumes the respective coefficient to be equal to 0. In order to test for the significance of the VDP , I was interested in the slope of the linear fit: for a p-value smaller than α , I rejected H_0 and consider the slope, i.e. the VDP , to be significantly different from 0.

To test whether the VDP s of two different conditions significantly deviate from each other, I used a general linear regression model with a categorical variable, $Type$, to differentiate between the two conditions analysed:

$$\log_2(c) = \log_2(c_0) + VDP_0 \cdot \log_2(V) + \delta_1 \cdot Type + \delta_2 \cdot Type \cdot \log_2(V) \quad (\text{B.1})$$

with c_0 and VDP_0 corresponding to the reference condition ($Type = 0$), δ_1 describing the average difference in the intercepts of the linear fits between the two conditions, and δ_2 describing the change in the slopes (VDP s) between the two conditions. In order to test for a significant difference between the two VDP s, I performed a two-tailed one-sample t-

test on δ_2 , with the null hypothesis H_0 assuming $\delta_2 = 0$, at a confidence level of $\alpha = 0.05$. For a p-value smaller than α , I rejected H_0 and consider the change between the two slopes to be significant, i.e. I consider the two *VDPs* to be significantly different from each other.

B.2 Comparison of population means

When comparing distributions of mean cell volumes determined with a Coulter counter, or mRNA concentrations determined with either RT-qPCR or smFISH, I performed the following statistical tests to assess whether the population means were significantly different from each other. First, I performed a Shapiro-Wilk test at a confidence level of $\alpha = 0.05$ to test whether the distributions were normally distributed. For normal distributions, I then performed a Bartlett test at a confidence level of $\alpha = 0.05$ to test whether equal variances of the distributions could be assumed. If this was the case, I performed a two-tailed, two sample t-test assuming equal variances with the null hypothesis H_0 assuming equal means, at a confidence level of $\alpha = 0.05$. If I could not assume equal variances, I performed a two-tailed, two sample t-test assuming unequal variances. For a p-value smaller than α , I rejected H_0 and consider the means of the distributions to be significantly different from each other.

If I could not assume normal distributions, after performing the Shapiro-Wilk test, I performed a Kruskal-Wallis test with the null hypothesis H_0 assuming that the distributions are from the same population, at a confidence level of $\alpha = 0.05$. For a p-value smaller than α , I rejected H_0 and consider the distributions to not be from the same population.

B.3 Error estimation of concentrations at a set cell volume

To calculate concentrations at a characteristic cell volume of 60 fL with respective error estimates, I evaluated the linear fits to the double logarithmic data at 60 fL and estimated

the 95 % confidence intervals of the fit at 60 fL. When normalising the concentration to a chosen value x , errors were calculated using error propagation:

$$\Delta y = y \cdot \sqrt{\left(\frac{\Delta c^2}{c^2}\right)^2 + \left(\frac{\Delta x^2}{x^2}\right)^2} \quad (\text{B.2})$$

with y being the new normalised concentration and c the previously calculated concentration. To estimate the error associated with the ratio between the concentrations at 60 fL in haploids and diploids, I used bootstrap analysis. Specifically, I treated the measurements of protein or mRNA concentration and corresponding cell volume as a set of linked variables, both for haploid and diploid cells. I then resampled $n = 10000$ populations of same size by random sampling with replacement from this experimental two-dimensional population. Next, I performed a linear regression on the double logarithmic data for each of the resampled populations and estimated the concentration at 60 fL, giving us a distribution of $n = 10000$ concentrations at 60 fL for both haploid and diploid cells. Finally, I randomly selected a concentration in each of those distributions, and divided the concentration for diploids by the concentration for haploids. I repeated this process 10000 times with replacement to obtain a distribution of $n = 10000$ concentration ratios, for which I calculated the median and the 2.5- and 97.5-percentiles.

Appendix C

qPCR primer

Table C.1 shows the results of the RT-qPCR measurements on deletion strains, performed by Daniela Bureik where possible in order to determine the specificity of the qPCR primers on histone genes. The qPCR primer sequences are shown in table C.2.

qPCR primer	MS63-1 [mean C_P^{Gene}]	Δ strain [C_P range]
HHO1	20.3 ± 0.1	no amplification
HTB2	16.8 ± 0.1	40.9 – no amplification
HHF1	17.7 ± 0.3	34.6 – no amplification
HHF2	19.5 ± 0.1	33.6 – 35.9
HHT1	18.0 ± 0.1	32.9 – no amplification
HHT2	19.0 ± 1.4	33.7 – no amplification

Table C.1: Results of RT-qPCR measurements on deletion strains to test for primer specificity.

Gene	qPCR primer direction	qPCR primer sequence (5' - 3')
<i>ACT1</i>	forward	AGTTGCCCCAGAAGAACACC
	reverse	GGACAAAACGGCTTGGATGG
<i>ENO2</i>	forward	TTGTTCCATCTGGTGCCTCC
	reverse	ACGAAAGCAGCAGCAATGAC
<i>HHF1</i>	forward	TACACCGAACACGCCAAGAG
	reverse	TTGCTTGTTGTTACCGTTTTCTT

Gene	qPCR primer direction	qPCR primer sequence (5' - 3')
<i>HHF2</i>	forward	ACGAAGAAGTCAGAGCCGTC
	reverse	ACCGATTGTTTAACCACCGATTG
<i>HHO1</i>	forward	ACCAGCAAAGGCAAGGAGAA
	reverse	AAAGCCGTGAGCCCTTCAAT
<i>HHT1</i>	forward	CAATCTTCTGCCATCGGTGC
	reverse	ACTGATGACAATCAACAACTATGA
<i>HHT2</i>	forward	AGCAAACACTCCACAATGGC
	reverse	CAAGGCAACAGTACCTGGCT
<i>HTA1</i>	forward	GTTGCCAAAGAAGTCTGCCA
	reverse	CAGTTTAGTTCCTTCCGCCTT
<i>HTA2</i>	forward	TCGCCCAAGGTGGTGTFFF
	reverse	TGATTTGCTTTGTTTCTTTTCAACT
<i>HTB1</i>	forward	TACACACATACAATGTCTGCTAAAG
	reverse	AGTGTCAGGGTGAGTTTGCTT
<i>HTB2</i>	forward	CCTCTGCCGCCGAAAAGAAA
	reverse	TCTTACCATCGACGGAGGTTG
<i>mCitrine</i>	forward	GAGCTGAAGGGCATCGACTT
	reverse	TTCTGCTTGTCGGCCATGAT
<i>RDN18</i>	forward	AACTCACCAGGTCCAGACACAATAAGG
	reverse	AAGGTCTCGTTCGTTATCGCAATTAAGC
<i>RPB1</i>	forward	CCAGAAGTGGTCACACCATATAA
	reverse	GGTCTCCGCTATCACGAATG
<i>RPB3</i>	forward	TGTGGGGTCTATTCCCGTTG
	reverse	CGCCCGTCATCATTACGTCT

Table C.2: Sequences of all qPCR primers used in this work.

Appendix D

Yeast strains

Table D.1 shows all strains used for this work. Strains generated by myself or my student Petia Adarska are denoted as KCY. Similarly, strains generated by Anika Seel are denoted as ASY, by Daniela Bureik as DBY and by Dr. Kurt Schmoller as KSY, all members of the Schmoller lab at HMGU. MMY116-2C, MS62-1 and MS63-1 were gifted by the Skotheim lab at Stanford University.

Name	Genotype	Description
ASY020-1	<i>Mat a/a; ADE2/ADE2, URA3/ura3, leu2/LEU2</i>	Non-inducible <i>WHI5</i> , diploid strain. Also used as microscopy background
ASY023-1	<i>Mat a/a; ADE2/ADE2, URA3/ura3, WHI5/whi5Δ::kanMX6-LexAprom-WHI5-ADH1term-LEU2, his3/his3::LexA-ER-AD-TF-HIS3</i>	Inducible <i>WHI5</i> , diploid strain. Used as microscopy background
DBY001-2	<i>Mat a; ADE2, htb2Δ::KlacURA3</i>	Non-inducible <i>WHI5</i> , haploid <i>htb2Δ</i> strain
DBY002-1	<i>Mat a; ADE2, whi5Δ::kanMX6-LexAprom-WHI5-ADH1term-LEU2, his3::LexA-ER-AD-TF-HIS3, htb2Δ::KlacURA3</i>	Inducible <i>WHI5</i> , haploid <i>htb2Δ</i> strain
DBY003-1	<i>Mat a; ADE2, whi5Δ::kanMX6-LexAprom-WHI5-ADH1term-LEU2, his3::LexA-ER-AD-TF-HIS3, hho1Δ::CglaTRP1</i>	Inducible <i>WHI5</i> , haploid <i>hho1Δ</i> strain

Name	Genotype	Description
DBY008-1	<i>Mat a; ADE2, whi5Δ::kanMX6-LexAprm-WHI5-ADH1term-LEU2, his3::LexA-ER-AD-TF-HIS3, hhf1Δ::CglaTRP1</i>	Inducible <i>WHI5</i> , haploid <i>hhf1Δ</i> strain
DBY009-1	<i>Mat a; ADE2, hhf2Δ::CglaTRP1</i>	Non-inducible <i>WHI5</i> , haploid <i>hhf2Δ</i> strain
DBY011-1	<i>Mat a; ADE2, hht1Δ::CglaTRP1</i>	Non-inducible <i>WHI5</i> , haploid <i>hht1Δ</i> strain
DBY013-1	<i>Mat a; ADE2, hht2Δ::CglaTRP1</i>	Non-inducible <i>WHI5</i> , haploid <i>hht2Δ</i> strain
DBY020-2	<i>Mat a; ADE2, ura3::CglaTRP1-HTB1prom-mCitrine-ADH1term-URA3</i>	Non-inducible <i>WHI5</i> , haploid strain with additional copy of <i>HTB1</i> promoter expressing <i>mCitrine</i>
DBY021-3	<i>Mat a; ADE2, ura3::CglaTRP1-HTB2prom-mCitrine-ADH1term-URA3</i>	Non-inducible <i>WHI5</i> , haploid strain with additional copy of <i>HTB2</i> promoter expressing <i>mCitrine</i>
DBY022-1	<i>Mat a; ADE2, ura3::CglaTRP1-HHF1prom-mCitrine-ADH1term-URA3</i>	Non-inducible <i>WHI5</i> , haploid strain with additional copy of <i>HHF1</i> promoter expressing <i>mCitrine</i>
DBY027-11	<i>Mat a; ADE2, ura3::CglaTRP1-HTB1prom-mCitrine-ADH1term-URA3, his3::ACT1prom-mKate2-ADH1term-HIS3, htb2Δ::LEU2</i>	Non-inducible <i>WHI5</i> , haploid <i>htb2Δ</i> strain with additional copy of <i>HTB1</i> promoter expressing <i>mCitrine</i> and additional copy of <i>ACT1</i> promoter expressing <i>mKate2</i>
DCY003-6	<i>Mat a; ADE2, htb1::HTB1-linker-mCitrine-ADH1term-URA3</i>	Non-inducible <i>WHI5</i> , haploid strain with <i>HTB1</i> tagged with <i>mCitrine</i>
DCY008-8	<i>Mat a; ADE2, ura3::CglaTRP1-HTB1prom-mCitrine-ADH1term-URA3, his3::ACT1prom-mKate2-ADH1term-HIS3</i>	Non-inducible <i>WHI5</i> , haploid strain with additional copy of <i>HTB1</i> promoter expressing <i>mCitrine</i> and additional copy of <i>ACT1</i> promoter expressing <i>mKate2</i>

Name	Genotype	Description
KCY001-3	<i>Mat a; ADE2, htb2::HTB2-linker-mCitrine-ADH1term-CglaTRP1, whi5Δ::kanMX6-LexAprom-WHI5-ADH1term-LEU2, his3::LexA-ER-AD-TF-HIS3</i>	Inducible <i>WHI5</i> , haploid strain with <i>HTB2</i> tagged with <i>mCitrine</i>
KCY002-3	<i>Mat a; ADE2, htb2::HTB2-linker-mCitrine-ADH1term-CglaTRP1</i>	Non-inducible <i>WHI5</i> , haploid strain with <i>HTB2</i> tagged with <i>mCitrine</i>
KCY005-1	<i>Mat a/a; ADE2/ADE2, whi5Δ::CglaTRP1/whi5Δ::kanMX6-LexAprom-WHI5-ADH1term-LEU2, his3/his3::LexA-ER-AD-TF-HIS3</i>	Inducible <i>WHI5</i> , diploid strain. Also used as microscopy background
KCY006-1	<i>Mat a/a; ADE2/ADE2, htb2Δ::KlacURA3/HTB2, whi5Δ::CglaTRP1/whi5Δ::kanMX6-LexAprom-WHI5-ADH1term-LEU2, his3/his3::LexA-ER-AD-TF-HIS3</i>	Inducible <i>WHI5</i> , diploid strain with one <i>HTB2</i> allele deleted
KCY007-2	<i>Mat a; ADE2, ura3::CglaTRP1-150bpHHF1prom-mCitrine-ADH1term-URA3</i>	Non-inducible <i>WHI5</i> , haploid strain with additional 150 bp of <i>HHF1</i> promoter (truncated 5' – 3') expressing <i>mCitrine</i>
KCY008-1	<i>Mat a; ADE2, ura3::CglaTRP1-300bpHHF1prom-mCitrine-ADH1term-URA3</i>	Non-inducible <i>WHI5</i> , haploid strain with additional 300 bp of <i>HHF1</i> promoter (truncated 5' – 3') expressing <i>mCitrine</i>
KCY009-1	<i>Mat a; ADE2, ura3::CglaTRP1-450bpHHF1prom-mCitrine-ADH1term-URA3</i>	Non-inducible <i>WHI5</i> , haploid strain with additional 450 bp of <i>HHF1</i> promoter (truncated 5' – 3') expressing <i>mCitrine</i>
KCY010-2	<i>Mat a; ADE2, ura3::CglaTRP1-600bpHHF1prom-mCitrine-ADH1term-URA3</i>	Non-inducible <i>WHI5</i> , haploid strain with additional 600 bp of <i>HHF1</i> promoter (truncated 5' – 3') expressing <i>mCitrine</i>
KCY011-1	<i>Mat a; ADE2, ura3::CglaTRP1-150bpHHF1prom-mCitrine-ADH1term-URA3, whi5Δ::kanMX6-LexAprom-WHI5-ADH1term-LEU2, his3::LexA-ER-AD-TF-HIS3</i>	Inducible <i>WHI5</i> , haploid strain with additional 150 bp of <i>HHF1</i> promoter (truncated 5' – 3') expressing <i>mCitrine</i>

Name	Genotype	Description
KCY012-1	<i>Mat a; ADE2, ura3::CglaTRP1-300bpHHF1prom-mCitrine-ADH1term-URA3, whi5Δ::kanMX6-LexAprom-WHI5-ADH1term-LEU2, his3::LexA-ER-AD-TF-HIS3</i>	Inducible <i>WHI5</i> , haploid strain with additional 300 bp of <i>HHF1</i> promoter (truncated 5' – 3') expressing <i>mCitrine</i>
KCY013-1	<i>Mat a; ADE2, ura3::CglaTRP1-450bpHHF1prom-mCitrine-ADH1term-URA3, whi5Δ::kanMX6-LexAprom-WHI5-ADH1term-LEU2, his3::LexA-ER-AD-TF-HIS3</i>	Inducible <i>WHI5</i> , haploid strain with additional 450 bp of <i>HHF1</i> promoter (truncated 5' – 3') expressing <i>mCitrine</i>
KCY014-1	<i>Mat a; ADE2, ura3::CglaTRP1-600bpHHF1prom-mCitrine-ADH1term-URA3, whi5Δ::kanMX6-LexAprom-WHI5-ADH1term-LEU2, his3::LexA-ER-AD-TF-HIS3</i>	Inducible <i>WHI5</i> , haploid strain with additional 600 bp of <i>HHF1</i> promoter (truncated 5' – 3') expressing <i>mCitrine</i>
KCY015-1	<i>Mat a; ADE2, ura3::CglaTRP1-150bpHTB1prom-mCitrine-ADH1term-URA3, whi5Δ::kanMX6-LexAprom-WHI5-ADH1term-LEU2, his3::LexA-ER-AD-TF-HIS3</i>	Inducible <i>WHI5</i> , haploid strain with additional 150 bp of <i>HTB1</i> promoter (truncated 5' – 3') expressing <i>mCitrine</i>
KCY016-1	<i>Mat a; ADE2, ura3::CglaTRP1-300bpHTB1prom-mCitrine-ADH1term-URA3, whi5Δ::kanMX6-LexAprom-WHI5-ADH1term-LEU2, his3::LexA-ER-AD-TF-HIS3</i>	Inducible <i>WHI5</i> , haploid strain with additional 300 bp of <i>HTB1</i> promoter (truncated 5' – 3') expressing <i>mCitrine</i>
KCY017-1	<i>Mat a; ADE2, ura3::CglaTRP1-450bpHTB1prom-mCitrine-ADH1term-URA3, whi5Δ::kanMX6-LexAprom-WHI5-ADH1term-LEU2, his3::LexA-ER-AD-TF-HIS3</i>	Inducible <i>WHI5</i> , haploid strain with additional 450 bp of <i>HTB1</i> promoter (truncated 5' – 3') expressing <i>mCitrine</i>

Name	Genotype	Description
KCY018-1	<i>Mat a; ADE2, ura3::CglaTRP1-600bpHTB1prom-mCitrine-ADH1term-URA3, whi5Δ::kanMX6-LexAprom-WHI5-ADH1term-LEU2, his3::LexA-ER-AD-TF-HIS3</i>	Inducible <i>WHI5</i> , haploid strain with additional 600 bp of <i>HTB1</i> promoter (truncated 5' – 3') expressing <i>mCitrine</i>
KCY019-1	<i>Mat a; ADE2, ura3::CglaTRP1-750bpHTB1prom-mCitrine-ADH1term-URA3, whi5Δ::kanMX6-LexAprom-WHI5-ADH1term-LEU2, his3::LexA-ER-AD-TF-HIS3</i>	Inducible <i>WHI5</i> , haploid strain with additional 750 bp of <i>HTB1</i> promoter (truncated 5' – 3') expressing <i>mCitrine</i>
KCY020-1	<i>Mat a; ADE2, ura3::CglaTRP1-150bpHTB1prom-mCitrine-ADH1term-URA3</i>	Non-inducible <i>WHI5</i> , haploid strain with additional 150 bp of <i>HTB1</i> promoter (truncated 5' – 3') expressing <i>mCitrine</i>
KCY021-1	<i>Mat a; ADE2, ura3::CglaTRP1-300bpHTB1prom-mCitrine-ADH1term-URA3</i>	Non-inducible <i>WHI5</i> , haploid strain with additional 300 bp of <i>HTB1</i> promoter (truncated 5' – 3') expressing <i>mCitrine</i>
KCY022-1	<i>Mat a; ADE2, ura3::CglaTRP1-450bpHTB1prom-mCitrine-ADH1term-URA3</i>	Non-inducible <i>WHI5</i> , haploid strain with additional 450 bp of <i>HTB1</i> promoter (truncated 5' – 3') expressing <i>mCitrine</i>
KCY023-4	<i>Mat a; ADE2, ura3::CglaTRP1-600bpHTB1prom-mCitrine-ADHterm-URA3</i>	Non-inducible <i>WHI5</i> , haploid strain with additional 600 bp of <i>HTB1</i> promoter (truncated 5' – 3') expressing <i>mCitrine</i>
KCY024-1	<i>Mat a; ADE2, ura3::CglaTRP1-750bpHTB1prom-mCitrine-ADH1term-URA3</i>	Non-inducible <i>WHI5</i> , haploid strain with additional 750 bp of <i>HTB1</i> promoter (truncated 5' – 3') expressing <i>mCitrine</i>
KCY027-4	<i>Mat a/a; ADE2/ADE2, htb2::HTB2-linker-mCitrine-ADH1term-CglaTRP1/htb2::HTB2-linker-mCitrine-ADH1term-KlacURA3</i>	Non-inducible <i>WHI5</i> , diploid strain with both <i>HTB2</i> alleles tagged with <i>mCitrine</i>

Name	Genotype	Description
KCY028-1	<i>Mat a/a; ADE2/ADE2, htb2::HTB2-linker-mCitrine-ADH1term-KlacURA3/htb2::HTB2-linker-mCitrine-ADH1term-CglaTRP1, whi5Δ::CglaTRP1/whi5Δ::kanMX6-LexAprom- WHI5-ADH1term-LEU2, his3/his3::LexA-ER-AD-TF-HIS3</i>	Inducible <i>WHI5</i> , diploid strain with both <i>HTB2</i> alleles tagged with <i>mCitrine</i>
KCY029-1	<i>Mat a/a; ADE2/ADE2, htb2Δ::KlacURA3/htb2::HTB2-linker-mCitrine-ADH1term-CglaTRP1, whi5Δ::CglaTRP1/whi5Δ::kanMX6-LexAprom- WHI5-ADH1term-LEU2, his3/his3::LexA-ER-AD-TF-HIS3</i>	Inducible <i>WHI5</i> , diploid strain with one <i>HTB2</i> allele deleted and the other <i>HTB2</i> allele tagged with <i>mCitrine</i>
KCY031-1	<i>Mat a/a; ADE2/ADE2, ura3::CglaTRP1-HTB1prom-mCitrine-ADH1term-URA3/ura3, WHI5/whi5Δ::kanMX6-LexAprom- WHI5-ADH1term-LEU2, his3/his3::LexA-ER-AD-TF-HIS3</i>	Inducible <i>WHI5</i> , diploid strain with additional copy of <i>HTB1</i> promoter expressing <i>mCitrine</i>
KCY032-2	<i>Mat a/a; ADE2/ADE2, ura3::CglaTRP1-HHF1prom-mCitrine-ADH1term-URA3/ura3, WHI5/whi5Δ::kanMX6-LexAprom- WHI5-ADH1term-LEU2, his3/his3::LexA-ER-AD-TF-HIS3</i>	Inducible <i>WHI5</i> , diploid strain with additional copy of <i>HHF1</i> promoter expressing <i>mCitrine</i>
KCY033-2	<i>Mat a/a; ADE2/ADE2, ura3::CglaTRP1-HTB2prom-mCitrine-ADH1term-URA3/ura3, WHI5/whi5Δ::kanMX6-LexAprom- WHI5-ADH1term-LEU2, his3/his3::LexA-ER-AD-TF-HIS3</i>	Inducible <i>WHI5</i> , diploid strain with additional copy of <i>HTB2</i> promoter expressing <i>mCitrine</i>
KCY035-3	<i>Mat a/a; ADE2/ADE2, ura3::CglaTRP1-ACT1prom-mCitrine-ADH1term-URA3/ura3, WHI5/whi5Δ::kanMX6-LexAprom- WHI5-ADH1term-LEU2, his3/his3::LexA-ER-AD-TF-HIS3</i>	Inducible <i>WHI5</i> , diploid strain with additional copy of <i>ACT1</i> promoter expressing <i>mCitrine</i>

Name	Genotype	Description
KCY038-1	<i>Mat a/a; ADE2/ADE2, ura3::CglaTRP1-300bpHTB1prom-mCitrine-ADH1term-URA3/ura3, leu2/LEU2</i>	Non-inducible <i>WHI5</i> , diploid strain with additional 300 bp of <i>HTB1</i> promoter (truncated 5' – 3') expressing <i>mCitrine</i>
KCY039-1	<i>Mat a/a; ADE2/ADE2, ura3::CglaTRP1-300bpHTB1prom-mCitrine-ADH1term-URA3/ura3, WHI5/whi5Δ::kanMX6-LexAprom-WHI5-ADH1term-LEU2, his3/his3::LexA-ER-AD-TF-HIS3</i>	Inducible <i>WHI5</i> , diploid strain with additional 300 bp of <i>HTB1</i> promoter (truncated 5' – 3') expressing <i>mCitrine</i>
KCY040-1	<i>Mat a/a; ADE2/ADE2, ura3::CglaTRP1-450bpHTB1prom-mCitrine-ADH1term-URA3/ura3, leu2/LEU2</i>	Non-inducible <i>WHI5</i> , diploid strain with additional 450 bp of <i>HTB1</i> promoter (truncated 5' – 3') expressing <i>mCitrine</i>
KCY041-1	<i>Mat a/a; ADE2/ADE2, ura3::CglaTRP1-450bpHTB1prom-mCitrine-ADH1term-URA3/ura3, WHI5/whi5Δ::kanMX6-LexAprom-WHI5-ADH1term-LEU2, his3/his3::LexA-ER-AD-TF-HIS3</i>	Inducible <i>WHI5</i> , diploid strain with additional 450 bp of <i>HTB1</i> promoter (truncated 5' – 3') expressing <i>mCitrine</i>
KCY043-1	<i>Mat a/a; ADE2/ADE2, ura3::CglaTRP1-300bpHHF1prom-mCitrine-ADH1term-URA3ura3, WHI5/whi5Δ::kanMX6-LexAprom-WHI5-ADH1term-LEU2, his3/his3::LexA-ER-AD-TF-HIS3</i>	Inducible <i>WHI5</i> , diploid strain with additional 300 bp of <i>HHF1</i> promoter (truncated 5' – 3') expressing <i>mCitrine</i>
KCY045-1	<i>Mat a/a; ADE2/ADE2, ura3::CglaTRP1-450bpHHF1prom-mCitrine-ADH1term-URA3/ura3, WHI5/whi5Δ::kanMX6-LexAprom-WHI5-ADH1term-LEU2, his3/his3::LexA-ER-AD-TF-HIS3</i>	Inducible <i>WHI5</i> , diploid strain with additional 450 bp of <i>HHF1</i> promoter (truncated 5' – 3') expressing <i>mCitrine</i>
KCY049-1	<i>Mat a; ADE2, ura3::CglaTRP1-HTB1prom-mCitrine-ADH1term-URA3, hir1Δ::natMX6, whi5Δ::kanMX6-LexAprom-WHI5-ADH1term-LEU2, his3::LexA-ER-AD-TF-HIS3</i>	Inducible <i>WHI5</i> , haploid <i>hir1Δ</i> strain with additional copy of <i>HTB1</i> promoter expressing <i>mCitrine</i>

Name	Genotype	Description
KCY050-2	<i>Mat a/a; ADE2/ADE2, htb1::HTB1-linker-mCitrine-ADH1term-KlacURA3/htb1::HTB1-linker-mCitrine-ADH1term-CglaTRP1</i>	Non-inducible <i>WHI5</i> , diploid strain with both <i>HTB1</i> alleles tagged with <i>mCitrine</i>
KCY051-1	<i>Mat a; ADE2, ura3::CglaTRP1-HTB2prom-mCitrine-ADH1term-URA3, hir1Δ::natMX6, whi5Δ::kanMX6-LexAprom-WHI5-ADH1term-LEU2, his3::LexA-ER-AD-TF-HIS3</i>	Inducible <i>WHI5</i> , haploid <i>hir1Δ</i> strain with additional copy of <i>HTB2</i> promoter expressing <i>mCitrine</i>
KSY212-2	<i>Mat a; ADE2, rrp6Δ::CglaTRP1</i>	Non-inducible <i>WHI5</i> , haploid <i>rrp6Δ</i> strain
KSY213-6	<i>Mat a; ADE2, rrp6Δ::CglaTRP1, whi5Δ::kanMX6-LexAprom-WHI5-ADH1term-LEU2, his3::LexA-ER-AD-TF-HIS3</i>	Inducible <i>WHI5</i> , haploid <i>rrp6Δ</i> strain
KSY214-1	<i>Mat a; ADE2, hir1Δ::CglaTRP1</i>	Non-inducible <i>WHI5</i> , haploid <i>hir1Δ</i> strain
KSY215-2	<i>Mat a; ADE2, hir1Δ::CglaTRP1, whi5Δ::kanMX6-LexAprom-WHI5-ADH1term-LEU2, his3::LexA-ER-AD-TF-HIS3</i>	Inducible <i>WHI5</i> , haploid <i>hir1Δ</i> strain
KSY219-3	<i>Mat a; ADE2, rtt106Δ::CglaTRP1, whi5Δ::kanMX6-LexAprom-WHI5-ADH1term-LEU2, his3::LexA-ER-AD-TF-HIS3</i>	Inducible <i>WHI5</i> , haploid <i>rtt106Δ</i> strain
KSY208-3	<i>Mat a; ADE2, ura3::mCitrine-ADH1term-URA3</i>	Non-inducible <i>WHI5</i> , haploid strain with additional <i>mCitrine</i> copy (not expressed)
KSY222-1	<i>Mat a; ADE2, ura3::CglaTRP1-HTB1prom-mCitrine-ADH1term-URA3, whi5Δ::kanMX6-LexAprom-WHI5-ADH1term-LEU2, his3::LexA-ER-AD-TF-HIS3</i>	Inducible <i>WHI5</i> , haploid strain with additional copy of <i>HTB1</i> promoter expressing <i>mCitrine</i>

Name	Genotype	Description
KSY223-3	<i>Mat a; ADE2, ura3::CglaTRP1-HHF1prom-mCitrine-ADH1term-URA3, whi5Δ::kanMX6-LexAprom-WHI5-ADH1term-LEU2, his3::LexA-ER-AD-TF-HIS3</i>	Inducible <i>WHI5</i> , haploid strain with additional copy of <i>HHF1</i> promoter expressing <i>mCitrine</i>
KSY225-2	<i>Mat a; ADE2, ura3::CglaTRP1-HTB2prom-mCitrine-ADH1term-URA3, whi5Δ::kanMX6-LexAprom-WHI5-ADH1term-LEU2, his3::LexA-ER-AD-TF-HIS3</i>	Inducible <i>WHI5</i> , haploid strain with additional copy of <i>HTB2</i> promoter expressing <i>mCitrine</i>
KSY226-3	<i>Mat a; ADE2, ura3::mCitrine-ADH1term-URA3, whi5Δ::kanMX6-LexAprom-WHI5-ADH1term-LEU2, his3::LexA-ER-AD-TF-HIS3</i>	Inducible <i>WHI5</i> , haploid strain with additional <i>mCitrine</i> copy (not expressed)
KSY229-1	<i>Mat a; ADE2, ura3::CglaTRP1-ACT1prom-mCitrine-ADH1term-URA3</i>	Non-inducible <i>WHI5</i> , haploid strain with additional copy of <i>ACT1</i> promoter expressing <i>mCitrine</i>
KSY230-1	<i>Mat a; ADE2, ura3::CglaTRP1-ACT1prom-mCitrine-ADH1term-URA3, whi5Δ::kanMX6-LexAprom-WHI5-ADH1term-LEU2, his3::LexA-ER-AD-TF-HIS3</i>	Inducible <i>WHI5</i> , haploid strain with additional copy of <i>ACT1</i> promoter expressing <i>mCitrine</i>
MMY116-2C	<i>Mat a; ADE2</i>	Non-inducible <i>WHI5</i> , haploid strain. Also used as microscopy background
MS62-1	<i>Mat a; ADE2, whi5Δ::kanMX6, his3::LexA-ER-AD-TF-HIS3</i>	β-estradiol dependent transcription factor, haploid <i>whi5Δ</i> strain
MS63-1	<i>Mat a; ADE2, whi5Δ::kanMX6-LexAprom-WHI5-ADH1term-LEU2, his3::LexA-ER-AD-TF-HIS3</i>	Inducible <i>WHI5</i> , haploid strain. Also used as microscopy background

Table D.1: Yeast strains used in this work. All strains are based on W303. *CglaTRP1* denotes the *TRP1* gene of the organism *C. glabrata*, *KlacURA3* denotes the *URA3* gene of the organism *K. lactis*.

References

- [Aiken et al., 2004] Aiken, C. E. M., Swoboda, P. P. L., Skepper, J. N., and Johnson, M. H. (2004). The direct measurement of embryogenic volume and nucleo-cytoplasmic ratio during mouse pre-implantation development. *Reproduction*, 128(5):527–535.
- [Alberts et al., 2002] Alberts, B., Johnson, A., Lewis, J., Raff, M., Roberts, K., and P., W. (2002). *Molecular Biology of the Cell*. Garland Science, New York.
- [Amodeo et al., 2015] Amodeo, A. A., Jukam, D., Straight, A. F., and Skotheim, J. M. (2015). Histone titration against the genome sets the DNA-to-cytoplasm threshold for the *Xenopus* midblastula transition. *Proceedings of the National Academy of Sciences of the United States of America*, 112(10):E1086–E1095.
- [Beggs et al., 2012] Beggs, S., James, T. C., and Bond, U. (2012). The PolyA tail length of yeast histone mRNAs varies during the cell cycle and is influenced by Sen1p and Rrp6p. *Nucleic Acids Research*, 40(6):2700–11.
- [Canavan and Bond, 2007] Canavan, R. and Bond, U. (2007). Deletion of the nuclear exosome component RRP6 leads to continued accumulation of the histone mRNA HTB1 in S-phase of the cell cycle in *Saccharomyces cerevisiae*. *Nucleic Acids Research*, 35(18):6268–6279.
- [Catala and Abou Elela, 2019] Catala, M. and Abou Elela, S. (2019). Promoter-dependent nuclear RNA degradation ensures cell cycle-specific gene expression. *Communications Biology*, 2(1):211.
- [Chan and Marshall, 2010] Chan, Y. H. M. and Marshall, W. F. (2010). Scaling properties of cell and organelle size. *Organogenesis*, 6(2):88–96.

- [Chandler-Brown et al., 2017] Chandler-Brown, D., Schmoller, K. M., Winetraub, Y., and Skotheim, J. M. (2017). The Adder Phenomenon Emerges from Independent Control of Pre- and Post-Start Phases of the Budding Yeast Cell Cycle. *Current Biology*, 27(18):2774–2783.
- [Chari et al., 2019] Chari, S., Wilky, H., Govindan, J., and Amodeo, A. A. (2019). Histone concentration regulates the cell cycle and transcription in early development. *Development (Cambridge)*, 146(19):dev177402.
- [Chen et al., 2020] Chen, Y., Zhao, G., Zahumensky, J., Honey, S., and Futcher, B. (2020). Differential Scaling of Gene Expression with Cell Size May Explain Size Control in Budding Yeast. *Molecular Cell*, 78:1–12.
- [Cherry et al., 2012] Cherry, J. M., Hong, E., Amundsen, C., Balakrishnan, R., Binkley, G., Chan, E. T., Christie, K. R., Costanzo, M. C., Dwight, S. S., Engel, S. R., Fisk, D. G., Hirschman, J. E., Hitz, B. C., Karra, K., Krieger, C. J., Miyasato, S. R., Nash, R. S., Park, J., Skrzypek, M. S., Simison, M., Weng, S., and Wong, E. D. (2012). Saccharomyces genome database: the genomics resource of budding yeast. *Nucleic Acids Research*, 40(Database issue):D700–D705.
- [Collart and Oliviero, 1993] Collart, M. A. and Oliviero, S. (1993). Preparation of Yeast RNA. *Current Protocols in Molecular Biology*, 23(1):13.12.1–13.12.5.
- [Conrad et al., 2014] Conrad, M., Schothorst, J., Kankipati, H. N., Van Zeebroeck, G., Rubio-Teixeira, M., and Thevelein, J. M. (2014). Nutrient sensing and signaling in the yeast *Saccharomyces cerevisiae*. *FEMS Microbiology Reviews*, 38(2):254–299.
- [Coulter, 1953] Coulter, W. H. (issued Oct. 20, 1953). Means for counting particles suspended in a fluid. *US patent 2656508*.
- [Cox et al., 2005] Cox, M. M., Nelson, D. L., and Lehninger, A. L. (2005). *Lehninger Principles of Biochemistry*. W. H. Freeman, San Francisco.

- [Crissman and Steinkamp, 1973] Crissman, H. A. and Steinkamp, J. A. (1973). Rapid, simultaneous measurement of dna, protein, and cell volume in single cells from large mammalian cell populations. *Journal of Cell Biology*, 59(3):766–771.
- [Cross and Smith, 1988] Cross, S. L. and Smith, M. M. (1988). Comparison of the structure and cell cycle expression of mRNAs encoded by two histone H3-H4 loci in *Saccharomyces cerevisiae*. *Molecular and Cellular Biology*, 8(2).
- [de Blois and Bean, 1970] de Blois, R. W. and Bean, C. P. (1970). Counting and Sizing of Submicron Particles by the Resistive Pulse Technique. *Rev. Sci. Instrum.*, 41(909).
- [Doncic et al., 2013] Doncic, A., Eser, U., Atay, O., and Skotheim, J. M. (2013). An Algorithm to Automate Yeast Segmentation and Tracking. *PLoS ONE*, 8(3):e57970.
- [Duina et al., 2014] Duina, A. A., Miller, M. E., and Keeney, J. B. (2014). Budding yeast for budding geneticists: A primer on the *Saccharomyces cerevisiae* model system. *Genetics*, 197(1):33–48.
- [Elliott and McLaughlin, 1979] Elliott, S. G. and McLaughlin, C. S. (1979). Regulation of rna synthesis in yeast. III. Synthesis during the cell cycle. *Molecular Genetics and Genomics*, 169:237–243.
- [Elliott et al., 1979] Elliott, S. G., Warner, J. R., and McLaughlin, C. S. (1979). Synthesis of ribosomal proteins during the cell cycle of the yeast *saccharomyces cerevisiae*. *Journal of Bacteriology*, 137:1048–1050.
- [Eriksson et al., 2011] Eriksson, P. R., Ganguli, D., and Clark, D. J. (2011). Spt10 and Swi4 Control the Timing of Histone H2A/H2B Gene Activation in Budding Yeast. *Molecular and Cellular Biology*, 31(3):557–572.
- [Eriksson et al., 2012] Eriksson, P. R., Ganguli, D., Nagarajavel, V., and Clark, D. J. (2012). Regulation of histone gene expression in budding yeast. *Genetics*, 191(1):7–20.
- [Eriksson et al., 2005] Eriksson, P. R., Mendiratta, G., McLaughlin, N. B., Wolfsberg, T. G., Mariño-Ramírez, L., Pompa, T. A., Jainerin, M., Landsman, D., Shen, C.-H.,

- and Clark, D. J. (2005). Global regulation by the yeast Spt10 protein is mediated through chromatin structure and the histone upstream activating sequence elements. *Molecular and Cellular Biology*, 25:9127–9137.
- [Feser et al., 2010] Feser, J., Truong, D., Das, C., Carson, J. J., Kieft, J., Harkness, T., and Tyler, J. K. (2010). Elevated Histone Expression Promotes Life Span Extension. *Molecular Cell*, 39(5):724–735.
- [Fillingham et al., 2009] Fillingham, J., Kainth, P., Lambert, J. P., van Bakel, H., Tsui, K., Peña-Castillo, L., Nislow, C., Figeys, D., Hughes, T. R., Greenblatt, J., and Andrews, B. J. (2009). Two-Color Cell Array Screen Reveals Interdependent Roles for Histone Chaperones and a Chromatin Boundary Regulator in Histone Gene Repression. *Molecular Cell*, 35(3):340–351.
- [Futcher, 1999] Futcher, B. (1999). Cell cycle synchronization. *Methods in Cell Science*, 21:79–86.
- [Galitski, 1999] Galitski, T. (1999). Ploidy regulation of gene expression. *Science*, 285:251–254.
- [Ginzberg et al., 2015] Ginzberg, M. B., Kafri, R., and Kirschner, M. (2015). On being the right (cell) size. *Science*, 348(6236):1245075–1 – 1245075–7.
- [Goehring and Hyman, 2012] Goehring, N. W. and Hyman, A. A. (2012). Organelle growth control through limiting pools of cytoplasmic components. *Current Biology*, 22(9):R330–R339.
- [Goffeau et al., 1996] Goffeau, A. ., Barrell, B. G., Bussey, H., Davis, R. W., Dujon, B., Feldmann, H., Galibert, F., Hoheisel, J. D., Jacq, C., Johnston, M., Louis, E. J., Mewes, H. W., Murakami, Y., Philippsen, P., Tettelinand, H., and Oliver, S. G. (1996). Life with 6000 genes. *Science*, 274(5287):546–567.
- [Gunjan and Verreault, 2003] Gunjan, A. and Verreault, A. (2003). A Rad53 Kinase-Dependent Surveillance Mechanism that Regulates Histone Protein Levels in *S. cerevisiae*. *Cell*, 115(5):537–549.

- [Haase and Reed, 2002] Haase, S. B. and Reed, S. I. (2002). Improved flow cytometric analysis of the budding yeast cell cycle. *Cell Cycle*, 1:117–121.
- [Haber, 2012] Haber, J. E. (2012). Mating-type genes and MAT switching in *Saccharomyces cerevisiae*. *Genetics*, 191(1):33–64.
- [Hamperl et al., 2014a] Hamperl, S., Brown, C. R., Garea, A. V., Perez-Fernandez, J., Bruckmann, A., Huber, K., Wittner, M., Babl, V., Stoeckl, U., and Deutzmann, R. (2014a). Compositional and structural analysis of selected chromosomal domains from *Saccharomyces cerevisiae*. *Nucleic Acids Research*, 42:e2.
- [Hamperl et al., 2014b] Hamperl, S., Brown, C. R., Perez-Fernandez, J., Huber, K., Wittner, M., Babl, V., Stöckl, U., Boeger, H., Tschochner, H., and Milkereit, P. (2014b). Purification of specific chromatin domains from single-copy gene loci in *Saccharomyces cerevisiae*. *Methods in Molecular Biology*, 1094:239–341.
- [Han et al., 1987] Han, M., Chang, M., Kim, U. J., and Grunstein, M. (1987). Histone H2B repression causes cell-cycle-specific arrest in yeast: Effects on chromosomal segregation, replication, and transcription. *Cell*, 48:589–597.
- [Hauer et al., 2017] Hauer, M. H., Seeber, A., Singh, V., Thierry, R., Sack, R., Amitai, A., Kryzhanovska, M., Eglinger, J., Holcman, D., Owen-Hughes, T., and Gasser, S. M. (2017). Histone degradation in response to DNA damage enhances chromatin dynamics and recombination rates. *Nature Structural and Molecular Biology*, 24:99–107.
- [Heldt et al., 2018] Heldt, F. S., Lunstone, R., Tyson, J. J., and Novák, B. (2018). Dilution and titration of cell-cycle regulators may control cell size in budding yeast. *PLoS Computational Biology*, 14(10):1–26.
- [Hereford et al., 1979] Hereford, L., Fahrner, K., Woolford, J., Rosbash, M., and Kaback, D. B. (1979). Isolation of yeast histone genes H2A and H2B. *Cell*, 18(4):1261–1271.
- [Jorgensen et al., 2007] Jorgensen, P., Edgington, N. P., Schneider, B. L., Rupes, I., Tyters, M., and Futcher, B. (2007). The size of the nucleus increases as yeast cells grow. *Molecular Biology of the Cell*, 18(9):3523–3532.

- [Jorgensen et al., 2002] Jorgensen, P., Nishikawa, J. L., Breikreutz, B. J., and Tyers, M. (2002). Systematic identification of pathways that couple cell growth and division in yeast. *Science*, 297(5580):395–400.
- [Joseph et al., 2017] Joseph, S. R., Pálffy, M., Hilbert, L., Kumar, M., Karschau, J., Zaburdaev, V., Shevchenko, A., and Vastenhouw, N. L. (2017). Competition between histone and transcription factor binding regulates the onset of transcription in zebrafish embryos. *eLife*, 6.
- [Kim et al., 2010] Kim, D., Hayles, J., Kim, D., Wood, V., Park, H.-O., Won, M., Yoo, H.-S., Duhig, T., Nam, M., Palmer, G., Han, S., Jeffery, L., Baek, S., Lee, H., Shim, Y. S., Lee, M., Kim, L., Heo, K.-S., Noh, E. J., Lee, A.-R., Jang, Y.-J., Chung, K.-S., Shin-Jung Choi, S.-J., Jo-Young Park, J.-Y., Park, Y., Kim, H. M., Park, S.-K., Park, H.-J., Kang, E.-J., Kim, H. B., Kang, H.-S., Park, H.-M., Kim, K., Song, K., Song, K. B., Nurse, P., and Hoe, K. (2010). Analysis of a genome-wide set of gene deletions in the fission yeast *schizosaccharomyces pombe*. *Nature Biotechnology*, 26(6):617–623.
- [Kim et al., 1988] Kim, U. J., Han, M., Kayne, P., and Grunstein, M. (1988). Effects of histone H4 depletion on the cell cycle and transcription of *Saccharomyces cerevisiae*. *The EMBO Journal*, 7(7):2211–2219.
- [Kukhtevich et al., 2020] Kukhtevich, I. V., Lohrberg, N., Padovani, F., Schneider, R., and Schmoller, K. M. (2020). Cell size sets the diameter of the budding yeast contractile ring. *Nature Communications*, 11:2952.
- [Kurat et al., 2014a] Kurat, C. F., Lambert, J.-P., Petschnigg, J., Friesen, H., Pawson, T., Rosebrock, A., Gingras, A.-C., Fillingham, J., and Andrews, B. (2014a). Cell cycle-regulated oscillator coordinates core histone gene transcription through histone acetylation. *Proceedings of the National Academy of Sciences*, 111(39):14124–14129.
- [Kurat et al., 2014b] Kurat, C. F., Recht, J., Radovani, E., Durbic, T., Andrews, B., and Fillingham, J. (2014b). Regulation of histone gene transcription in yeast. *Cellular and Molecular Life Sciences*, 71(4):599–613.

- [Laissue et al., 2017] Laissue, P. P., Alghamdi, R. A., Tomancak, P., Reynaud, E. G., and Shroff, H. (2017). Assessing phototoxicity in live fluorescence imaging. *Nature Methods*, 14:657–661.
- [Lanz et al., 2021] Lanz, M. C., Zatulovskiy, E., Swaffer, M. P., Zhang, L., Zhang, S., You, D. S., Marinov, G., McAlpine, P., Elias, J. E., and Skotheim, J. M. (2021). Increasing cell size remodels the proteome and promotes senescence. *bioRxiv*, doi: 10.1101/2021.07.29.454227.
- [Lee et al., 2005] Lee, K. M., Miklos, I., Du, H., Watt, S., Szilagy, Z., Saiz, J. E., Madabhushi, R., Penkett, C. J., Sipiczki, M., Bähler, J., and Fisher, R. P. (2005). Impairment of the TFIIH-associated CDK-activating kinase selectively affects cell cycle-regulated gene expression in fission yeast. *Molecular biology of the cell*, 16(6):2734–2745.
- [Lee and Young, 2013] Lee, T. I. and Young, R. A. (2013). Transcriptional regulation and its misregulation in disease. *Cell*, 152(6):1237–1251.
- [Libuda and Winston, 2006] Libuda, D. E. and Winston, F. (2006). Amplification of histone genes by circular chromosome formation in *Saccharomyces cerevisiae*. *Nature*, 443(7114):1003–1007.
- [Libuda and Winston, 2010] Libuda, D. E. and Winston, F. (2010). Alterations in DNA replication and histone levels promote histone gene amplification in *Saccharomyces cerevisiae*. *Genetics*, 184(4):985–997.
- [Lin and Amir, 2018] Lin, J. and Amir, A. (2018). Homeostasis of protein and mRNA concentrations in growing cells. *Nature Communications*, 9(4496).
- [Lloyd, 2013] Lloyd, A. C. (2013). The regulation of cell size. *Cell*, 154(6):1194–1205.
- [Marguerat and Bähler, 2012] Marguerat, S. and Bähler, J. (2012). Coordinating genome expression with cell size. *Trends in Genetics*, 28(11):560–565.

- [Marguerat et al., 2012] Marguerat, S., Schmidt, A., Codlin, S., Chen, W., Aebersold, R., and Bähler, J. (2012). Quantitative analysis of fission yeast transcriptomes and proteomes in proliferating and quiescent cells. *Cell*, 151:671–683.
- [Mariño-Ramírez et al., 2006] Mariño-Ramírez, L., Jordan, I., and Landsman, D. (2006). Multiple independent evolutionary solutions to core histone gene regulation. *Genome Biology*, 7:R122.
- [Meeks-Wagner and Hartwell, 1986] Meeks-Wagner, D. and Hartwell, L. H. (1986). Normal stoichiometry of histone dimer sets is necessary for high fidelity of mitotic chromosome transmission. *Cell*, 44(1):43–52.
- [Mena et al., 2017] Mena, A., Medina, D. A., García-Martínez, J., Begley, V., Singh, A., Chávez, S., Muñoz-Centeno, M. C., and Pérez-Ortín, J. E. (2017). Asymmetric cell division requires specific mechanisms for adjusting global transcription. *Nucleic Acids Research*, 45(21):12401–12412.
- [Merlini et al., 2013] Merlini, L., Dudin, O., and Martin, S. G. (2013). Mate and fuse: how yeast cells do it. *open Biology*, 3(3):130008.
- [Miller et al., 2011] Miller, C., Schwalb, B., Maier, K., Schulz, D., Dümecke, S., Zacher, B., Mayer, A., Sydow, J., Marcinowski, L., and Dölken, L. (2011). Dynamic transcriptome analysis measures rates of mRNA synthesis and decay in yeast. *Molecular Systems Biology*, 7(1):458.
- [Moran et al., 1990] Moran, L., Norris, D., and Osley, M. A. (1990). A yeast H2A-H2B promoter can be regulated by changes in histone gene copy number. *Genes and Development*, 4(5):752–763.
- [Morgan, 2007] Morgan, D. O. (2007). *Cell Cycle: Principles of Control*. New Science Press Ltd, London.
- [Mortimer et al., 1992] Mortimer, R. K., Contopoulou, C. R., and King, J. S. (1992). Genetic and physical maps of *Saccharomyces cerevisiae*. *Yeast*, 8(10):817–902.

- [Mortimer and Johnston, 1986] Mortimer, R. K. and Johnston, J. R. (1986). Genealogy of principal strains of the yeast genetic stock center. *Genetics*, 113(1):35–34.
- [Mueller et al., 2013] Mueller, F., Senecal, A., Tantale, K., Marie-Nelly, H., Ly, N., Collin, O., Basyuk, E., Bertrand, E., Darzacq, X., and Zimmer, C. (2013). FISH-quant: automatic counting of transcripts in 3D FISH images. *Nature Methods*, 10(4):277–278.
- [Myers et al., 2013] Myers, J. A., Curtis, B. S., and Curtis, W. R. (2013). Improving accuracy of cell and chromophore concentration measurements using optical density. *BMC Biophysics*, 6. 4.
- [Nash et al., 1988] Nash, R., Tokiwa, G., Anand, S., Erickson, K., and Futcher, A. B. (1988). The *WHI1+* gene of *Saccharomyces cerevisiae* tethers cell division to cell size and is a cyclin homolog. *EMBO Journal*, 7(13):4335–4346.
- [Neiman, 2011] Neiman, A. M. (2011). Sporulation in the budding yeast *Saccharomyces cerevisiae*. *Genetics*, 189(3):737–765.
- [Neumann and Nurse, 2007] Neumann, F. R. and Nurse, P. (2007). Nuclear size control in fission yeast. *Journal of Cell Biology*, 179(4):593–600.
- [Norris and Osley, 1987] Norris, D. and Osley, M. A. (1987). The two gene pairs encoding H2A and H2B play different roles in the *Saccharomyces cerevisiae* life cycle. *Molecular and Cellular Biology*, 7(10):3473–3481.
- [Ogur et al., 1952] Ogur, M., Minckler, S., Lindegren, G., and Lindegren, C. C. (1952). The nucleic acids in a polyploid series of *Saccharomyces*. *Archives of Biochemistry and Biophysics*, 40(1):175–184.
- [Olivares-Marin et al., 2018] Olivares-Marin, I. K., González-Hernández, J. C., Regalado-Gonzalez, C., and Madrigal-Perez, L. A. (2018). *Saccharomyces cerevisiae* exponential growth kinetics in batch culture to analyze respiratory and fermentative metabolism. *Journal of Visualized Experiments*, 139:58192.

- [Örd et al., 2019] Örd, M., Venta, R., Möll, K., Valk, E., and Loog, M. (2019). Cyclin-Specific Docking Mechanisms Reveal the Complexity of M-CDK Function in the Cell Cycle. *Molecular Cell*, 75(1):76–89.
- [Orjalo and Johannsson, 2016] Orjalo, Jr., A. V. and Johannsson, H. E. (2016). Stellaris® RNA fluorescence *in situ* hybridization for the simultaneous detection of immature and mature long noncoding RNAs in adherent cells. *Methods in Molecular Biology*, 1402:119–134.
- [Osley, 1991] Osley, M. (1991). The Regulation Of Histone Synthesis In The Cell Cycle. *Annual Review of Biochemistry*, 60(1):827–861.
- [Osley and Lycan, 1987] Osley, M. and Lycan, D. (1987). Trans-acting regulatory mutations that alter transcription of *Saccharomyces cerevisiae* histone genes. *Molecular and Cellular Biology*, 7(12):4204–4210.
- [Osley et al., 1986] Osley, M. A., Gould, J., Kim, S., Kane, M., and Hereford, L. (1986). Identification of sequences in a yeast histone promoter involved in periodic transcription. *Cell*, 45(4):537–544.
- [Ottoz et al., 2014] Ottoz, D. S., Rudolf, F., and Stelling, J. (2014). Inducible, tightly regulated and growth condition-independent transcription factor in *Saccharomyces cerevisiae*. *Nucleic Acids Research*, 42(17):e130.
- [Padovan-Merhar et al., 2015] Padovan-Merhar, O., Nair, G. P., Biaesch, A. G., Mayer, A., Scarfone, S., Foley, S. W., Wu, A. R., Churchman, L. S., Singh, A., and Raj, A. (2015). Single Mammalian Cells Compensate for Differences in Cellular Volume and DNA Copy Number through Independent Global Transcriptional Mechanisms. *Molecular Cell*, 58(2):339–352.
- [Picot et al., 2012] Picot, J., Guerin, C. L., Le Van Kim, C., and Boulanger, C. M. (2012). Flow cytometry: retrospective, fundamentals and recent instrumentation. *Cytotechnology*, 64(2):109–130.

- [Pir et al., 2012] Pir, P., Gutteridge, A., Wu, J., Rash, B., Kell, D. B., Zhang, N., and Oliver, S. G. (2012). The genetic control of growth rate: a systems biology study in yeast. *BMC Systems Biology*, 6(4):1752–0509.
- [Rafelski et al., 2012] Rafelski, S. M., Viana, M. P., Zhang, Y., Chan, Y. H. M., Thorn, K. S., Yam, P., Fung, J. C., Li, H., Costa, L. D. F., and Marshall, W. F. (2012). Mitochondrial network size scaling in budding yeast. *Science*, 338(6108):822–824.
- [Raj et al., 2008] Raj, A., van den Bogaard, P., Rifkin, S. A., van Oudenaarden, A., and Tyagi, S. (2008). Imaging individual mRNA molecules using multiple singly labeled probes. *Nature Methods*, 5(10):877–879.
- [Ralser et al., 2012] Ralser, M., Kuhl, H., Ralser, M., Werber, M., Lehrach, H., Breitenbach, M., and Timmermann, B. (2012). The *Saccharomyces cerevisiae* W303-K6001 cross-platform genome sequence: insights into ancestry and physiology of a laboratory mutt. *Open Biology*, 2(8):120093.
- [Robert, 2015] Robert, L. (2015). Size sensors in bacteria, cell cycle control, and size control. *Frontiers in Microbiology*, 6(515).
- [Schindelin et al., 2012] Schindelin, J., Arganda-Carreras, I., Frise, E., Kaynig, V., Longair, M., Pietzch, T., Preibisch, S., Rueden, C., Saalfeld, S., Schmid, B., Tinevez, J.-Y., White, D. J., Hartenstein, V., Eliceiri, K., Pomancak, P., and Cardona, A. (2012). Fiji: an open-source platform for biological-image analysis. *Nature Methods*, 9:676–682.
- [Schmidt and Schibler, 1995] Schmidt, E. E. and Schibler, U. (1995). Cell size regulation, a mechanism that controls cellular RNA accumulation: consequences on regulation of the ubiquitous transcription factors Oct1 and NF-Y and the liver-enriched transcription factor DBP. *Journal of Cell Biology*, 128:467–483.
- [Schmoller and Skotheim, 2015] Schmoller, K. M. and Skotheim, J. M. (2015). The Biosynthetic Basis of Cell Size Control. *Trends in Cell Biology*, 25(12):793–802.

- [Schmoller et al., 2015] Schmoller, K. M., Turner, J. J., Kõivomägi, M., and Skotheim, J. M. (2015). Dilution of the cell cycle inhibitor Whi5 controls budding-yeast cell size. *Nature*, 526(7572):268–272.
- [Schulz et al., 2013] Schulz, D., Schwalb, B., Kiesel, A., Baejen, C., Torkler, P., Gagneur, J., Soeding, J., and Cramer, P. (2013). Transcriptome surveillance by selective termination of noncoding RNA synthesis. *Cell*, 155(5):1075–1087.
- [Seel et al., 2022] Seel, A., Padovani, F., Finster, A., Mayer, M., Bureik, D., Osman, C., Klecker, T., and Schmoller, K. M. (2022). Regulation with cell size ensures mitochondrial DNA homeostasis during cell growth. *bioRxiv*, doi: 10.1101/2021.12.03.471050.
- [Sharma et al., 2006] Sharma, N., Marguerat, S., Mehta, S., Watt, S., and Bähler, J. (2006). The fission yeast Rpb4 subunit of RNA polymerase II plays a specialized role in cell separation. *Molecular genetics and genomics : MGG*, 276(6):545–554.
- [Smith and Murray, 1983] Smith, M. M. and Murray, K. (1983). Yeast H3 and H4 histone messenger RNAs are transcribed from two non-allelic gene sets. *Journal of Molecular Biology*, 169:641–661.
- [Stockert and Blazquez-Castro, 2017] Stockert, J. C. and Blazquez-Castro, A. (2017). *Fluorescence Microscopy in Life Sciences*. Bentham Science Publishers, Sharjah.
- [Sun et al., 2012] Sun, M., Schwalb, B., Schulz, D., Pirkl, N., Etzold, S., L., L., Maier, K. C., Seizl, M., Tresch, A., and Cramer, P. (2012). Comparative dynamic transcriptome analysis (cDTA) reveals mutual feedback between mrna synthesis and degradation. *Genome Research*, 22:1350–1359.
- [Sun et al., 2020] Sun, X. M., Bowman, A., Priestman, M., Bertaux, F., Martinez-Segura, A., Tang, W., Whilding, C., Dormann, D., Shahrezaei, V., and Marguerat, S. (2020). Size-Dependent Increase in RNA Polymerase II Initiation Rates Mediates Gene Expression Scaling with Cell Size. *Current Biology*, 30(7):1217–1230.
- [Swaffer et al., 2021a] Swaffer, M. P., Kim, J., Chandler-Brown, D., Langhinrichs, M., Marinov, G. K., Greenleaf, W. J., Kundaje, A., Schmoller, K. M., and Skotheim,

- J. M. (2021a). Transcriptional and chromatin-based partitioning mechanisms uncouple protein scaling from cell size. *Molecular Cell*, 81(23):4861–4875.E7.
- [Swaffer et al., 2021b] Swaffer, M. P., Marinov, G. K., Zheng, H., Jones, A. W., Greenwood, J., Kundaje, A., Snijders, A. P., Greenleaf, W. J., Reyes-Lamothe, R., and Skotheim, J. M. (2021b). RNA polymerase II dynamics and mRNA stability feedback determine mRNA scaling with cell size. *bioRxiv*, doi: 10.1101/2021.09.20.461005.
- [Tsihlaki and FitzHarris, 2016] Tsihlaki, E. and FitzHarris, G. (2016). Nucleus down-scaling in mouse embryos is regulated by cooperative developmental and geometric programs. *Scientific Reports*, 6:28040.
- [Turner et al., 2012] Turner, J. J., Ewald, J. C., and Skotheim, J. M. (2012). Cell size control in yeast. *Current Biology*, 22(9):R350–R359.
- [von der Haar, 2008] von der Haar, T. (2008). A quantitative estimation of the global translational activity in logarithmically growing yeast cells. *BMC Systems Biology*, 2:87–101.
- [Watson et al., 1987] Watson, J. V., Chambers, S. H., and Smith, P. J. (1987). With a Definable G1 Peak. *Cytometry*, 8:1–8.
- [Williamson and Scopes, 1961] Williamson, D. H. and Scopes, A. W. (1961). The distribution of nucleic acids and protein between different sized yeast cells. *Experimental Cell Research*, 24:151–153.
- [Wu et al., 2010] Wu, C. Y., Alexander Rolfe, P., Gifford, D. K., and Fink, G. R. (2010). Control of transcription by cell size. *PLoS Biology*, 8(11):e1000523.
- [Wu and Pollard, 2005] Wu, J.-Q. and Pollard, T. D. (2005). Counting cytokinesis proteins globally and locally in fission yeast. *Science*, 310(5746):310–314.
- [Xu et al., 1992] Xu, H., Kim, U., Schuster, T., and Grunstein, M. (1992). Identification of a new set of cell cycle-regulatory genes that regulate s-phase transcription of histone genes in *Saccharomyces cerevisiae*. *Molecular and Cellular Biology*, 12:5249–5259.

- [Zacharias et al., 2002] Zacharias, D. A., Violin, J. D., Newton, A. C., and Tsien, R. Y. (2002). Partitioning of lipid-modified monomeric GFPs into membrane microdomains of live cells. *Science*, 296(5569):913–916.
- [Zatulovskiy et al., 2020] Zatulovskiy, E., Zhang, S., Berenson, D. F., Topacio, B. R., and Jan, M. (2020). Cell growth dilutes the cell cycle inhibitor Rb to trigger cell division. *Science*, 369(6502):466–471.
- [Zernike, 1942a] Zernike, F. (1942a). Phase contrast, a new method for the microscopic observation of transparent objects part I. *Physica*, 9(7):686–698.
- [Zernike, 1942b] Zernike, F. (1942b). Phase contrast, a new method for the microscopic observation of transparent objects part II. *Physica*, 9(10):974–986.
- [Zettel et al., 2003] Zettel, M. F., Garza, L. R., Cass, A. M., Myhre, R. A., Haizlip, L. A., Osadebe, S. N., Sudimack, D. W., Pathak, R., Stone, T. L., and Polymenis, M. (2003). The budding index of *Saccharomyces cerevisiae* deletion strains identifies genes important for cell cycle progression. *FEMS Microbiology Letters*, 223(2):253–258.
- [Zhang et al., 2002] Zhang, J., Schneider, C., Ottmers, L., Rodriguez, R., Day, A., Markwardt, J., and Schneider, B. L. (2002). Genomic scale mutant hunt identifies cell size homeostasis genes in *S. cerevisiae*. *Current biology: CB*, 12:1992–2001.
- [Zhurinsky et al., 2010] Zhurinsky, J., Leonhard, K., Watt, S., Marguerat, S., Bähler, J., and Nurse, P. (2010). A coordinated global control over cellular transcription. *Current Biology*, 20(22):2010–2015.
- [Zunder and Rine, 2012] Zunder, R. M. and Rine, J. (2012). Direct Interplay among Histones, Histone Chaperones, and a Chromatin Boundary Protein in the Control of Histone Gene Expression. *Molecular and Cellular Biology*, 32(21).

Scientific curriculum vitae

Scientific education:

- 2011 - 2014, Technical University Munich, B. Sc. in Physics
- 2014 - 2017, Technical University Munich, M. Sc. in Condensed Matter Physics
- 2017 - 2020, Ludwig-Maximilians-University Munich, Doctoral student in Biology
- 2017 - 2021, Helmholtz Centre Munich, Doctoral researcher at the Institute of Functional Epigenetics

Poster presentations related to this thesis:

- 2017 December 14-15, HMGU Stem Cell Center opening symposium, Munich, Germany
- 2018 June 26-29, 10th Salk Institute Cell Cycle meeting, San Diego, USA
- 2019 April 1-3, “Chromatin and Epigenetics: Inheritance and Design” meeting, Munich, Germany
- 2019 June 3-6, Trieste Cell Cycle meeting, Trieste, Italy

Oral presentations related to this thesis:

- 2019 December 7-11, ASCB/EMBO meeting, Washington DC, USA
- 2020 September 9, Cell Size & Growth seminar series, online
- 2021 May 17, RIKEN - HMGU joint Epigenetics Seminar, online
- 2021 June 22-25, 11th Salk Institute Cell Cycle meeting, online

Publications**Related to this thesis:**

- Claude, K.-L., Bureik, D., Chatzitheodoridou, D., Adarska, P., Singh, A., and Schmoller, K. M. (2021) Transcription coordinates histone amounts and genome content. *Nature Communications*, 12:4202.

Unrelated to this thesis:

- Niebuur, B.-J., Ko, C.-H., Zhang, X., Claude, K.-L., Chiappisi, L., Schulte, A., and Papadakis, C. M. (2020). Pressure Dependence of the Cononsolvency Effect in Aqueous Poly(N-isopropylacrylamide) Solutions: A SANS Study. *Macromolecules*, 53(10):3946.
- Ko, C.-H., Claude, K.-L., Niebuur, B.-J., Jung, F. A., Kang, J.-J., Schanzenbach, D., Frielinghaus, H., Barnsley, L. C., Wu, B., Pipich, V., Schulte, A., Müller-Buschbaum, P., Laschewsky, A., and Papadakis, C. M. (2020). Temperature-Dependent Phase Behavior of the Thermoresponsive Polymer Poly(N-isopropylmethacrylamide) in an Aqueous Solution. *Macromolecules*, 53(16):6816.